UNIVERSITY OF CALIFORNIA SAN DIEGO

Neuronal Reprogramming to Study Human Brain Aging and Disease

A dissertation submitted in partial satisfaction
of the requirements for the Doctor of Philosophy

in

Neurosciences

by

Joseph Roger Herdy III

Committee in charge:

Professor Fred Gage, Co-Chair
Professor Gene Yeo, Co-Chair
Professor Doug Galasko
Professor Christopher Glass

2023

The dissertation of Joseph Herdy is approved, and it is acceptable in quality and form for publication on microfilm and electronically.

University of California San Diego

2023

DEDICATION

I would like to dedicate this work to the persons who have donated their cells and tissues to science and have allowed us to do this rewarding work. To all my family who have shown me with magnificent love and support through these years. To all my friends and colleagues who have expanded my mind both in and out of science and without whom I would live a much less enriching life. And finally to the social structures that have brought me from Alabama to California and have given me the privilege to contribute to the pursuit of collective human knowledge.

EPIGRAPH

“Ah, there’s nothing more exciting than science. You get all the fun of sitting still, being quiet, writing down numbers, paying attention… Science has it all.”

- Principal Skinner

TABLE OF CONTENTS

LIST OF FIGURES

ACKNOWLEDGEMENTS

I would like to acknowledge the members of the Gage and Mertens labs for their support and friendship over the years. I feel incredibly lucky to have been able to spend time in a lab like Rusty's and to learn from his mentorship and draw on his passion for science and discovery. I would also like to thank Jerome for teaching me more or less everything I know about cell biology and for always being a source of encouragement and inspiration during my training. There have been so many others who have contributed to my science journey over the years that it would be impossible to list them all, but I would especially like to thank Jennifer Erwin for introducing me to the world of human genetics, and Ravi Agarwal, Lukas Karbacher, Dina Zangwill, Zoya Ansari and all the other students and technicians who helped pursue the ideas for this thesis. I would also like to thank the other PhD students in the lab, Steve Johnston, David Adamovich, Jasmin Revana, Sheila Steiner, Sarah Fernandes, Mike Cuocco, and Christina Lim for their comradery and putting up with discussing obscure ideas. The same goes for the students in the Mertens lab: Larissa Traxler, Sophie Eichhorner, Lucia Zhou Yang, Jessica Lagerwall, and Oli Borgogno who showed me hospitality and friendship in the Alps.

I would also like to acknowledge the funding from the National Institute of Health, the AHA Allen Initiative, and the Milky Way Foundation for their generous funding for this research.

Chapter 1, in full, is a reprint of the material as it appears in:. Joseph Herdy, Simon Schafer, Yongsung Kim, Zoya Ansari, Dina Zangwill, Manching Ku, Apua Paquola, Hyungjun Lee, Jerome Mertens, Fred H Gage (2019) Chemical modulation of transcriptionally enriched signaling pathways to optimize the conversion of fibroblasts into neurons eLife 8:e41356 https://doi.org/10.7554/eLife.41356. The dissertation author was the primary investigator and author of this paper.

Chapter 2, in full, is a reprint of the material as it appears in: Herdy, J. R., Traxler, L., Agarwal, R. K., Karbacher, L., Schlachetzki, J. C. M., Boehnke, L., Zangwill, D., Galasko, D., Glass, C. K., Mertens, J., & Gage, F. H. (2022). Increased post-mitotic senescence in aged human

neurons is a pathological feature of Alzheimer's disease. Cell stem cell, 29(12), 1637–1652.e6. https://doi.org/10.1016/j.stem.2022.11.010. The dissertation author was the primary investigator and author of this paper.

VITA

2012 Bachelor of Science, University of Alabama in Huntsville

2014 Master of Science, University of Kentucky

2023 Doctor of Philosophy, University of California San Diego

PUBLICATIONS

Joseph R. Herdy, Larissa Traxler, Ravi K. Agarwal, Lukas Karbacher, Johannes C.M. Schlachetzki, Lena Boehnke, Dina Zangwill, Doug Galasko, Christopher K. Glass, Jerome Mertens & Fred H. Gage. “Increased Post-Mitotic Senescence in Aged Human Neurons is a Pathological Feature of Alzheimer’s Disease” Cell Stem Cell (2022).

Joseph R. Herdy, Simon Schafer, Yongsung Kim, Zoya Ansari, Dina Zangwill, Manching Ku, Apua Paquola, Hyungjun Lee, Jerome Mertens, Fred H. Gage. “Chemical modulation of transcriptionally enriched signaling pathways to optimize the conversion of fibroblasts into neurons”. eLIFE (2019).

Joseph R. Herdy, Lukas Karbacher, Jerome Mertens. “One Big Step to a Neuron, Two Small Steps for miRNAs”. Preview. Cell Stem Cell (2021).

Jerome Mertens, Joseph R. Herdy, Larissa Traxler, Simon T. Schafer, Johannes C.M. Schlachetzki, Lena Böhnke, Dylan A. Reid, Hyungjun Lee, Dina Zangwill, Diana P. Fernandes, Ravi K. Agarwal, Raffaella Lucciola, Lucia Zhou-Yang, Lukas Karbacher, Frank Edenhofer, Shani Stern, Steve Horvath, Apua C.M. Paquola, Christopher K. Glass, Shauna H. Yuan, Manching Ku, Attila Szücs, Lawrence S.B. Goldstein, Douglas Galasko, Fred H. Gage, “Age-dependent instability of mature neuronal fate in induced neurons from Alzheimer’s patients.” Cell Stem Cell, (2021).

Larissa Traxler, Joseph R. Herdy, Davide Stefanoni, Sophie Eichhorner, Silvia Pelucchi, Attila Szücs, Alice Santagostino, Yongsung Kim, Ravi K Agarwal, Johannes C M Schlachetzki, Christopher K Glass, Jessica Lagerwall, Douglas Galasko, Fred H Gage, Angelo D'Alessandro, JeromeMertens. “Warburg-like metabolic transformation underlies neuronal degeneration in sporadic Alzheimer's disease”. Cell Metabolism (2022).

Larissa Traxler1 Raffaella Lucciola, Joseph R. Herdy, Jeffrey R. Jones, Jerome Mertens, Fred H. Gage. Neural cell state shifts and fate loss in ageing and age-related diseases. Nature Reviews: Neurology. (2023).

Lena Böhnke, Lucia Zhou-Yang, Silvia Pelucchi, Flora Kogler, Daniela Frantal, Florian Schön, Stina Lagerström, Oliver Borgogno, Jennifer Baltazar, Joseph R. Herdy, Sarah Kittel-Schneider, Michaela Defrancesco, and Jerome Mertens. “Chemical Replacement of Noggin with Dorsomorphin Homolog 1 for Cost-Effective Direct Neuronal Conversion” Cellular Reprogramming (2022).

Shinichi Fukuda, Akhil Varshney, Benjamin J. Fowler, Shao-bin Wang, Siddharth Narendran, Kameshwari Ambati, Tetsuhiro Yasuma, Joseph Magagnoli, Hannah Leung, Shuichiro Hirahara, Yosuke Nagasaka, Reo Yasuma, Ivana Apicella, Felipe Pereira, Ryan D. Makin, Eamonn Magner, Xinan Liu, Jian Sun, Mo Wang, Kirstie Baker, Kenneth M. Marion, Xiwen Huang, Elmira Baghdasaryan, Meenakshi Ambati, Vidya L. Ambati, Akshat Pandey, Lekha Pandya, Tammy Cummings, Daipayan Banerjee, Peirong Huang, Praveen Yerramothu, Genrich V. Tolstonog, Ulrike Held, Jennifer A. Erwin, Apua C. M. Paquola, Joseph R. Herdy, Yuichiro Ogura, Hiroko Terasaki, Tetsuro Oshika, Shaban Darwish, Ramendra K. Saghar Mozaffari, Deepak Bhattarai,

Kyung Bo Kim, James W. Hardin, Charles L. Bennett, David R. Hinton, Timothy E. Hanson, Christian Röver, Keykavous Parang, Nagaraj Kerur, Jinze Liu, Brian C. Werner, S. Scott Sutton, Srinivas R. Sadda, Gerald G. Schumann, Bradley D. Gelfand, Fred H. Gage, Jayakrishna Ambati. “Cytoplasmic synthesis of endogenous Alu complementary DNA via reverse transcription and implications in age-related macular degeneration”. PNAS (2021).

Lena Böhnke, Larissa Traxler, Joseph R. Herdy, Jerome Mertens “Human neurons to model aging: A dish best served old”. Drug Discovery Today: Disease Models (2019).

Dr. Ana Jovicic , Dr. Jerome Mertens , MSteven Boeynaems , Elke Bogaert ,Miss Noo Chai , Ms. Shizuka Yamada , Mr. Joseph Paul , Shuying Sun,Joseph R. Herdy , Mr. Gregor Bieri , Nicholas Kramer , Dr. Fred Gage, Prof. Ludo Van Den Bosch , Wim Robberecht “Modifiers of C9orf72 DPR toxicity implicate nucleocytoplasmic transport impairments in c9FTD/ALS”. Nature Neuroscience (2015).

Jerome Mertens, Apuã C. M. Paquola, Manching Ku, Emily Hatch, Lena Böhnke, Shauheen Ladjevardi, Sean McGrath, Benjamin Campbell, Hyungjun Lee, Joseph R. Herdy, J. Tiago Gonçalves, Tomohisa Toda, Yongsung Kim, Jürgen Winkler, Jun Yao, Martin Hetzer and Fred H. Gage “Directly Reprogrammed Human Neurons Retain Aging-Associated Transcriptomic Signatures and Reveal Age-Related Nucleocytoplasmic Defects”. Cell Stem Cell (2015). Best of Cell Stem Cell 2015

Jennifer A. Erwin, Apuã C.M. Paquola, Tatjana Singer, Iryna Gallina, Mark Novotny, Carolina Quayle, Tracy Bedrosian, Cheyenne R. Butcher, Joseph R. Herdy, Roger S. Lasken, Alysson R. Muotri, Fred H. Gage “L1-associated genomic regions are deleted in somatic cells of the healthy human brain” Nature Neuroscience (2016).

Yongsung Kim, Xinde Zheng, Zoya Ansari, Mark C. Bunnell, Joseph R. Herdy, Larissa Traxler, Hyungjun Lee, Apua C.M. Paquola, Chrysanthi Blithikioti, Manching Ku, Johannes C.M. Schlachetzki, Jürgen Winkler, Frank Edenhofer, Christopher K. Glass, Andres A. Paucar, Baptiste N. Jaeger, Son Pham, Leah Boyer, Benjamin C. Campbell, Tony Hunter, Jerome Mertens, Fred H. Gage “Mitochondrial Aging Defects Emerge in Directly Reprogrammed Human Neurons due to Their Metabolic Profile” Cell Reports (2018).

Paige E. Herman, Angelos Papatheodorou, Stephanie A. Bryant, Courtney K. M. Waterbury, Joseph R. Herdy, Anthony A. Arcese, Joseph D. Buxbaum, Jeramiah J. Smith, Jennifer R. Morgan & Ona Bloom “Highly conserved molecular pathways, including Wnt signaling, promote functional recovery from spinal cord injury in lampreys” Scientific Reports (2018).

Vladimir A. Timoshevskiy, Joseph R. Herdy, Jeramiah James Smith “Cellular and Molecular Features of Developmentally Programmed Genome Rearrangements in a Vertebrate (Sea Lamprey: Petromyzon marinus)” PLOS Genetics (2016).

Bryant SA, Joseph R. Herdy, Amemiya CT, Smith JJ. “Characterization of Somatically-Eliminated Genes During Development of the Sea Lamprey (Petromyzon marinus)” Mol Biol Evol. (2016).

Leland Cseke and Joseph R. Herdy, "Extraction/Characterization of DNA" Cell Biology Protocols Module, Methods Navigator, Ed. P. \Michael Conn, Elsevier (2012).

ABSTRACT OF THE DISSERTATION

Neuronal Reprogramming to Study Human Brain Aging and Disease

by

Joseph Roger Herdy III

Doctor of Philosophy in Neurosciences

University of California San Diego 2023

Professor Fred H. Gage, Co-Chair

Professor Gene Yeo, Co-Chair

The individual unit of computation in the human brain is the neuron. To advance our understanding of the human brain, we need to generate relevant cellular models of human neurons *in vitro*. Direct conversion of human somatic fibroblasts into induced neurons (iNs) allows for the generation of functional neurons while bypassing any stem cell intermediary stages. Although iN technology has an enormous potential for modeling age-related diseases, as well as therapeutic approaches, the technology faces limitations due to variable conversion efficiencies and a lack of thorough understanding of the signaling pathways directing iN conversion. Here, I introduce a new all-in-one inducible lentiviral system that simplifies fibroblast transgenesis for the two pioneer transcription factors, Ngn2 and Ascl1, and a small molecule cocktail that markedly improves iN yields and sheds new insight into the mechanisms influencing direct iN conversion. Next, I will apply the iN protocol on a cohort of Alzheimer's disease (AD) and healthy age matched control donor samples to model age-related molecular phenotypes in AD neurons. I previously

found that AD brains have significantly higher proportions of neurons that express senescence markers, and their distribution indicates bystander effects. AD patient-derived iNs exhibit strong transcriptomic, epigenetic, and molecular biomarker signatures that illuminate a specific human neuronal senescence-like state. AD iN single-cell transcriptomics revealed that senescent neurons face oncogenic challenges, and metabolic dysfunction, and they display a proinflammatory signature. Integrative profiling of the inflammatory secretome of AD iNs and patient cerebral spinal fluid revealed a neuronal senescence-associated-secretory-phenotype, that can trigger astrogliosis in human astrocytes. Finally, I show that targeting senescence-like neurons with senotherapeutics could be a novel strategy for preventing or treating AD.

INTRODUCTION

To improve our understanding of the human brain we need access to its cellular components. Human neural cells are challenging to access due to the invasive nature necessary to acquire them, and consequently our understanding of human brain cellular biology has lagged behind animal models where these tissues can be readily derived. An alternative strategy is to manipulate the fate of a more easily accessible cell to the cell type of interest. During development, naïve embryonic cells undergo patterned differentiation to give rise to defined somatic cell types that perform specialized functions and are locked into a developmental fate. Under normal circumstances, cells maintain this fate for the remainder of the life of the organism, and a loss of fate is typically associated with pathologies like cancer. The manipulation of cellular fate and setting a cell back in developmental time was demonstrated in 1962 by Gurdon when differentiated epithelial cells were transplanted from tadpoles into enucleated frog eggs (GURDON 1962). Although the efficiency was low, some of these transferred nuclei were able to give rise to normal tadpoles demonstrating that their nuclei contained all the genetic information necessary for the formation of all other cell types in a normal feeding tadpole. However, the signaling factors present in the oocytes that were necessary for mediating this reprogramming were unknown for many decades.

The next breakthrough came in 2006 when Takahashi and Yamanaka demonstrated that oocyte based reprogramming could be recapitulated in mice by the overexpression of four defined transcription factors (Oct4, Sox2, Klf4, and c-Myc) which together produced pluripotent stem cells that resembled inner mass embryonic cells and could give rise to all three germ layers and therefore every somatic cell in adult mammals (Takahashi and Yamanaka 2006). These induced pluripotent stem cells (iPSCs) have since become a field of study in their own right, and have led to thousands of publications as investigators have developed protocols for differentiating iPSCs into the cell types of interest. Importantly, iPSC technology works in human cells, and a relatively non-invasive skin biopsy provides a human cellular source that can be used to reprogram to

iPSCs and then differentiated into the target cell type, vastly improving our understanding of human cell biology.

One of the fields that has benefitted the most from iPSC-based reprogramming is human cellular neuroscience, as neural progenitor cells (NPCs) and their progeny can be readily generated from human iPSCs. iPSC differentiations have been used to produce a vast array of human neuronal cell types and have led to major discoveries in molecular neuroscience (Dolmetsch and Geschwind 2011). Neuronal reprogramming paradigms have aided in the development of the cellular disease modeling field, where cohorts of patients with genetic or sporadic neuropsychiatric disorders and healthy controls can be collected, their cells differentiated into neurons, and tested to determine the molecular basis of disease in these patients. This strategy has contributed to our understanding of many human diseases, including epilepsy, autism, and schizophrenia (Liu et al. 2012; Kiskinis et al. 2014; Yoon et al. 2014). As our understanding of genetic markers of human neuronal subtypes improves and the complexity of iPSC reprogramming models advances, we will have the capacity to produce more physiologically relevant tissues and circuits to study more complex brain systems to understand their function and intervene in cases of damage or disease.

Although iPSC-based paradigms have been instrumental in human cellular neuroscience, there are some limitations to the technology. Among these limitations is the erasure of the molecular age of the donor (Mertens et al. 2015b). During cellular reprogramming, iPSCs transit an embryo-like state, which is a highly selective process associated with complete epigenetic remodeling and immense cell proliferation. Consequently, iPSCs and their derivatives have been found to be largely rejuvenated (Horvath 2013). However, many human neurodegenerative diseases occur only in the elderly, and aging is by far the major risk factor for diseases like Alzheimer's and Parkinson's. Therefore, retaining the human aging component in afflicted cell types is essential for disease modeling and testing therapies.

To circumvent the age limitations of iPSCs, we have taken advantage of a more recent

reprogramming paradigm of direct transdifferentiation. Transdifferentiation involves the overexpression of transcription factors for the target cell type of interest to directly convert differentiated cells from one cell type to another without transitioning through a stem cell intermediary. With two pro-neuronal transcription factors and a small molecule cocktail of SMAD inhibitors, BMP inhibitors, and other enhancers human fibroblasts can be directly converted into mature neurons which faithfully maintain the age of their donor (Thomas Vierbuchen and Austin Ostermeier and Zhiping 2010; Mertens et al. 2015a). This technique has been used to identify age related phenotypes in human neurons and has advanced our understanding of Alzheimer's disease, ALS, and other neuronal aging phenotypes (Traxler et al. 2022; Meng-Lu Liu and Tong Zang and Chun-Li 2016; Christine 2016). However, one important limitation of this technique is the lower overall efficiency of the transdifferentiation process from fibroblasts compared to iPSCs.

To address these technical limitations, in the first chapter of this dissertation, I present a streamlined protocol for iN generation. I developed an all-in-one lentiviral system for the efficient delivery of NGN2 and ASCL1 for iN differentiation. I collected timeline RNAseq of iN conversion to identify pathways upregulated during iN differentiation and tested small molecules to increase the iN yield and boost the numbers of cells that can successfully convert to neurons. The results of this chapter constitute a state-of-the-art iN transdifferentiation protocol that can be used to generate aged-equivalent human neurons for molecular evaluation.

As noted above, the capacity to produce aged human neurons is of great importance for understanding neurodegenerative diseases, as aging is by far the largest risk factor for developing a myriad of neurodegenerative disorders. The most common age-related neurodegenerative disorder is Alzheimer's Disease (AD). Despite decades of research and billions of dollars of spending AD remains a condition with no viable pharmaceutical intervention. Indeed, in recent years there have been high profile failures in clinical trials and controversies over drugs coming to market without a demonstrated capacity to reduce or slow dementia in AD patients. Why has the AD field struggled while treatments of other aging diseases have greatly advanced over the

same period? One reason is the difficult nature of studying the aged human brain. Unlike conditions like cancer where the affected tissues can be biopsied and studied in the lab, only indirect measurements can be obtained from the aged human brain without an invasive surgery. Further, there are still fundamental gaps in our understanding of the pathogenesis of AD. AD is a largely sporadic disease, with familial early onset forms accounting for only 5% of all cases, yet many cellular and animal models rely on these rare mutations to induce disease-relevant phenotypes and, consequently, narrow the window of discovery for molecular mechanisms of the disease to a minority of cases. However, using iN technology, we now have the capability to compare age equivalent human neurons from sporadic or familial AD and healthy age-matched control patients to elucidate age-specific molecular mechanisms of disease in human cells.

In the second chapter, I use our improved iN protocol on a cohort of AD and healthy age matched control neurons to identify molecular phenotypes of AD in aged human neurons. Therein, I discovered a small population of neurons that enter into cellular senescence that were also present in the human brain. iNs from AD patients expressed more senescence related genes, had a senescence permission epigenome, and endogenously presented many molecular markers of senescence. Senescent neurons have impaired synaptic function and neuroinflammatory properties and could be an early source of inflammation in the pathogenesis of AD. Finally, I show that these cells can be targeted with senescence eliminating drugs, indicating that removal of senescent neurons could be a therapeutic avenue for AD.

References

Christine, J. Huh and Bo Zhang and Matheus B. Victor and Sonika Dahiya and Luis F. Z. Batista and Steve Horvath and Andrew S. Yoo. 2016. "Maintenance of Age in Human Neurons Generated by Microrna-Based Neuronal Conversion of Fibroblasts." *eLife* 5 (9 , pmid = 27644593 , publisher = eLife Sciences Publications Ltd). https://dx.doi.org/10.7554/eLife.18648.

Dolmetsch, R., and D. H. Geschwind. 2011. "The Human Brain in a Dish: The Promise of Ipsc-Derived Neurons." *Cell* 145, no. 6 (Jun 10): 831-4. https://dx.doi.org/10.1016/j.cell.2011.05.034.

GURDON, J. B. 1962. "The Developmental Capacity of Nuclei Taken from Intestinal Epithelium Cells of Feeding Tadpoles." *J Embryol Exp Morphol* 10 (Dec): 622-40.

Horvath, S. 2013. "Dna Methylation Age of Human Tissues and Cell Types." *Genome Biol* 14, no. 10: R115. https://dx.doi.org/10.1186/gb-2013-14-10-r115.

Kiskinis, E., J. Sandoe, L. A. Williams, G. L. Boulting, R. Moccia, B. J. Wainger, S. Han, T. Peng, S. Thams, S. Mikkilineni, C. Mellin, F. T. Merkle, B. N. Davis-Dusenbery, M. Ziller, D. Oakley, J. Ichida, S. Di Costanzo, N. Atwater, M. L. Maeder, M. J. Goodwin, J. Nemesh, R. E. Handsaker, D. Paull, S. Noggle, S. A. McCarroll, J. K. Joung, C. J. Woolf, R. H. Brown, and K. Eggan. 2014. "Pathways Disrupted in Human Als Motor Neurons Identified through Genetic Correction of Mutant Sod1." *Cell Stem Cell* 14, no. 6 (Jun 05): 781-95. https://dx.doi.org/10.1016/j.stem.2014.03.004.

Liu, G. H., J. Qu, K. Suzuki, E. Nivet, M. Li, N. Montserrat, F. Yi, X. Xu, S. Ruiz, W. Zhang, U. Wagner, A. Kim, B. Ren, Y. Li, A. Goebl, J. Kim, R. D. Soligalla, I. Dubova, J. Thompson, J. Yates, C. R. Esteban, I. Sancho-Martinez, and J. C. Izpisua Belmonte. 2012. "Progressive Degeneration of Human Neural Stem Cells Caused by Pathogenic Lrrk2." *Nature* 491, no. 7425 (Nov 22): 603-7. https://dx.doi.org/10.1038/nature11557.

Meng-Lu Liu and Tong Zang and Chun-Li, Zhang. 2016. "Direct Lineage Reprogramming Reveals Disease-Specific Phenotypes of Motor Neurons from Human Als Patients." *Cell reports* 14 (1): 115-128 , pmid = 26725112 , publisher = Elsevier. https://dx.doi.org/10.1016/j.celrep.2015.12.018.

Mertens, J., A. C. M. Paquola, M. Ku, E. Hatch, L. Bohnke, S. Ladjevardi, S. McGrath, B. Campbell, H. Lee, J. R. Herdy, J. T. Goncalves, T. Toda, Y. Kim, J. Winkler, J. Yao, M. W. Hetzer, and F. H. Gage. 2015a. "Directly Reprogrammed Human Neurons Retain Aging-Associated Transcriptomic Signatures and Reveal Age-Related Nucleocytoplasmic Defects." *Cell Stem Cell* 17, no. 6 (Dec 3): 705-718. https://dx.doi.org/10.1016/j.stem.2015.09.001.

Mertens, J., A. C. M. Paquola, M. Ku, E. Hatch, L. Böhnke, S. Ladjevardi, S. McGrath, B. Campbell, H. Lee, J. R. Herdy, J. T. Gonçalves, T. Toda, Y. Kim, J. Winkler, J. Yao, M. W. Hetzer, and F. H. Gage. 2015b. "Directly Reprogrammed Human Neurons Retain Aging-Associated Transcriptomic Signatures and Reveal Age-Related Nucleocytoplasmic Defects." *Cell Stem Cell* 17, no. 6 (Dec 03): 705-718. https://dx.doi.org/10.1016/j.stem.2015.09.001.

Takahashi, K., and S. Yamanaka. 2006. "Induction of Pluripotent Stem Cells from Mouse Embryonic and Adult Fibroblast Cultures by Defined Factors." *Cell* 126, no. 4 (Aug 25): 663-76. https://dx.doi.org/10.1016/j.cell.2006.07.024.

Thomas Vierbuchen and Austin Ostermeier and Zhiping, P. Pang and Yuko Kokubu and Thomas C. Südhof and Marius Wernig. 2010. "Direct Conversion of Fibroblasts to Functional Neurons by Defined Factors." *Nature* 463 (2): 1035-1041 , pmid = 20107439. https://dx.doi.org/10.1038/nature08797.

Traxler, L., J. R. Herdy, D. Stefanoni, S. Eichhorner, S. Pelucchi, A. Szücs, A. Santagostino, Y. Kim, R. K. Agarwal, J. C. M. Schlachetzki, C. K. Glass, J. Lagerwall, D. Galasko, F. H. Gage, A. D'Alessandro, and J. Mertens. 2022. "Warburg-Like Metabolic Transformation Underlies Neuronal Degeneration in Sporadic Alzheimer's Disease." *Cell Metab* 34, no. 9 (Sep 06): 1248-1263.e6. https://dx.doi.org/10.1016/j.cmet.2022.07.014.

Yoon, K. J., H. N. Nguyen, G. Ursini, F. Zhang, N. S. Kim, Z. Wen, G. Makri, D. Nauen, J. H. Shin, Y. Park, R. Chung, E. Pekle, C. Zhang, M. Towe, S. M. Hussaini, Y. Lee, D. Rujescu, D. St Clair, J. E. Kleinman, T. M. Hyde, G. Krauss, K. M. Christian, J. L. Rapoport, D. R. Weinberger, H. Song, and G. L. Ming. 2014. "Modeling a Genetic Risk for Schizophrenia in Ipscs and Mice Reveals Neural Stem Cell Deficits Associated with Adherens Junctions and Polarity." *Cell Stem Cell* 15, no. 1 (Jul 03): 79-91. https://dx.doi.org/10.1016/j.stem.2014.05.003.

CHAPTER 1: Chemical modulation of transcriptionally enriched signaling pathways to optimize the conversion of fibroblasts into neurons.

Abstract

Direct conversion of human somatic fibroblasts into induced neurons (iNs) allows for the generation of functional neurons while bypassing any stem cell intermediary stages. Although iN technology has an enormous potential for modeling age-related diseases, as well as therapeutic approaches, the technology faces limitations due to variable conversion efficiencies and a lack of thorough understanding of the signaling pathways directing iN conversion. Here, we introduce a new all-in-one inducible lentiviral system that simplifies fibroblast transgenesis for the two pioneer transcription factors, Ngn2 and Ascl1, and markedly improves iN yields. Further, our timeline RNA-Seq data across the course of conversion has identified signaling pathways that become transcriptionally enriched during iN conversion. Small molecular modulators were identified for four signaling pathways that reliably increase the yield of iNs. Taken together, these advances provide an improved toolkit for iN technology and new insight into the mechanisms influencing direct iN conversion.

Introduction

Human somatic cells such as skin fibroblasts can be directly converted into cultures of functional induced neurons (iNs) by the overexpression of pro-neuronal transcription factors (Zhiping 2011b; Stuart 2011). As opposed to induced pluripotent stem cell (iPSC) reprogramming and differentiation, direct iN conversion bypasses the pluripotent stage as well as any other stem cell-like stages and preserves epigenetic information of their donor's age, making it a particularly valuable tool to study aging and aging-related disorders(Jerome Mertens and Apuã 2015; Victor et al. 2018; Yu Tang and Meng-Lu Liu and Tong Zang and Chun-Li 2017). iN technology has also shown promise in vivo as a strategy to replace damaged cells following brain injury by direct conversion of non-neuronal cell types into neurons directly within the nervous system(Marisa Karow and Rodrigo Sánchez and Christian Schichor and Giacomo Masserdotti and Felipe Ortega

and Christophe Heinrich and Sergio Gascón and Muhammad 2012; Christophe Heinrich and Robert Blum and Sergio Gascón and Giacomo Masserdotti and Pratibha Tripathi and Rodrigo Sánchez and Steffen Tiedt and Timm Schroeder and Magdalena Götz and Benedikt 2010). Using combinations of pro-neuronal and region-/subtype-specific transcription factors, a variety of neuronal subtypes has been produced via direct conversion(Massimiliano Caiazzo and Maria Teresa Dell'Anno and Elena Dvoretskova and Dejan Lazarevic and Stefano Taverna and Damiana Leo and Tatyana 2011; Esther 2011; Matheus 2014; Vadodaria et al. 2016; Rachel Tsunemoto and Sohyon Lee and Attila Szűcs and Pavel Chubukov and Irina Sokolova and Joel 2018).

Because iN conversion lacks a proliferating stem cell intermediate, the iN numbers obtained are largely dependent on conversion efficiency; therefore, great efforts have been undertaken to improve iN process yields. The identification and the combination of Ngn2 with Ascl1 as two pro-neuronal pioneer transcription factors that can induce neuronal identity in non-neuronal cells have been key features in the advancement of this technology(Philipp Koch and Oliver, Brüstle 2012; Meng-Lu Liu and Tong Zang and Yuhua Zou and Joshua 2013; Jerome Mertens and Apuã 2015; Orly 2013; Derek 2016). The efficient delivery of Ngn2/Ascl1 into fibroblasts, and their robust, controllable transgene expression, left room for improvement and, because variations in the transduction and conversion efficiencies from different donors are common limitations, we have developed a new all-in-one lentiviral system for inducible Ngn2/Ascl1 expression called UNA.

Chemical modulation of several cellular signaling pathways has been shown to improve iN conversion and thus enable iN technology as a legitimate alternative to iPSC differentiation. Inhibition of TGF-b/SMAD signaling via blockade of AKT kinases, inhibition of GSK-3b signaling (Philipp Koch and Oliver, Brüstle 2012), adenylyl cyclase activation (Philipp Koch and Oliver, Brüstle 2012; Meng-Lu Liu and Tong Zang and Yuhua Zou and Joshua 2013; Sergio Gascón and Elisa Murenu and Giacomo Masserdotti and Felipe Ortega and Gianluca 2016), inhibition of REST

(Giacomo Masserdotti and Sébastien Gillotin and Bernd Sutor and Daniela Drechsel and Martin Irmler and Helle 2015; Jiang and Zhiqiang Cai and Hui Sun and Kang Zhang and Yi Zhang and Ju Chen and Xiang-Dong, Fu 2013), induction of canonical Bcl-2 signaling, and inhibition of lipid oxidation pathways via ferroptosis inhibition (Marisa Karow and Rodrigo Sánchez and Christian Schichor and Giacomo Masserdotti and Felipe Ortega and Christophe Heinrich and Sergio Gascón and Muhammad 2012) have all been shown to greatly promote iN conversion. However, because these known signaling pathway modulators have either been adopted from iPSC differentiation (Stuart 2009)(Chambers et al. 2009) or are the result of educated guessing or simply of trial-and-error experiments, no systematic efforts have been made to utilize broad and unbiased datasets to identify the pathways and corresponding modulators that orchestrate iN conversion. We sought to optimize the iN conversion media composition with small molecular pathway modulators to reach efficient iN conversion even in suboptimal human fibroblast lines. To that end, we have performed timeline RNAseq transcriptome analysis over the time course of direct iN conversion and have discovered four pathways that are instrumental in iN conversion. Based on these pathways, we identified four small molecules that could be combined into an improved iN conversion medium, ZPAK, which reliably boosted iN conversion of young and old fibroblasts into epigenetically age-equivalent iNs.

Materials and Methods

Direct Conversion of Human Fibroblasts into iNs

Primary human dermal fibroblasts from donors between 0 and 88 years of age were obtained from the Coriell Institute Cell Repository, the University Hospital in Erlangen and Shiley-Marcos Alzhiemer's Disease Research Center (Supplemental Table T1.1). Protocols were previously approved by the Salk Institute Institutional Review Board and informed consent was obtained from all subjects. Fibroblasts were cultured in DMEM containing 15% tetracycline-free fetal bovine serum and 0.1% NEAA (Thermo Fisher Scientific), transduced with lentiviral particles for EtO and XTP-Ngn2:2A:Ascl1 (E+N2A), or the combined tetOn system cassette consisting of the rtTAAdv.

[Clonech] driven by the UbC promoter, Ngn2:2A:Ascl1 under control of the TREtight promoter [Clontech], and a puromycin-resistance gene driven by the PGK promoter (UNA, Fig.1A) and expanded in the presence of G418 (200 µg/ml; Thermo Fisher Scientific) and puromycin (1 µg/ml; Sigma Aldrich), or puromycin only, respectively, as 'iN-ready' fibroblast cell lines. Following at least three passages after viral transduction, 'iN-ready' fibroblasts were trypsinized and pooled into high densities (30.000 – 50.000 cells per cm2 ; appx. a 2:1 – 3:1 split from a confluent culture) and, after 24h, the medium was changed to neuron conversion (NC) or NC+ZPAK medium based on DMEM:F12/Neurobasal (1:1) for three weeks. NC contains the following supplements: N2 supplement, B27 supplement (both 1x; Thermo Fisher Scientific), doxycycline (2 µg/ml, Sigma Aldrich), Laminin (1 µg/ml, Thermo Fisher Scientific Scientific), dibutyryl cyclic-AMP (500 µg/ml, Sigma Aldrich), human recombinant Noggin (150 ng/ml; Preprotech), LDN-193189 (5 µM; Fisher Scientific Co) and A83-1 (5 µM; Santa Cruz Biotechnology Inc.), CHIR99021 (3 µM, LC Laboratories), Forskolin (5 µM, LC Laboratories) and SB-431542 (10 µM; Cayman Chemicals). ZPAK contains the following supplements: Pyrintegrin (1 µM; Tocris), ZM336372 (.175 µM; Cayman), AZ960 (0.1 µM; Cayman), and KC7F2 (7.5 µM; Fischer Scientific). Medium was changed every third day. For further maturation up to six weeks, iNs were switched to BrainPhys (STEMCELL Technologies)-based neural maturation media (NM) containing N2, B27, GDNF, BDNF (both 20 ng/ml, R&D), dibutyryl cyclicAMP (500 µg/ml, Sigma Aldrich), doxycycline (2 µg/ml, Sigma-Aldrich) and laminin (1 µg/ml, Thermo Fisher Scientific). For maturation on astrocytes for morphological analysis and calcium imaging, iNs were carefully trypsinized during week 4 and replated on a feeder layer of mouse astrocytes and cultured in NM media containing 1% KOSR (Thermo Fisher Scientific).

Whole Transcriptome mRNA Sequencing and Methylation Array

Total bulk RNA was extracted from fibroblasts and converting iNs at all collected time points using Trizol LS reagent (Thermo Fischer). RNA integrity (RIN) numbers were assessed using the Agilent TapeStation before library preparation. RNA-Seq libraries were prepared using the

TruSeq Stranded mRNA Sample Prep Kit according to the manufacturer's instructions (Illumina). Libraries were sequenced single-end 50 bp using the Illumina HiSeq 2500 platform. Read trimming was performed using TrimGalore, read mapping was performed using STAR, raw counts were generated using HTseq variance stabilizing transformation normalization (vst) and differential expression analysis was performed in DEseq2. Pathway and network analysis was performed using Ingenuity Pathway Analysis (Qiagen) from FPKM normalized HTseq generated gene counts under the time course analysis module. Pathways with a Z-Score ≥ 3 (99% confidence interval) were considered for further study.

Total genomic DNA was extracted from bulk fibroblasts and flow cytometry sorted PSA-NCAM+ 21 day iNs as described below with the DNeasy Blood and Tissue Kit (Qiagen). DNA methylation assays were performed on the MethylationEPIC BeadChip as per the standard manufacturer's protocol (Illumina). Raw intensity idat files were processed and analyzed using the R packages ChAMP (Morris 2014) or Rnbeads (Assenov et al. 2014); arrays were normalized using the BMIQ procedure (Teschendorff et al. 2013).

Flow Cytometry Assessment of PSA-NCAM, ECAD/NCAD, Cell Proliferation, and Mitochondrial Membrane Polarization

For PSA-NCAM analysis, iNs were detached using TrypLE and stained for PSA-NCAM directly conjugated to PE (Miltenyl Biotec; 1:50) for 1h at 4 °C in sorting buffer (250 mM myo-inositol and 5 mg/ml polyvinyl alcohol, PVA, in PBS) containing 1% KOSR. Cells were washed and resuspended in sorting buffer containing EDTA and DNAse and filtered using a 40 µm cell strainer. For co-staining with NCAD and ECAD, cells were detached and prepared as above and stained for N-CAD:APC (Miltenyl Biotec, CD325, 1:20) and E-CAD:PE (Miltenyl Biotec, CD324, 1:11). To determine the effect of AZ960 on proliferation of fibroblast cell lines, the cellular divisions were quantified with the CellTrace CFSE proliferation assay (Thermo Fisher). 1.2 x 106 fibroblasts at full density on a single well of a six-well plate (9 cm2) were split into two 60-mm plates (21 cm2) and proliferated in DMEM containing 15% tetracycline-free fetal bovine serum and 0.1% NEAA

(Life Technologies), 2.5 µM of CellTrace CFSE proliferation dye (Invitrogen), and 0.1 µM AZ960 for 48h. Mitochondrial membrane potential was analyzed using the MitoProbe JC-1 assay kit (Thermo Fisher, M34152). In all cases analysis was conducted on the FACS Canto II platform.

Image collection and analysis

Cells were transferred to tissue culture-treated ibidi µ-slides for imaging. Cells were fixed with 4% PFA for 20 min at room temperature and washed 3 x 15 minutes with TBS, followed by a 1h block with TBS + 4% bovine serum albumin and 0.1% Triton X-100 (TBS++). Primary antibodies (Anti-NeuN, 1:200, EMD Millipore; Anti-ßIII-tubulin, 1:3000, Covance; Phalloidin CruzFluor 488 Conjugate, 1:1000, SCBT) were applied overnight at 4°C. After washing as described above, samples were incubated in 1:250 donkey anti-mouse, chicken, or rabbit secondary antibody for 2h at room temperature. Nuclear staining was done with DAPI (1/10,000; Sigma-Aldrich). After washing, slides were mounted in PVA-DAPCO (Sigma Aldrich). Confocal images were taken on Zeiss LSM780 or Zeiss AiryScan series confocal microscope. All data for one experiment were acquired from cells cultured and processed in parallel on the same microscope with the exact same setting reused. For analysis, 2-µm confocal sections through the nuclear layer were acquired from three confocal z stacks. Neurolucida software was used for manual tracing of entire neuronal processes, and data were analyzed using NeuroExplorer (MicroBrightField Inc). All tracings were performed in a blinded manner. For phalloidin staining, automatic thresholding in ImageJ was used to binarize the images and green fluorescence intensity was calculated minus background intensity. At least 50 different cells were analyzed in each experiment, and the mean +/- SEM optical density (OD) was then calculated.

Calcium Imaging

iNs converted in NC or NC+ZPAK were transduced with lentiviral particles for CAG-GCAMP5G and LV-hSyn-dsRed at 21 days of conversion and replated on astrocytes for maturation as described above. Calcium imaging were performed four weeks after plating on astrocytes. Imaging was performed in BrainPhys media (Stemcell Technologies) on a Yokogawa Cell

Voyager 1000 Spinning Disk Confocal Microscope. We only analyzed 10 cells per field that were hSyn-dsRed+ and exhibited neuron identity. Calcium responses were calculated as the change in fluorescence intensity (ΔF) over the initial fluorescence intensity (F-F0)/F0,in which F is the fluorescence at a given time point and F0 was calculated as the average of the first five inactive fluorescence measurements at the start of imaging. A non-response area for each recording was measured for background subtraction, and imaging bleach was corrected for using the ImageJ plugin Fiji (NIH, Bethesda, MD). The threshold for a positive calcium event was defined as local maxima when fluorescence response within a soma exceeded a value greater than three standard deviations above the mean.

SYBR qPCR

Bulk mRNA was extracted as described above, and 1 μg of RNA was then reverse transcribed using the Superscript III Reverse Transcriptase kit (Thermo Fisher). Quantitative differences in gene expression were determined by real-time qPCR using SYBR Green Master Mix (Bio-Rad) and a spectrofluorometric thermal cycler (CFX384, Bio-Rad). Values are presented as the ratio of target mRNA to GAPDH expression obtained for each time point and treatment. Primer sequences used are the following:

MNX1: GATGCCCGACTTCAACTCCC, GCCGCGACAGGTACTTGTT

MAP2: CTCAGCACCGCTAACAGAGG, CATTGGCGCTTCGGACAAG

CCND2:TTTGCCATGTACCCACCGTC, AGGGCATCACAAGTGAGCG

MYOG:GGGGAAAACTACCTGCCTGTC, AGGCGCTCGATGTACTGGAT

MEF2C:CTGGTGTAACACATCGACCTC, GATTGCCATACCCGTTCCCT

NCAM1:GTCCTGCTCCTGGTGGTTGT, TGACCGCAATGCACATGAA

NCAM2:GACGTGCCATCCAGTCCCTA, ATGGGAGTCCGGTTTGTTGA

CAMK2A:AACCTTGGCTCCAGCATGAA, AAGGGAGACAGGAGGCCTTG

GAPDH:TGCACCACCAACTGCTTAGC, GGCATGGACTGTGGTCATGAG

Western blot analysis

Cell lysates were prepared in Lysis buffer A (20 mM Tris pH 7.5, 100 mM NaCl, 1 mM EDTA, 2 mM EGTA, 50 mM β -glycerophosphate, 50 mM NaF, 1 mM sodium vanadate, 2 mM dithiothreitol, proteinase inhibitor cocktail (Roche) and 1% Triton X-100 and subjected to Western blot according to the standard procedures. The primary antibody used was rabbit mAb STAT3 (1:1000, Cell Signaling, 79D7, #4904).

Statistical Analysis

Statistical values for RNA-Seq and CpG methylation data were corrected for false discovery rates (FDR) using the Benjamini-Hochberg method implemented in R. Statistical tests of quantitative data were calculated using GraphPad Prism 7 software, with the method indicated for each figure. Significance evaluation are marked as *p<0.05; **p<0.01; ***p<0.005 and ****p<0.001.

Results

An optimized all-in-one viral system simplifies fibroblast transduction and increases conversion efficiency.

Lentiviral delivery of pro-neuronal transcription factors is the most widely used technique for direct iN conversion due to its outstanding efficiency and relative ease to use (Louise 2015). Successful strategies involve the use of constitutive or inducible expression of either only a single pioneer factor, such as Ngn2 or Ascl1 (Meng-Lu Liu and Tong Zang and Yuhua Zou and Joshua 2013; Derek 2016), a combination of a pioneer factor with secondary factors (Zhiping 2011a; Thomas Vierbuchen and Austin Ostermeier and Zhiping 2010), a combination of a pioneer factor with subtype-specifying transcription factors (Massimiliano Caiazzo and Maria Teresa Dell'Anno and Elena Dvoretskova and Dejan Lazarevic and Stefano Taverna and Damiana Leo and Tatyana 2011; Meng-Lu Liu and Tong Zang and Chun-Li 2016; Vadodaria, et al. 2016; Rachel Tsunemoto and Sohyon Lee and Attila Szűcs and Pavel Chubukov and Irina Sokolova and Joel 2018), or the use of two coupled pioneer factors (Philipp Koch and Oliver, Brüstle 2012; Jerome Mertens and Apuã 2015). Typically, these factors are distributed across several lentiviral vectors; however, given that lentiviral transduction is not 100% efficient and because an individual fibroblast must

be transduced with two or more viruses to survive chemical selection and successfully reprogram, this strategy left room for improvement. To eliminate the need for co-infection, we combined the tetOn system cassette consisting of the rtTAAdv. [Clonech] driven by the UbC promoter, the iN cassette consisting of Ngn2:2A:Ascl1 under control of the TREtight promoter [Clontech], and a puromycin-resistance gene driven by the PGK promoter to yield the UNA construct (Fig1.1A, Sup Fig S1.4). To test the efficiency of UNA compared to our conventional two-vector system (EtO+N2A), we selected fibroblasts from three individual donors that had not yielded optimal iN conversion efficiencies in the past (Fig1.1B and Suppl. Table T1.1). Dermal fibroblasts were transduced with similar titers of either EtO+N2A or UNA, selected by puromycin or puromycin/G418, respectively, and converted to iNs using our previously described conversion medium (NC) containing noggin as well as the small molecules CHIR-99021 (GSK3ß inhibitor), SB-431542, LDN-193189, A-83-01 (ALK inhibitors), forskolin, and db-cAMP (cAMP increase) (Mertens et al. 2015; Philipp Koch and Oliver, Brüstle 2012). Following three weeks of conversion, cells were live-stained for the neural surface marker PSA-NCAM, which stains reprogrammed iNs but not fibroblasts (Fig1.1C). Flow cytometry revealed that UNA-derived iNs exhibited significantly more PSA-NCAM-positive cells than E+N2A, boosting efficiencies by up to 90-100% for the two suboptimal fibroblast lines, but also increasing efficiencies of the lines that already converted well by 30±8% (Fig1.1D-E). In addition, immunocytochemical co-staining for the neuronal markers ßIII-tubulin and NeuN revealed that UNA iNs were on average twice as likely to be positive for NeuN or ßIII-tubulin (Fig1.1F-H). Based on these experiments, we reasoned that the use of the single all-in-one lentiviral vector UNA was notably easier and less prone to experimental error, as well as significantly more efficient in generating larger numbers of mature iNs compared to a multiple vector strategy.

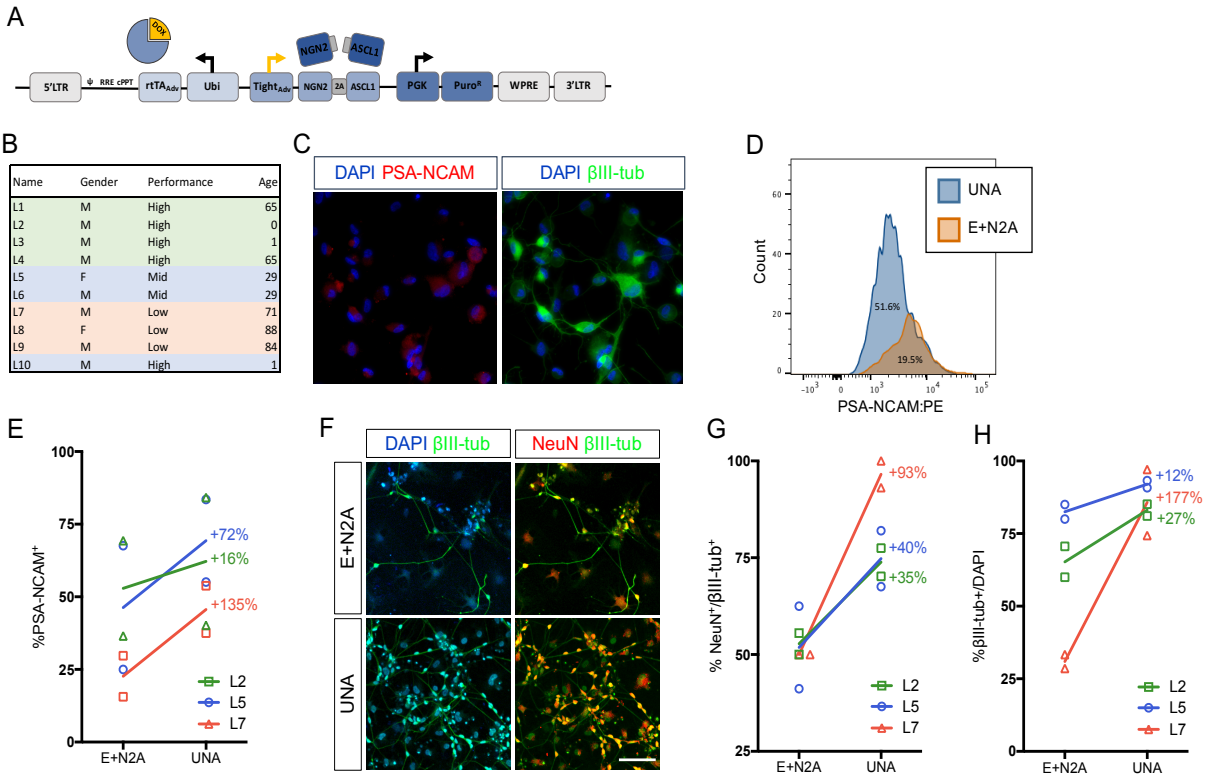

Figure 1.1. An optimized all-in-one viral system simplifies fibroblast transduction and increases conversion efficiency. A. Schematic of all-in-one lentiviral system for inducible overexpression of N2A for iN conversion. **B.** Cell lines of varying conversion efficiencies used for comparison **C.** Immunocytochemical analysis of iNs following three weeks of conversion, stained with βIII-tubulin, PSA-NCAM, and DAPI. The scale bar represents 20 μm. **D.** Flow cytometry histogram plots of PSA-NCAM:PE-stained iNs following 3 weeks of conversion with UNA (blue) or E:N2A (Orange) lentiviral systems. **E.** Comparison of % PSA-NCAM:PE+ cells from three 3 lines (L2,L5,L7) reprogrammed with E+N2A or UNA (3 biological and 2 technical replicates). **F.** Immunocytochemical analysis of E:N2A or UNA iNs following three 3 weeks of conversion, stained with βIII-tubulin, NeuN, and DAPI. Scale bar represents 100 μm. **G-H** Quantification of immunocytochemical staining in **F**. (3 biological and 2 technical replicates).

Time based RNAseq identifies signaling pathways directing iN conversion.

As pathways influential in controlling the direct conversion process continue to be found, we decided to investigate the transcriptional dynamics during reprogramming to identify the pathways that orchestrate iN conversion. We gathered RNAseq data from bulk fibroblasts as well as cells undergoing conversion for 1, 2, 3, 6, 18, and 24 days (Line 10, Fig1.2A). Using the Ingenuity Pathway Analysis software tool (IPA; Qiagen Inc.), we identified more than 500 pathways called to be significantly transcriptionally enriched or depleted (-2 > Z-Score > 2) as conversion proceeded (Suppl. Table T1.2); of these, we selected 10 of the most enriched pathways for further experimental testing (Suppl. Table T1.3). Based on the regulated genes and overlap of the called pathways, we selected one small molecule activator and one inhibitor for each of the 10 pathways, with the strategy of initiating diametrically opposing regulation of a given pathway. Each of the 20 compounds had been previously reported to be effective in tissue culture (Suppl. Table T1.3). Preference was given to molecules that targeted an intersection of two or more called pathways rather than specifically targeting the canonical signaling cascade of one pathway. When screening for PSA-NCAM-positive cells by flow cytometry following 21 days in NC plus the respective compound, four compounds were found to significantly ($P < .05$) increase the frequency of PSA-NCAM-positive iNs (Fig1.2C-E and Suppl. Fig. S1.1 and Suppl. Table T1.3). Interestingly, the compound that acted in the opposite direction decreased iN conversion efficiency (Fig1.2C-D and Suppl. Fig. S1.1 and Suppl. Table T1.3). These four conversion booster compounds were Pyrintegrin (PY; Integrin activator), AZ960 (AZ; Jak2 inhibitor), ZM336372, (ZM; Raf-1 activator), and KC7F2 (KC; HIF1α inhibitor) (Fig1.2C). The iNs derived in NC plus any of these four compounds resulted in a significant ($P < .01$) increase in the number of NeuN- and ßIII-tubulin-positive cells compared to those derived in NC medium alone (Fig1.2F-H, Suppl. Fig S1.5). Importantly, the combination of all four compounds (ZPAK) resulted in an even higher iN yield than any of the compounds individually (Suppl. Fig S1.10). This combination of all four molecules with the NC medium will henceforth be referred to as ZPAK.

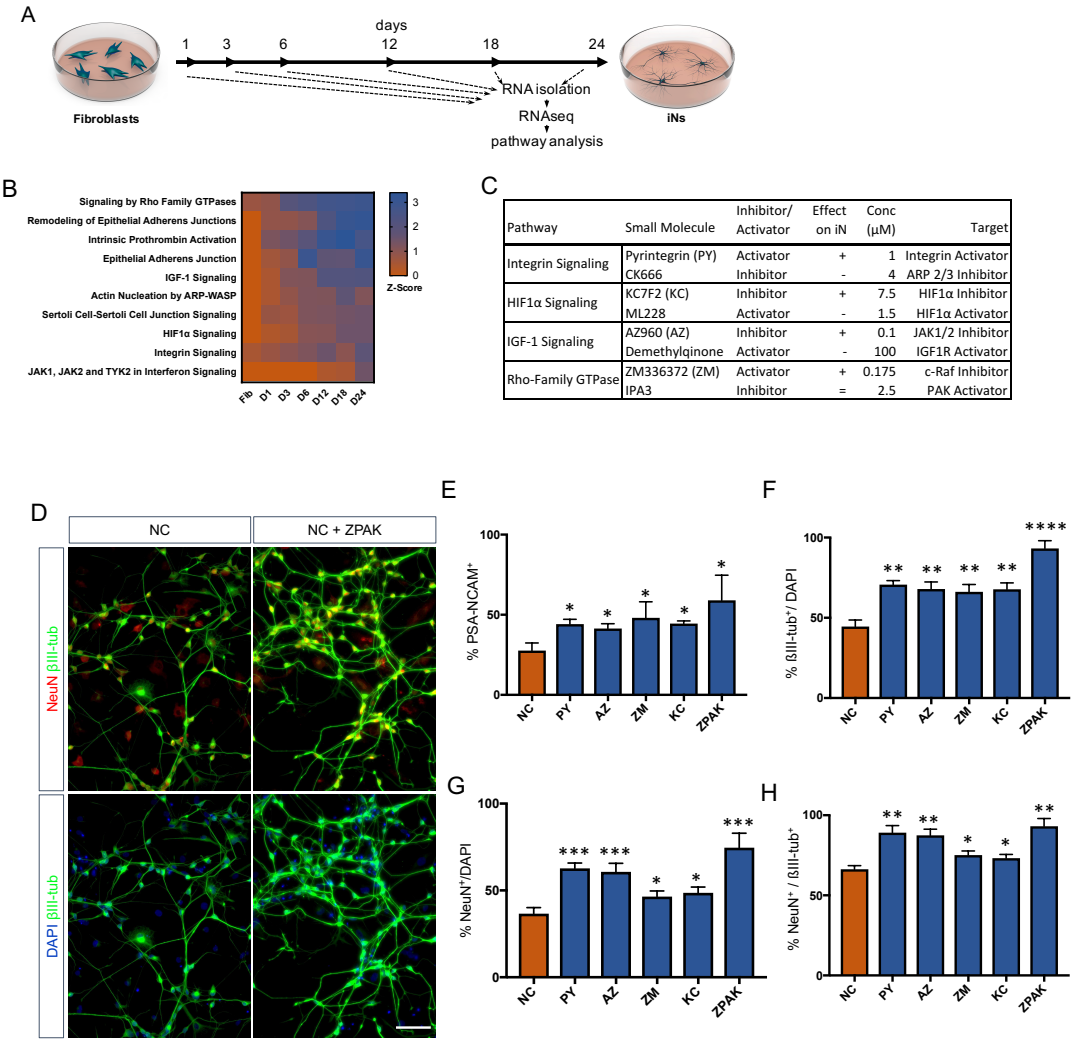

Pathway	Small Molecule	Inhibitor/ Activator	Effect on iN	Conc (μM)	Target
Integrin Signaling	Pyrintegrin (PY)	Activator	+	1	Integrin Activator
	CK666	Inhibitor	-	4	ARP 2/3 Inhibitor
HIF1α Signaling	KC7F2 (KC)	Inhibitor	+	7.5	HIF1α Inhibitor
	ML228	Activator	-	1.5	HIF1α Activator
IGF-1 Signaling	AZ960 (AZ)	Inhibitor	+	0.1	JAK1/2 Inhibitor
	Demethylqinone	Activator	-	100	IGF1R Activator
Rho-Family GTPase	ZM336372 (ZM)	Activator	+	0.175	c-Raf Inhibitor
	IPA3	Inhibitor	=	2.5	PAK Activator

Figure 1.2. Time-based RNAseq identifies signaling pathways influential during iN conversion. A. Schematic for timeline of RNA isolation during neuronal reprogramming of L10 **B.** Activation Z-Score of the indicated signaling pathway as called by IPA Comparison Analysis during neuronal reprogramming. Z-Scores represent a statistical measure of the match between the expected relationship direction and observed gene expression of a given pathway, with z-scores >2 considered significant. **C.** Description of small molecules selected to inhibit or activate branches of pathways identified in **B.** Effect on iN conversion is based on increased % PSA-NCAM+ cells by flow cytometry, with + indicating increased PSA-NCAM %, - reduced PSA-NCAM %, and = no effect on PSA-NCAM %. **D.** Immunocytochemical analysis of neural markers in NC or NC+ZPAK iNs (L1, L5, L9) following three weeks of conversion, stained with βIII-tubulin, NeuN, and DAPI. Scale bar represents 100 μm. Representative image from L1. **E.** flow cytometry quantification of %PSA-NCAM+ cells in iNs (L1, L5, L9) converted in NC and NC+ ZPAK supplements. **F-H.** Quantification of immunocytochemical staining in **D**. Results are shown as mean ± SEM. * $P < 0.05$; ** $P < 0.01$; *** $P < 0.001$; **** $P < 0.0001$, $n = 3$ biological replicates. Significance values were calculated by t test.

ZPAK induces a defined neuronal transcription that more closely relates to the adult brain transcriptome than NC alone.

To investigate the changes induced on the transcriptional level by the ZPAK cocktail, we again performed time series RNAseq from fibroblasts from three donors that were converted to iNs in NC or NC+ZPAK for 5, 10, 15, and 20 days (Fig1.3A; three biological replicates from four time points, 24 samples total). Comparing FPKM normalized gene counts for the conversion process for both conditions, we detected that the transcriptomes induced by NC or NC+ZPAK were highly correlated, with a Pearson correlation coefficient of ≥.85 for all sampled time points (Fig1.3C), indicating broad transcriptional similarities between the iN process in NC and NC+ZPAK. Comparing the top 100 upregulated and top 100 downregulated genes for the conversion process for both conditions, we detected an 80% and 93% overlap, respectively (Fig1.3B). Consistently, glutamatergic neuron-specific genes Unc-13 homolog A (UNC13A), AMPA receptor auxiliary protein 2 (CNIH2), NMDA1 (GRIN1), GluK5 (GRIK5), GluK2 (GRIK2) and vGLUT1 (SLC17A7), and the GABAergic neuron-specific genes phospholipase C like 2 (PLCL2), dopamine receptor D2 (DRD2), cannabinoid receptor 1 (CNR1) and glutamate decarboxylase 1 (GAD1) were found to be generally expressed at similar levels in NC and NC+ZPAK at 20 days of conversion (Fig1.3D, Suppl. Fig S1.9). Markers of dopaminergic, serotonergic, and cholinergic lineages were not consistent in expression and were not commonly observed in D20 iNs (Fig1.3D, Suppl. Fig S1.7). We next performed differential expression analysis between all NC and NC+ZPAK time points, revealing 143 genes that were significantly differentially expressed (Suppl. Table T1.4, padj <.05). Hierarchical clustering demonstrated a clear separation of NC and NC+ZPAK groups except for two NK samples at the earliest point of conversion (Fig1.3E). These significant transcriptional differences point to a more defined neuronal transcriptome initiated in NC+ZPAK compared to NC. Interestingly, we observed consistently increased expression of neuron-specific genes NCAM1/2 (Neural Cell Adhesion), MNX1 (Neural Homeobox), MAP2 (Neural Microtubule Protein), and CAMK2 (Central Nervous

System Kinase) in NC+ZPAK but lower expression levels of cyclins such as CCND2 (Cyclin D2) as well as the myogenic factors MEF2 (Myocyte Enhancer Factor) and MYOG (Myogenin), which are known to limit fibroblast to neuronal reprogramming, in NC+ZPAK (Fig1.3F, Suppl. Fig S1.8, Suppl. Fig S1.11).

Next, gene ontology (GO) enrichment analysis revealed that genes upregulated in NC (log2FC>1) were only enriched for three neuronal GO terms - GO:0034220 Ion transmembrane transport, GO:0006811 ion transport, and GO:0099537 Trans-synaptic signaling - whereas GO terms enriched in genes upregulated in NC+ZPAK included many GO terms categorized for neural development (GO:0021953 Central Nervous System Neuron Differentiation, GO:0007272/0008366 Ensheathement of Neurons/Axons, GO:0021700 Developmental Maturation), synapse development (GO:0007416 Synapse Assembly, GO:0050808 Synapse Organization, GO:0007268 Chemical Synaptic Transmission), neural activity (GO:0001964 Startle Response), and membrane potential maintenance (GO:0006811,0098660,0006811 Regulation of Ion Transport, Inorganic Ion Transport, Ion Transport)(Fig1.3G, Suppl. Fig S1.9)(Fran Supek and Matko Bošnjak and Nives Škunca and Tomislav 2011). When comparing the average and median expression of the genes in these GO terms, we observed consistent upregulation in NC+ZPAK (Suppl. Fig S1.9). These data indicate that NC+ZPAK yields iNs with a more defined and probably more human brain-like transcriptional profile. To assess neuronal enrichment in a threshold-free manner, and to quantify overlap of expression with adult brain, we employed the rank-rank hypergeometric overlap (RRHO) test(Seema 2010). Briefly, this method generates a map of the transcriptional overlap between any two systems by comparing two ranked lists of differentially expressed genes. We applied this method to compare the overlap of NC versus NC-ZPAK to fibroblast versus adult brain (Allen Institute) to evaluate the extent to which either condition more closely resembled adult brain gene expression. Using RRHO, we observed a pronounced bias in the overlap of NC-ZPAK with adult brain, indicating that, relative to NC, NC-ZPAK iNs were indeed more similar to brain expression patterns (Fig1.3H). To make

a direct comparison of the functional maturity of NC to NC+ZPAK iNs, we performed calcium imaging of NC and NC+ZPAK iNs, revealing that NC+ZPAK iNs have more spontaneous calcium transients than iNs cultured in NC alone (Suppl. Fig S1.6). As calcium transients have been established as a reliable readout of neural activity in vitro, this direct comparison between NC and NC+ZPAK iNs provides further evidence that ZPAK is producing a more mature and defined neuronal state (Spitzer 2011). Taken together, these data indicate that NC-ZPAK iNs possess a transcriptional profile more closely resembling that of mature neurons and that the original fibroblast transcriptional program, as well as other non-neuronal directions, were substantially reduced or absent.

To gain a better understanding of how each of the four pathway modulators improves iN conversion, we sought to obtain a more detailed understanding of the individual processes influenced by ZM, PY, AZ, and KC.

Figure 1.3. ZPAK induces a more defined neuronal transcription that more closely relates to the adult brain transcriptome. A. Schematic for timeline RNA isolation during neuronal reprogramming of L2, L5, & L7 at fibroblast and 5, 10, 15, and 20 days of conversion **B.** Heatmap of FPKM normalized counts of the top 100 correlating (+) and top 100 inverse correlating (-) genes (FPKM ≥ 1) for day 5, 10, 15 and 20 of neuronal reprogramming with NC or NC+ZPAK. Orange = low expression, blue = high expression **C.** Correlate R values of FPKM normalized counts from 25,610 genes during neuronal reprogramming with NC or NC+ZPAK cocktail. **D.** Heatmap showing relative expression of the glutamatergic neuron-specific genes Unc-13 homolog A (UNC13A), AMPA receptor auxiliary protein 2 (CNIH2),NMDA1 (GRIN1), GluK5 (GRIK5), GluK2 (GRIK2) and vGLUT1 (SLC17A7), GABAergic neuron-specific genes phospholipase C like 2 (PLCL2), dopamine receptor D2 (DRD2), cannabinoid receptor 1 (CNR1) and glutamate decarboxylase 1 (GAD1), Serotonergic neuron-specific genes ETS transcription factor (FEV), serotonin transporter 1 (SLC6A4), and tryptophan hydroxylase (TPH1), Dopaminergic neuron-specific genes tyrosine hydroxylase (TH), dopamine transporter 1 (SLC6A3), forkhead box A2 (FOXA2), potassium voltage-gated channel subfamily J member 6 (KCNJ6), nuclear receptor subfamily 4 group A member 2(NR4A2), and LIM homeobox transcription factor 1 beta (LMX1B), and cholinergic neuron-specific genes vesicular acetylcholine transporter (SLC18A3), and choline O-acetyltransferase (ChAT); normalized by row. **E.** Heatmap of 143 significantly (*p-adj* < 0.05) differentially expressed genes between NC and NC+ZPAK at 5, 10, 15 and 20 days of reprogramming (*n* = 3). **F.** FPKM normalized counts of five representative neuron specification genes - Neural Cell Adhesion Molecule 2 (NCAM2), Neural Cell Adhesion Molecule 1 (NCAM1), Motor Neuron and Pancreas Homeobox 1 (MNX1), Microtubule-associated Protein 2 (MAP2), Calcium/Calmodulin Dependent Protein Kinase II (CAMK2) - and three representative fibroblast-to-iN limiting genes - Cyclin D2 (CCND2), Myogenin (MYOG), and Myocyte enhancer factor-2 (MEF2) - over time during fibroblast-to-iN conversion with NC (orange) or NC+ZPAK (blue). **G.** Gene ontology (GO) enrichment analysis of genes upregulated in NC or NC+ZPAK ($log_2FC>1$). Results are shown as REVIGO (Supek et al., 2011) scatterplots in which similar GO terms are grouped in arbitrary two-dimensional space based on semantic similarity. Each circle indicates a specific GO term and circle sizes are indicative of how many genes are included in each term, where larger circles indicate greater numbers of genes that are included in that GO term. Colors indicate the level of significance of enrichment of the GO term by log_{10} p-value. **H.** Rank-rank hypergeometric overlap (RRHO) map (Plaisier et al. 2010) comparing the gene expression differences between NC and NC+ZPAK to expression differences between matched fibroblasts and adult human brain (Allen Brainspan). Each pixel represents overlap between NC or NC+ZPAK to fibroblast or adult brain transcriptome, color-coded according to the $-log_{10}$p value of a hypergeometric test (step size = 100). On the map, the extent of shared genes upregulated in NC+ZPAK and adult brain is displayed in the top right corner, whereas the shared genes upregulated in NC and fibroblasts are displayed in the bottom left corner (see schematic in Supp Fig S2).

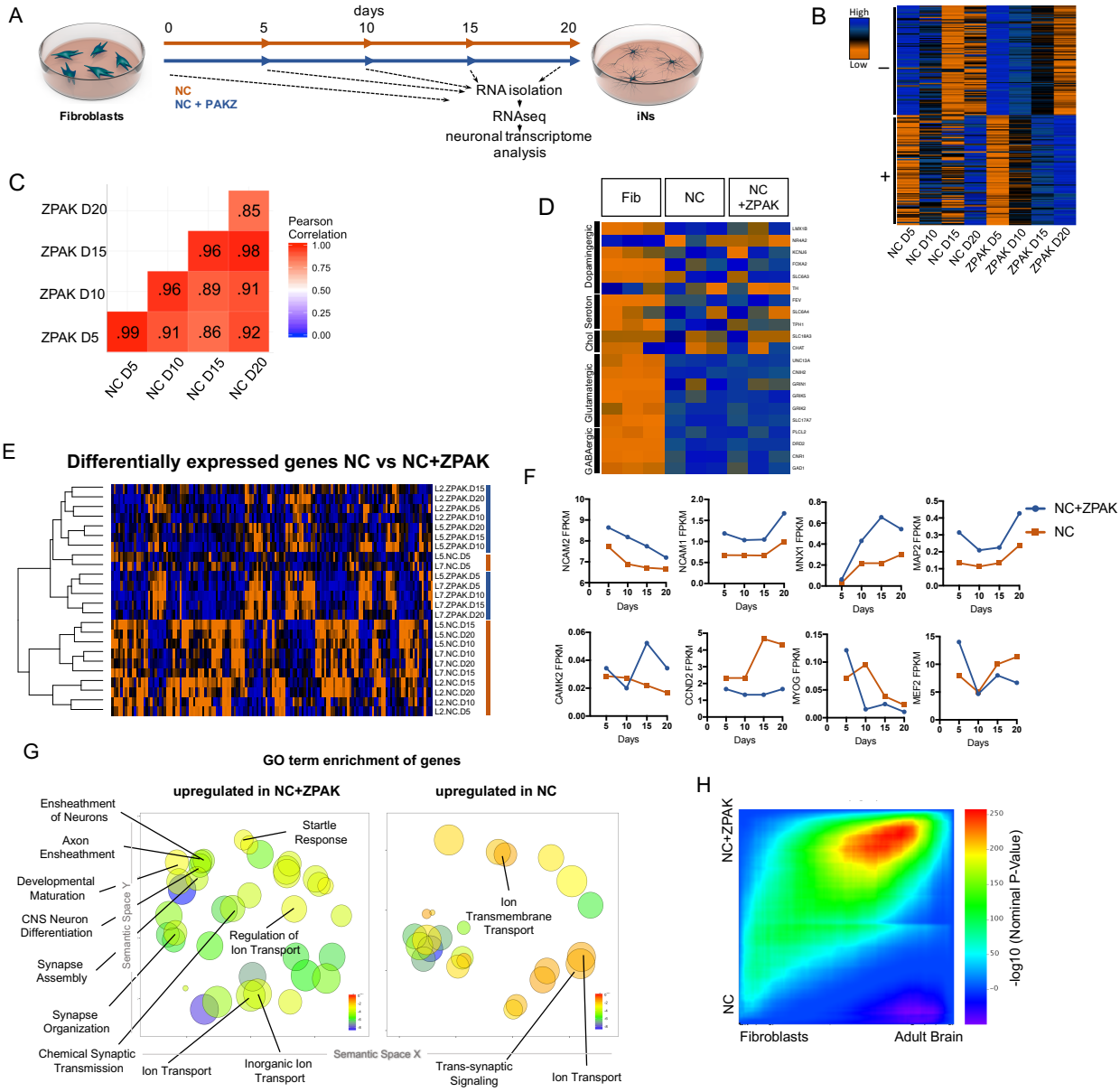
A
days
0
5
10
15
20
Fibroblasts
NC
NC + PAKZ
RNA isolation
RNAseq
neuronal transcriptome analysis
iNs
B
High
Low
NC D5
NC D10
NC D15
NC D20
ZPAK D5
ZPAK D10
ZPAK D15
ZPAK D20
C
ZPAK D20
ZPAK D15
ZPAK D10
ZPAK D5
.85
.96 .98
.96 .89 .91
.99 .91 .86 .92
Pearson Correlation
1.00
0.75
0.50
0.25
0.00
D
Fib
NC
NC +ZPAK
Dopaminergic
Chol Seroton
Glutamatergic
GABAergic
E
Differentially expressed genes NC vs NC+ZPAK
F
NC+ZPAK
NC
NCAM2 FPKM
NCAM1 FPKM
MNX1 FPKM
MAP2 FPKM
CAMK2 FPKM
CCND2 FPKM
MYOG FPKM
MEF2 FPKM
Days
G
GO term enrichment of genes
upregulated in NC+ZPAK
upregulated in NC
Ensheathment of Neurons
Axon Ensheathment
Developmental Maturation
CNS Neuron Differentiation
Synapse Assembly
Synapse Organization
Chemical Synaptic Transmission
Startle Response
Regulation of Ion Transport
Ion Transport
Inorganic Ion Transport
Semantic Space Y
Semantic Space X
Ion Transmembrane Transport
Trans-synaptic Signaling
Ion Transport
H
NC+ZPAK
NC
Fibroblasts
Adult Brain
-log10 (Nominal P-Value)

Inhibition of JAK2 removes fibroblasts from the cell cycle and promotes mesenchymal-to-epithelial transition (MET).

Removal of fibroblasts from the cell cycle has been reported to improve neuronal reprogramming (Houbo Jiang and Zhimin Xu and Ping Zhong and Yong Ren and Gaoyang Liang and Haley 2015; Meng-Lu Liu and Tong Zang and Yuhua Zou and Joshua 2013). Based on the enrichment of the IGF-1 signaling and the specific transcriptional footprint called by the IPA software, we selected the JAK2 inhibitor AZ as a promising and well-characterized inhibitor, because IGF1/IGF1R is known to enhance cell cycle entry of fibroblasts (DiCicco-Bloom 2009; Sean 2016) and signals through the JAK2 substrate STAT3 (Ailian Xiong and Zhengduo Yang and Yicheng Shen and Jia Zhou and Qiang 2014; Kitamura 1999; Ying Zhang and Rik 1999) (Fig1.4A). We therefore asked whether AZ removed fibroblasts from the cell cycle to enable direct conversion. As expected, Western blot analysis for STAT3 revealed that converting fibroblasts cultured in NC showed a decrease in STAT3 within the first six days of conversion, and the addition of AZ strongly promoted this decrease (Fig1.4B). Using carboxyfluorescein succinimidyl ester (CFSE) to examine cell divisions by flow cytometry, we consistently detected that fibroblasts cultured with 0.1 μM AZ or ZPAK went through significantly fewer divisions than fibroblasts cultured in control medium (Fig1.4C,D). Importantly, flow cytometry for DAPI staining did not detect elevated toxicity in AZ-treated cells. Change in the cell phenotype from multipolar mesenchymal cells to polarized epithelial cells is an important developmental process known as the mesenchymal-epithelial transition (MET) (Christine 2007). MET machinery plays an important role during direct conversion of fibroblasts to neurons (Feng and Fuhui Wang and Xiao Zhang and Yiping Guo and Duanqing Pei and Hui, Zheng 2017), and p-STAT3 dimers directly promote epithelial-to-mesenchymal transition (EMT)-related gene expression (Michael 2014). Perturbations in STAT3 signaling have been linked to MET (Chuan-hai Zhang and Feng-Lin Guo and Ge-Liang Xu and Wei-Dong Jia and Yong-Sheng 2014; Laloraya 2014). Therefore, we monitored the E-Cadherin to N-Cadherin switch during iN conversion in NC and in NC+AZ (and

2004; Samy Lamouille and Jian Xu and Rik 2014) and found that AZ induced a more rapid switch towards E-Cadherin (Fig1.4D), a switch that is a classic hallmark of MET (Elena Scarpa and Andrá 2015; Xiaoju Zhang and Guangzhi Liu and Yi Kang and Zhaogang Dong and Qiyu Qian and Xitao 2013).

Activation of Integrin and Rho signaling promotes neuronal complexity.

The morphological changes a fibroblast has to undergo to transform into a neuron are substantial, and we have observed a pronounced increase in neuronal complexity in ZPAK compared to NC (Fig1.2B). To determine which ZPAK molecules primarily facilitate these structural modifications, we used ßIII-tubulin-based tracing and scoring to assess the neuronal complexities of iN cultures derived in NC containing either PY, ZM, AZ, or KC; we found that both PY and ZM produced significantly increased complexity scores (Fig1.4E-F). Interestingly, PY was shown previously to promote integrin β1 stability and signaling of human pluripotent stem cells (Yue Xu and Xiuwen Zhu and Heung Sik Hahm and Wanguo Wei and Ergeng Hao and Alberto Hayek and Sheng 2010), and we reasoned that PY also enhanced integrin-dependent attachment to extracellular matrices of iNs, thereby promoting neurite outgrowth and interactions (Fig1.4G). Based on the fact that ZM is a Raf-1 activator, we reasoned that the structural complexity increase in NC+ZM was associated with increased F-actin activity (Fig1.4G). Thus, we stained fibroblasts cultured with ZM or PY for 48 hours with fluorescent phalloidin, which revealed a marked increase in phalloidin signal by ZM and also a significant increase by PY (Fig1.4H-I). These results are consistent with the reported roles of Raf-1 activation and actin polymerizations in organizing cytoskeletal shape and neuronal morphology (Karin Ehrenreiter and Daniela Piazzolla and Vanishree Velamoor and Izabela Sobczak and 2005; Yi-Ping 2012; Miquel Bosch and Jorge Castro and Takeo Saneyoshi and Hitomi Matsuno and Mriganka Sur and Yasunori 2014), and they suggest that ZM and PY promote morphological rearrangements that occur during direct neuronal reprogramming by different but overlapping means.

Inhibition of HIF1α signaling promotes oxidative phosphorylation in iNs.

Consistent with our timeline transcriptome data, the transcription factor HIF1α has been reported to be one of the top downregulated factors during direct neuronal conversion from a variety of originating cell types (Mohammad Reza Omrani and Moein Yaqubi and Abdulshakour 2018). Increased oxidative phosphorylation is a hallmark of neuronal identity, and glycolysis has been reported to limit neural reprogramming in many protocols (Xinde Zheng and Leah Boyer and Mingji Jin and Jerome Mertens and Yongsung Kim and Li Ma and Li Ma and Michael Hamm and Fred 2016; Sergio Gascón and Elisa Murenu and Giacomo Masserdotti and Felipe Ortega and Gianluca 2016; Mak 2016). As HIF1α is a major inhibitor of oxidative phosphorylation (OXPHOS) and a mediator of glycolysis, we hypothesized that KC, a HIF1α inhibitor, improved iN conversion by facilitating OXPHOS (Fig1.4J). Using the JC1 dye, a cationic dye that accumulates in energized mitochondria with high membrane potentials(Chen 1991), we found that cultures at one, two and three weeks of conversion had higher mitochondrial membrane potentials in the presence of KC at all time points and significantly higher mitochondrial membrane potentials by week three (Fig1.4K, Suppl. Fig S1.3). These data are consistent with a HIF1α blockade initiated by KC promoting the metabolic switch towards OXPHOS that is necessary for iN conversion.

Figure 1.4. Cellular mechanisms influenced by ZPAK-mediated reprogramming. A. Schematic diagram of AZ targeting confluence of IGF1R and JAK2 signaling pathways. **B.** Western blot analysis of protein levels of STAT3 assessed at one, three, and six days in L6 fibroblast media containing PY, ZM, AZ or control media. **C.** CFSE stained L1, L5, and L8 fibroblasts cultured with control, AZ-containing medium, or ZPAK-containing medium for 48 hours after plating at 50% confluency. Boxes indicate percentages of cells that have undergone at least one cellular division. **D.** Quantification of % dividing cell reduction in ZPAK from C. Results are shown as mean ± SD. n = 3, ** $P < 0.01$. Significance values were calculated by t-test. **E.** Two color flow cytometry analysis of E-cadherin (E-Cad) and N-cadherin (N-Cad) expression in L10 and L6 fibroblast-to-iN conversion in NC or NC+AZ. Increasing ratios of E-Cad/N-Cad are indicative of the mesenchymal-to-epithelial switch. **F.** Representative Neurolucida reconstruction of L1 reprogrammed for 21 days in NC or NC+ZPAK medium. Scale bar 100 μm **G.** Neurolucida complexity scores of iNs derived from NC or NC + ZPAK components. Complexity scores were normalized to cell number by counterstaining with DAPI to count cell bodies. Results are shown as mean ± SD. n = 3, * $P < 0.05$. **H.** Schematic diagram of PY and ZM interaction with cytoskeletal dynamics. **I.** L1 fibroblasts cultured for 48h with ZM, PY, or CTL medium labeled for F-Actin with FITC Phallodidin and nuclei with DAPI. Scale bar 20 μm. **J.** Integrated signal density of FITC phalloidin stain from H. Signal density was normalized to cell numbers by DAPI. Results are shown as mean ± SEM. n = 3, *** $P < 0.001$. **K.** Schematic diagram of KC targeting HIF1α to inhibit glycolysis and promote oxidative phosphorylation (OXPHOS). **L.** Mitochondria in L10, L4, & L2 iNs cultured for 21 days in NC or NC+KC stained with JC-1 and measured for membrane depolarization by flow cytometry. Increased ratios of aggregate (PE) to diffuse (FITC) JC-1 are indicative of increased mitochondrial membrane potential. Results are shown as mean ± SD. n = 3. Significance values were calculated by t-test.

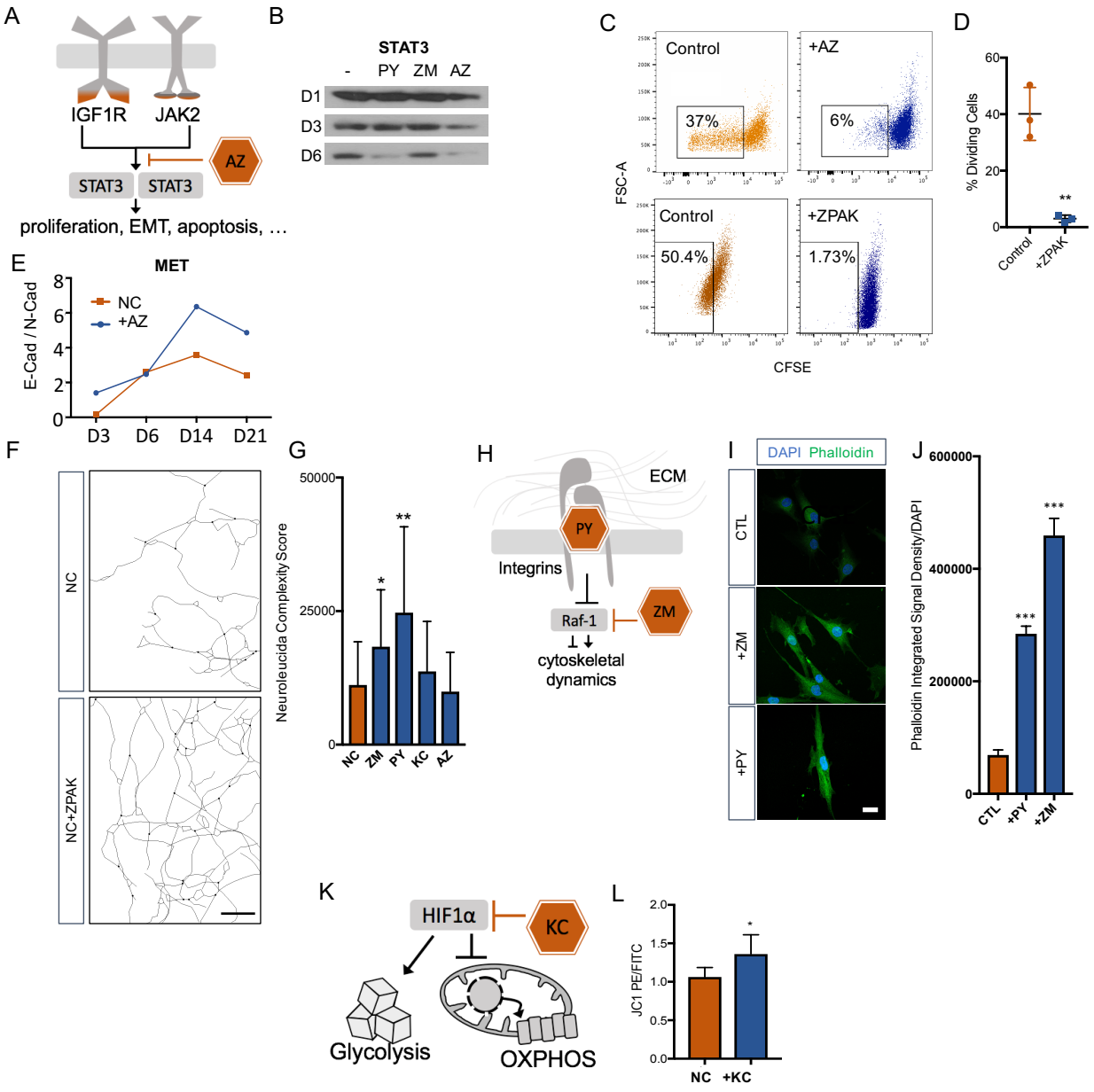
A
IGF1R
JAK2
AZ
STAT3
STAT3
proliferation, EMT, apoptosis, …
B
STAT3
- PY ZM AZ
D1
D3
D6
C
Control
+AZ
37%
6%
Control
+ZPAK
50.4%
1.73%
FSC-A
CFSE
D
% Dividing Cells
Control
+ZPAK
E
MET
E-Cad / N-Cad
NC
+AZ
D3 D6 D14 D21
F
NC
NC+ZPAK
G
Neuroleucida Complexity Score
NC ZM PY KC AZ
H
ECM
PY
Integrins
Raf-1
ZM
cytoskeletal dynamics
I
DAPI Phalloidin
CTL
+ZM
+PY
J
Phalloidin Integrated Signal Density/DAPI
CTL +PY +ZM
K
HIF1α
KC
Glycolysis
OXPHOS
L
JC1 PE/FITC
NC +KC

Epigenetic signatures of donor age are preserved in ZPAK-derived iNs.

One unique characteristic of direct iN conversion compared to iPSC reprogramming and subsequent neuronal differentiation is the retention of the cellular marks of aging (Jerome Mertens and Apuã 2015; Yu Tang and Meng-Lu Liu and Tong Zang and Chun-Li 2017; Victor, et al. 2018; Meng-Lu Liu and Tong Zang and Chun-Li 2016). As our additional ZPAK pathway modulators might impact the cellular age of the derived iNs, we sought to verify that ZPAK did not affect the epigenetic age of derived iNs based on age-dependent DNA methylation (Meaghan 2015). Similar to other global aging features, age-dependent DNA methylation of CpGs has been shown to be preserved in iNs (Huh et al. 2016) and reverts to a predicted prenatal age even in iPSCs from donors older then 90 years of age (Valentina Lo Sardo and William Ferguson and Galina 2016). We quantified CpG methylation for 850,000 sites for two young (0 and 1 years), two middle age (both 29 years), and two old (71 and 87 years) purified iN cultures in NC+ZPAK, as well as one young (1 year) and one old (87 years) unconverted fibroblast culture. Based on the top 5,000 differentially methylated regions identified using ChAMP (Tiffany 2014) we observed a clear difference between young and old donors, with middle-age donors showing an intermediate age-dependent CpG methylation pattern (Fig1.5A). Most importantly, the methylation patterns of the young and old NC+ZPAK iNs were largely unchanged compared to their parental fibroblasts (Fig1.5A). To apportion the majority of the variation, principal component analysis (PCA) based on all 850,000 CpGs consistently clearly separated the samples with respect to their age as the strongest component (Fig1.5B). Taken together, these results indicate that age-dependent DNA methylation patterns are maintained during ZPAK-assisted iN conversion and that NC+PAKZ is suitable to efficiently generate human neuronal models that recapitulate age-associated epigenetic changes.

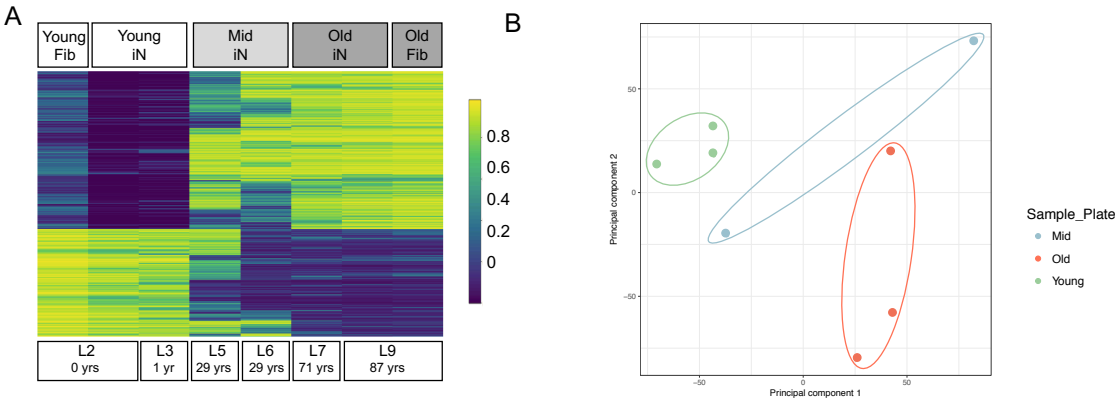

Figure 1.5. Epigenetic signatures of donor age are preserved in ZPAK-derived iNs. A. Heat map showing the top 5,000 significantly (padj < 0.05) differentially methylated CpGs between iNs generated by NC+ZPAK from two young (0, 1 years), two middle age (29 years), and two old (71, 87 years) donors, and one young and one old untreated fibroblast (0, 87 years, respectively). Each line represents a single probe. High methylation levels are shown in yellow, low methylation is shown in blue. Methylation of one young and one old paired, unconverted fibroblast is shown next to its iN counterpart. **B.** Principal Component Analysis (PCA) of the methylation profiles of two young iNs, one young fibroblast, two middle age iNs, two old iNs, and one old fibroblast cell line. All iNs were reprogrammed with NC+ZPAK medium. Plot shows principal component 1 and principal component 2 for each sample. Samples closer to each other in principal component space are similar in their methylation profiles.

Discussion

Significant gaps remain in our understanding of the mechanisms influencing neuronal specification during direct reprogramming. Consequently, iN yields from current protocols are often paltry, necessitating large numbers of converting cells to get sufficient successfully reprogrammed iNs for experimental analysis. Further, improvements to these protocols are largely based on trial and error, with few predictive tools available. In this study, we leveraged RNAseq data to uncover several key molecular events that can be targeted with small molecules to improve iN yield. These modifications, combined with our streamlined lentiviral system, provide a state-of-the-art improvement in current iN direct reprogramming protocols and shed insight into mechanisms driving neuronal specification during reprogramming.

Efficiently overcoming competing cellular programs has long been a challenge in the somatic reprogramming field. Here, we report that ZPAK causes a more thorough elimination of competing fibroblast programs on the transcriptional level than classic medium, as represented by both upregulation of neuron-specific genes and, importantly, downregulation of myogenic and fibroblast-specific genes known to limit neuronal specification during late reprogramming. These transcriptional changes are accompanied by other important phenotypes associated with neuronal fate, including removal of cells from the cell cycle, increased mitochondrial membrane potential, increased GCAMP activity, and enhanced mesenchymal to epithelial plasticity. There has also been an increased recognition of the important role of cytoskeleton remodeling during somatic cell reprogramming (Kumi Sakurai and Indrani Talukdar and Veena 2014; Jun Guo and Yuexiu Wang and Frederick Sachs and Fanjie 2014). Neurons have elaborate cytoskeleton structures that are highly specialized and critical for proper function. As the morphological changes from a fibroblast to a neuron are substantial, we were interested to discover that two of our compound modifications, ZM and PY, were associated with increased neuronal morphological complexity in addition to increasing iN yield. This phenotype was accompanied by an increase in F-Actin activity, a potent component of cellular plasticity. Cytoskeleton remodeling is associated

with sheer stress, and the actin cytoskeleton can sense and respond to these stresses with apoptotic signals. Therefore, we propose that the inclusion of ZM and PY in direct neuronal reprogramming could promote cytoskeleton reorganization and spare converting fibroblasts from mechanical stress-induced apoptosis. Our findings illustrate the important contribution actin structure makes during reprogramming and suggests that increased cellular structural plasticity could be a fruitful strategy for improving neuronal lineage commitment during reprogramming.

Classic direct conversion protocols, which we and others have used to differentiate fibroblasts to mature human neurons, are highly inefficient and fail to successfully reprogram the majority of input cells. Additionally, a significant heterogeneity exists in the reprogrammed pool, with many cells existing in a state that is not quite fibroblast, not quite neuron. Although many relevant phenotypes have been found between patient and control neuronal cultures reprogrammed in currently used media, we predict that new phenotypes might be revealed from studying neurons in conditions that more thoroughly commit fibroblasts to neuronal fate specification and, in turn, might lead to the discovery of more effective treatments for neurological disorders. Further, as iNs have shown promise in cell replacement therapies, we propose that using culture conditions that completely commit fibroblasts to the neuronal lineage will result in an increased therapeutic potential of iNs for possible neuronal replacement. Importantly, ZPAK improves iN yields even at very late fibroblast passages that could be required to produce therapeutic numbers of cells (Suppl. Fig S1.12). Although 100% efficiency in establishing neuronal specification remains elusive, the development of new neuronal reprogramming techniques, such as UNA and ZPAK media, takes us one step closer to this goal.

Chapter 1, in full, is a reprint of the material as it appears in: Joseph Herdy, Simon Schafer, Yongsung Kim, Zoya Ansari, Dina Zangwill, Manching Ku, Apua Paquola, Hyungjun Lee, Jerome Mertens, Fred H Gage (2019) Chemical modulation of transcriptionally enriched signaling pathways to optimize the conversion of fibroblasts into neurons eLife 8:e41356

https://doi.org/10.7554/eLife.41356. The dissertation author was the primary investigator and author of this paper.

Supplemental Table T1.1: Human fibroblasts used in this study.

Age (yr)	ID	Full Name	Sex	Fibroblast Source	Fibroblast RNAseq/ MethylCHIP Passage
65	L1	14096	M	ADRC	NA
0	L2	BJ CRL-2522	M	Coriell	p13
1	L3	AG08498	M	Coriell	p16
65	L4	8150	M	ADRC	NA
29	L5	ERF1	F	Erlangen	p14
29	L6	AG04054	M	Coriell	p12
71	L7	UKERfO3H-X-	M	Erlangen	p11
88	L8	3158LG	M	ADRC	NA
84	L9	3383	M	ADRC	p17
1	L10	AG08498	M	Coriell	p9

Supplemental Table T1.3: Expanded small molecule information.

Chemical (Abbreviation)	Pathway	Inhibitor/Activator	Effect on iN	IC50 (uM)	Supplier	Reference
Pyrintegrin (PY)	Integrin Signaling	Activator	+	2	Tocris	Xu, Yue et al. (2010)
CK666 (CK)	Integrin Signaling	Inhibitor	-	4	Sigma	Burke, Thomas A., et al. (2014)
PamCSK4 (PM)	JAK1, JAK2 and TYK2 Interferon Sig	Activator	-	12	Tocris	Manukyan, Maria, et al. (2005)
Pf3758309 (PF)	JAK1, JAK2 and TYK2 Interferon Sig	Inhibitor	+	0.0187	Cayman	Murray, Brion W., et al. (2010)
SU6656 (SU)	Epithelial Adherens Junction	Inhibitor	-	0.28	Cayman	Woodcock, Simon A., (2009)
Angiotensin II (AN)	Epithelial Adherens Junction	Activator	=	0.0015	Tocris	Suzuki, Yusuke, et al. (2003)
KC7F2 (KC)	HIF1α Signaling	Inhibitor	+	15	Tocris	Narita, Takuhito, et al. (2009)
ML228 (ML)	HIF1α Signaling	Activator	-	1.5	Tocris	Theriault, Jimmy R., (2012)
Demethylasterriquinone B1 (DM)	IGF-1 Signaling	Activator	-	100	Sigma	Webster, Nicholas JG, Kaapjoo Park, and Michael C. Pirrung. (2003)
AZ960 (AZ)	IGF-1 Signaling	Inhibitor	+	0.002	Cayman	Gozgit, Joseph M., (2008)
Ehop-016 (EH)	Actin Nucleation by ARP-WASP	Inhibitor	-	1.1	Selleckchem	Montalvo-Ortiz, Brenda L., et al. (2012)
PI3 Kinase act (PI)	Actin Nucleation by ARP-WASP	Activator	+	0.65	SC Biotech	Noh, Min Young, et al. (2013)
IPA3 (IP)	Rho-Family GTPase	Inhibitor	=	2.5	Tocris	Murakoshi, Hideji, Hong Wang, and Ryohei Yasuda. (2011)
ZM336372 (ZM)	Rho-Family GTPase	Activator	+	0.07	Tocris	Van Gompel, Jamie J., et al. (2005)
pkg inhibitor (PK)	Sertoli Junction Signaling	Activator	-	86	Cayman	Wexler, Eric M., Patric K. Stanton, and Scott Nawy. (1998)
U46619 (U4)	Sertoli Junction Signaling	Inhibitor	-	0.032	Cayman	Reese, Jeff, et al. wall. (2009)
syk inhbitor (SY)	Remodeling of Epithelial Adherens	Inhibitor	=	0.005	Cayman	Lai, Justine YQ, et al. (2003)
NSC87877 (NS)	Remodeling of Epithelial Adherens	Activator	-	0.355	Cayman	Song, Mina, et al. (2009)
dabigatram (DB)	Intrinsic Prothrombin Activation	Inhibitor	=	0.0045	Cayman	Ebner, Thomas, Klaus Wagner, and Wolfgang Wienen. (2010)
Thrombin TRAP6 (TR)	Intrinsic Prothrombin Activation	Activator	-	0.8	Tocris	Rudroff, Claudia, et al. (1998)

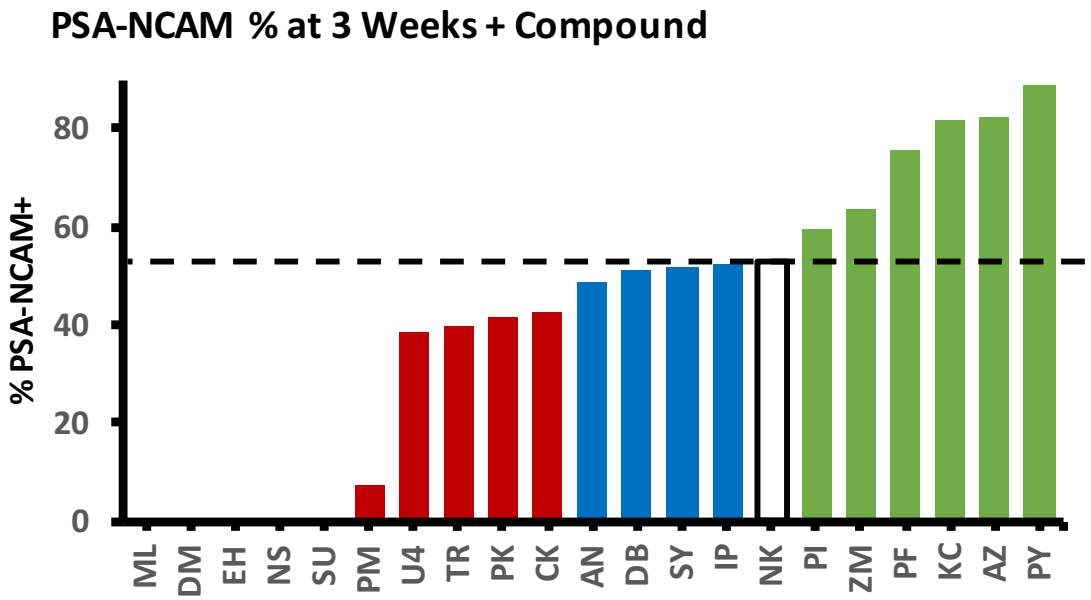

Supplemental Figure S1.1. Effect of screened small molecules on %PSA-NCAM yield of iNs. Dashed line represents NC (NK) control. Molecules with a score of 0 were lethal during direct conversion.

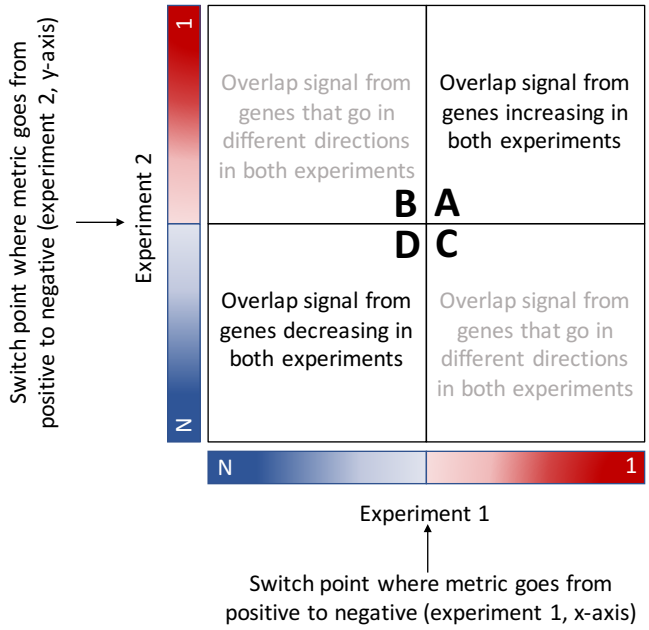

Supplemental Figure S1.2. RRHO schematic adapted from RRHO User Guide (Plaisier et al. 2010)

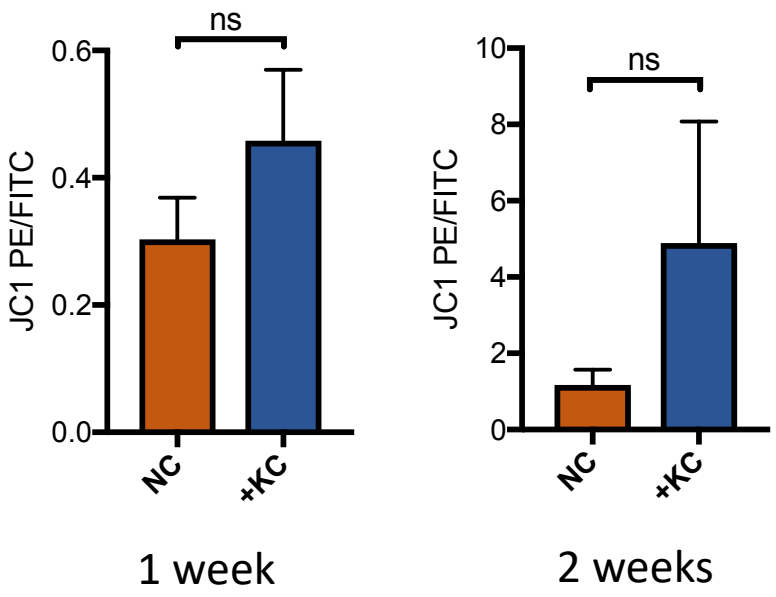

Supplemental Figure S1.3. Mitochondria in L10, L4, & L2 iNs cultured for one or two weeks in NC or NC+KC, stained with JC-1 and measured for membrane depolarization by flow cytometry. Increased ratios of aggregate (PE) to diffuse (FITC) JC-1 are indicative of increased mitochondrial membrane potential. Results are shown as mean ±

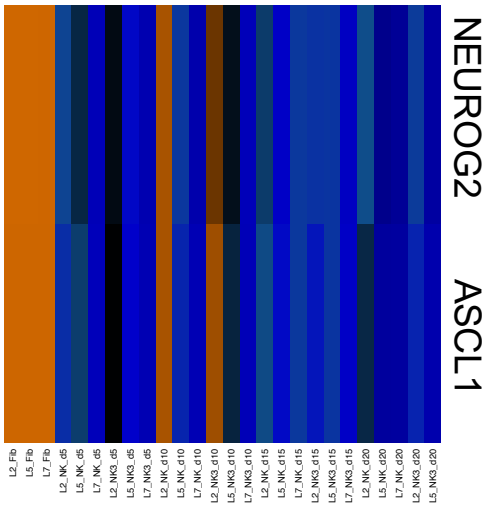

Supplemental Figure S1.4. Heatmap of FPKM normalized counts of Neurog2 and Ascl1. Dox-induced expression of Neurog2 and Ascl1 was maintained for all 20 days of conversion with NC and NC+ZPAK.

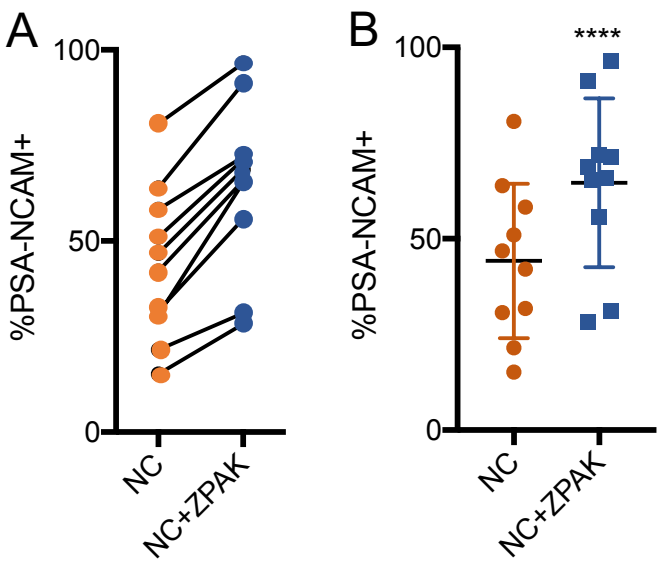

Supplemental Figure S1.5: % yield of PSA-NCAM+ iNs from all 10 lines used in this study. **A.** % change of PSA-NCAM+ cells for all lines converted in NC or NC+ZPAK. **B.** Dot plot demonstrating significantly increased PSA-NCAM+ cell yield with NC+ZPAK. Results are shown as mean ± SD. *n* = 10, ****p<0.00.1. Significance values were calculated by paired t-test.

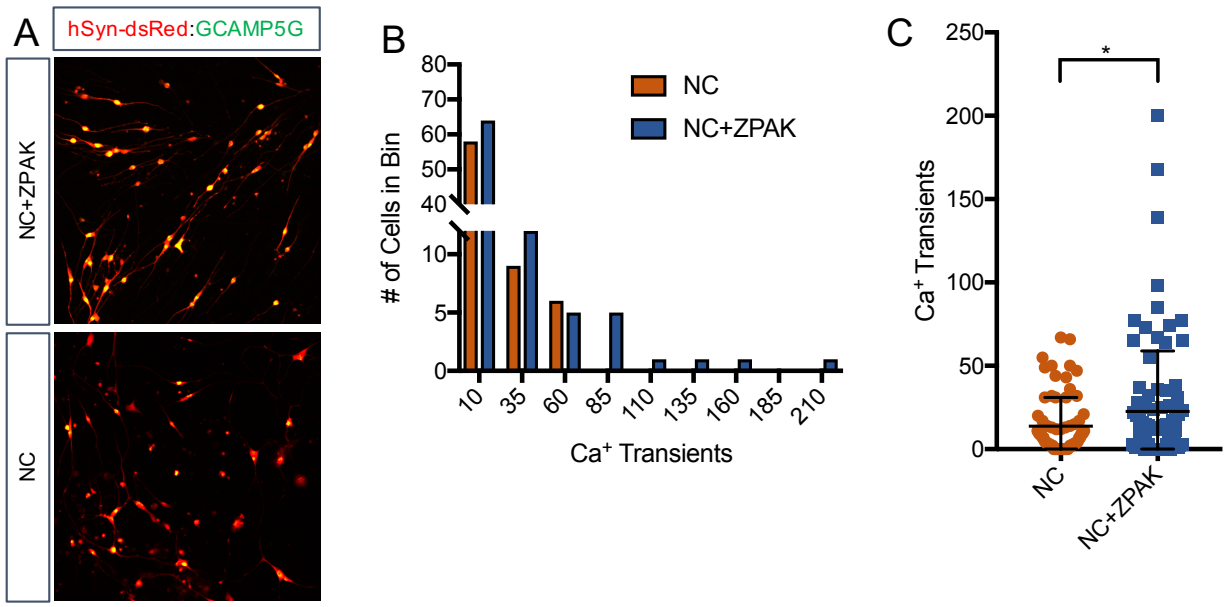

Supplemental Figure S1.6. Calcium imaging reveals increased spontaneous activity in NC+ZPAK iNs. **A.** Representative image of iNs cultured with NC or NC+ZPAK and transduced with lentiviral particles for GCAMP5G or hSyn-dsRed. Ten areas of overlap in yellow per field with coexpression of hSyn and GCAMP were considered for calcium activity. **B.** Histogram of number of calcium transients in four cell lines (L4, L2, L9, L8) converted in NC or NC+ZPAK. At almost all levels of spontaneous activity, there are more active ZPAK iNs compared to NC alone. Additionally, the most active neurons we observed were converted in NC+ZPAK. **C.** Comparison of the activity of all cells (n=160) quantified in this experiment shows a significantly increased level of spontaneous activity in NC+ZPAK iNs. Results are shown as mean ± SD. * $P < 0.05$. Significance values were calculated by t-test.

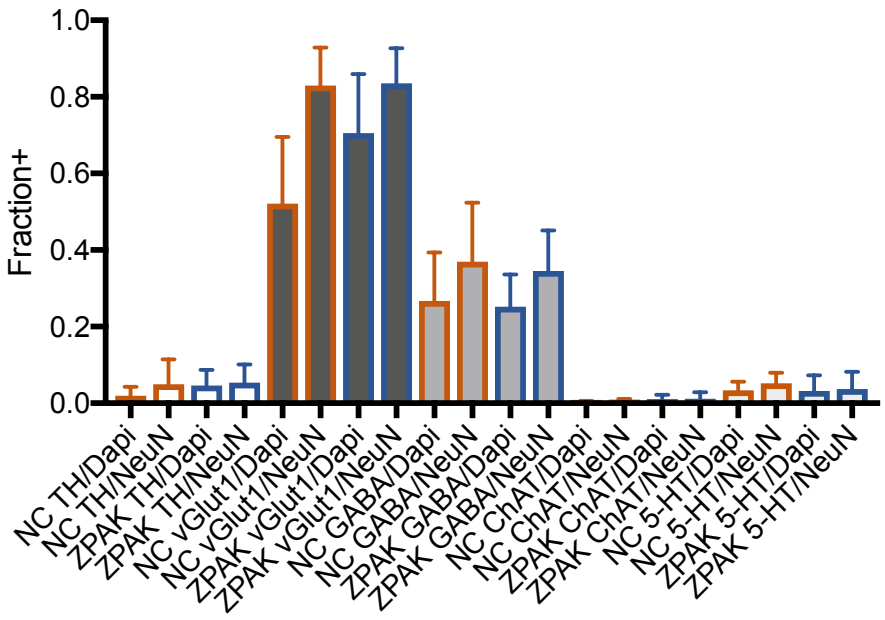

Supplemental Figure S1.7: Immunocytochemical quantification of neuron subtype markers TH (Dopamingeric), vGlut1 (Glutamatergic), GABA (GABAergic), ChAT (Cholinergic), and 5-HT (Serotonergic) in NC and NC+ZPAK iNs.

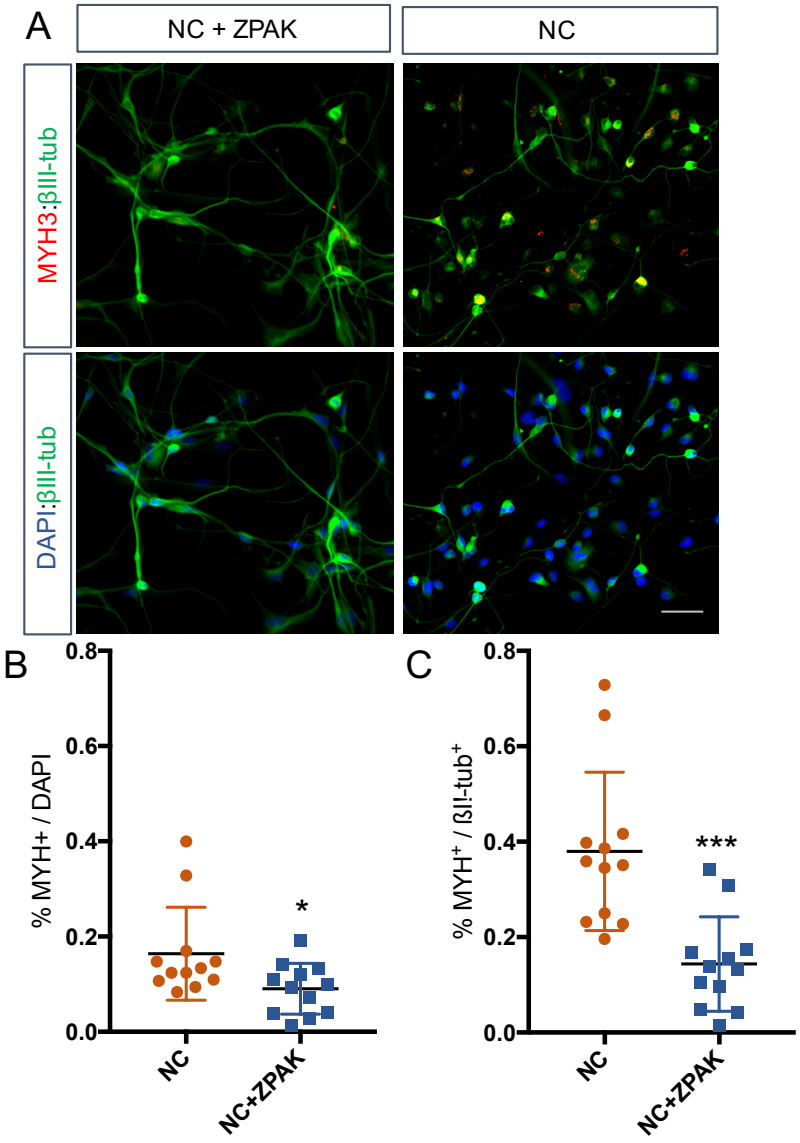

Supplemental Figure S1.8. Immunocytochemical analysis of MYH3 expression in L1, L4 and L8 NC and NC+ZPAK iNs. **A.** Representative image of MYH3 staining in NC and NC+ZPAK iNs. Scale bar represents 100 µm. **B.** Quantification of MYH3-positive cells per dapi-positive nuclei. **C.** Quantification of MYH3-positive cells per βIII-tub-positive cells. Results are shown as mean ± SD. * $P < 0.05$, *** $P < 0.001$.

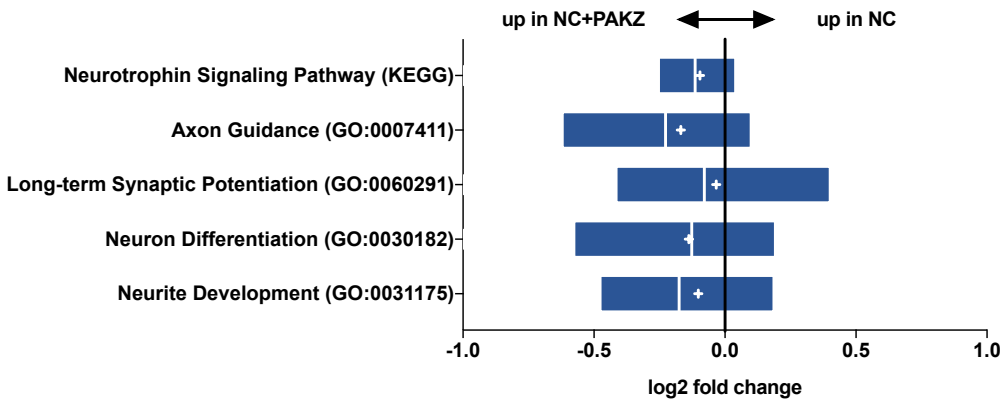

Supplemental Figure S1.9. Gene set expression analysis. Predefined and validated gene sets from GO and KEGG for neuron function show enrichment in mean and median expression in NC+ZPAK over NC.

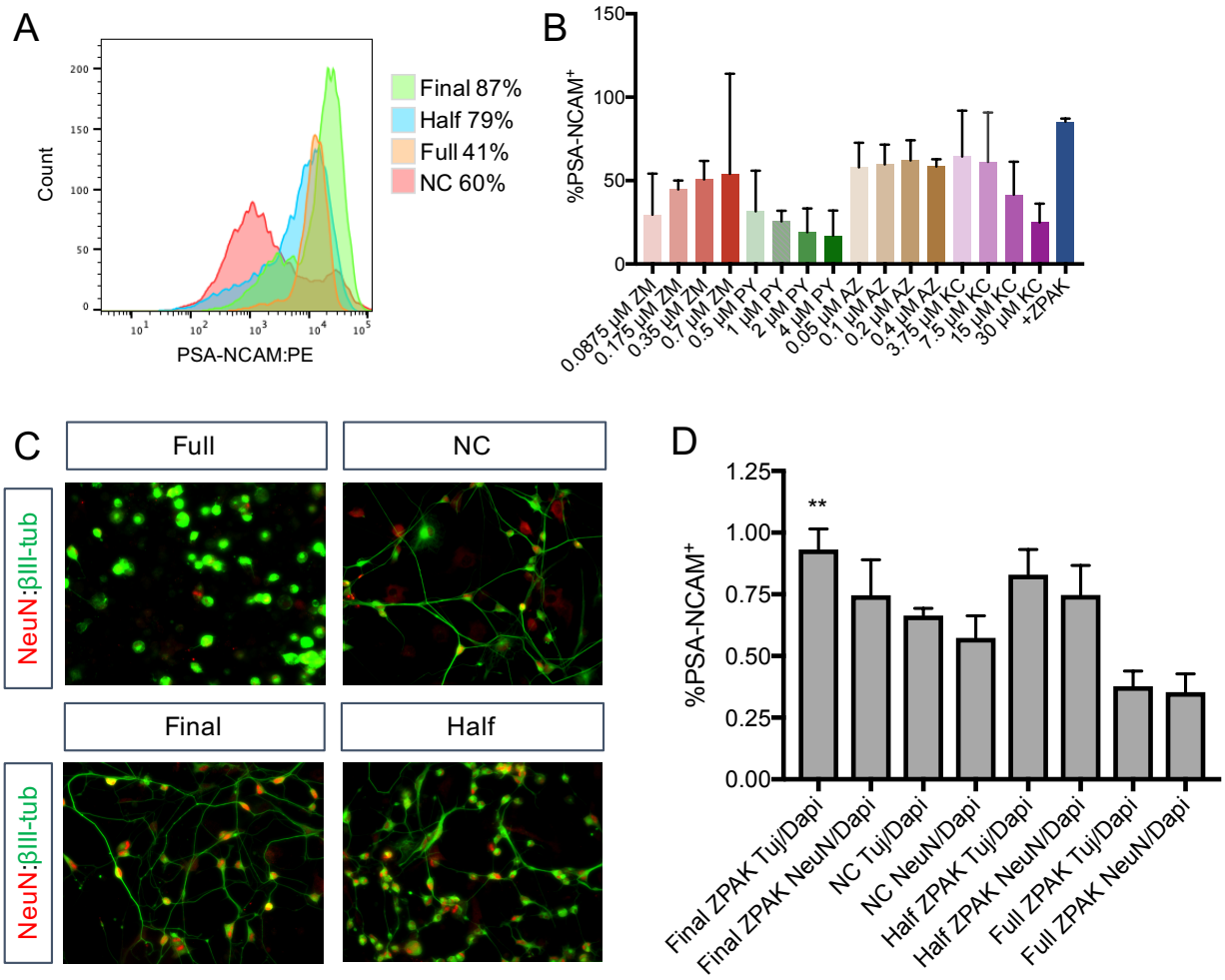

Supplemental Figure S1.10: Concentration optimization of ZPAK cocktail. **A.** Flow cytometry analysis of % PSA-NCAM$^+$ L1 cells cultured with NC or NC + Full ZPAK (4 µM PY, 30 µM KC, 0.4 µM AZ, and 0.7 µM ZM), Half ZPAK (2 µM PY, 15 µM KC, 0.2 µM AZ, and 0.35 µM ZM), and Final ZPAK (1 µM PY, 7.5 µM KC, 0.1 µM AZ, and 0.175 µM ZM). **B.** Flow cytometry analysis of % PSA-NCAM$^+$ L1, L4, and L8 cells cultured with the indicated concentrations of PY, KC, AZ, ZM, and Final ZPAK. **C.** Representative image of iNs produced from Full, Half, and Final ZPAK concentrations and NC alone. **D.** Quantification of results from C. Results are shown as mean ± SD. ** $P < 0.01$. Significance values were calculated by t-test.

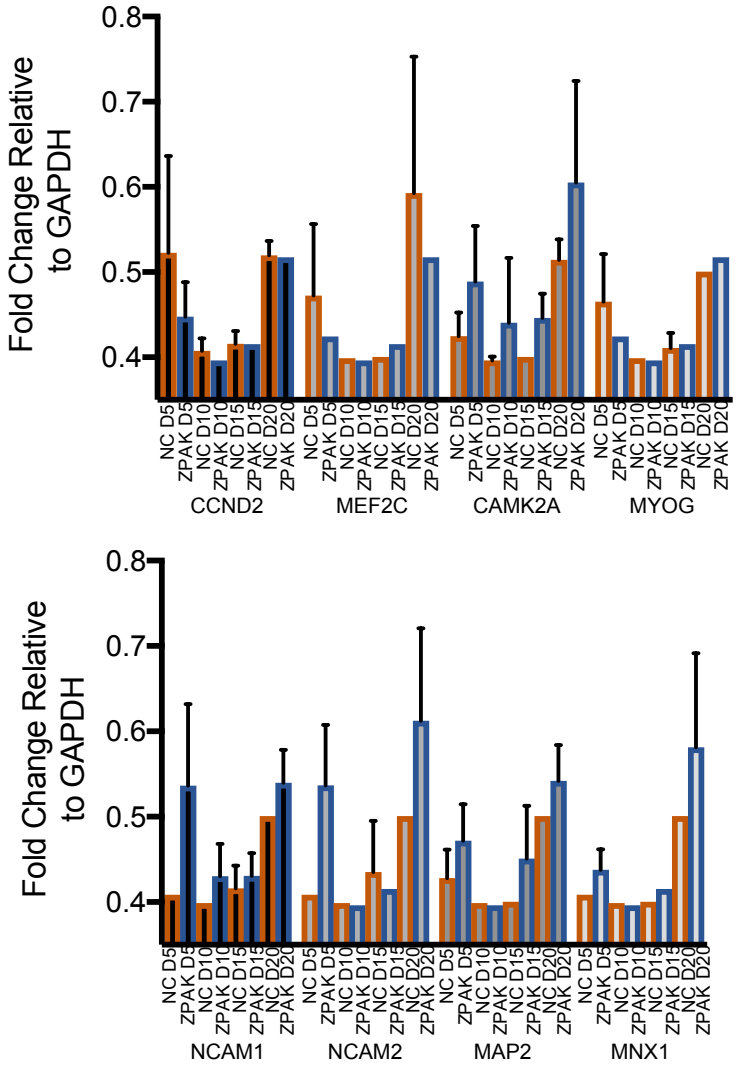

Supplemental Figure S1.11. Fold change of genes activated or suppressed by ZPAK assessed by SYBR qPCR in L2, L5, and L7 at D5, 10, 15, and 20 of conversion relative to GAPDH

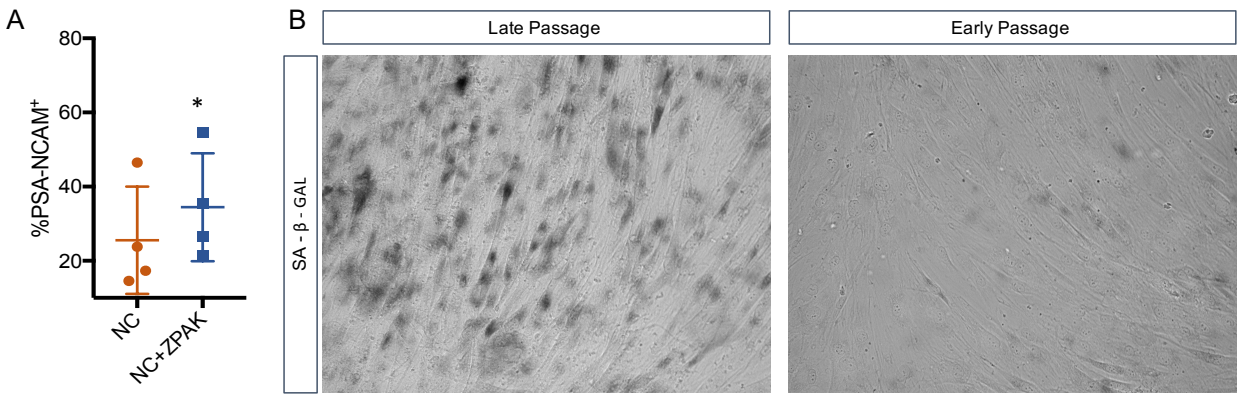

Supplemental Figure S1.12. High passage iN conversion in NC and NC+ZPAK. **A**: % yield of PSA-CNAM+ iNs from four lines (L1, L4, L10, L8) of late passage (>30) fibroblasts converted in NC or NC+ZPAK. **B**: representative brightfield images of early (p6) and late passage (p33) fibroblasts stained with senescence marker SA-B-Gal. Results are shown as mean ± SD. *n* = 4, * P < 0.05. Significance values were calculated

Chapter 1, in full, is a reprint of the material as it appears in: Joseph Herdy, Simon Schafer, Yongsung Kim, Zoya Ansari, Dina Zangwill, Manching Ku, Apua Paquola, Hyungjun Lee, Jerome Mertens, Fred H Gage (2019) Chemical modulation of transcriptionally enriched signaling pathways to optimize the conversion of fibroblasts into neurons eLife 8:e41356 https://doi.org/10.7554/eLife.41356. The dissertation author was the primary investigator and author of this paper.

References

Ailian Xiong and Zhengduo Yang and Yicheng Shen and Jia Zhou and Qiang, Shen. 2014. "Transcription Factor Stat3 as a Novel Molecular Target for Cancer Prevention." *Cancers* 6 (4): 926-957 , pmid = 24743778. https://dx.doi.org/10.3390/cancers6020926.

S. Nakajima and Ryuichiro Doi and Eiji Toyoda and Shoichiro Tsuji and Michihiko Wada and Masayuki Koizumi and Sidhartha S Tulachan and Daisuke Ito and Kazuhiro Kami and Tomohiko Mori. 2004. "N-Cadherin Expression and Epithelial-Mesenchymal Transition in Pancreatic Carcinoma." *Clinical Cancer Research* 10 (6): 4125-4133 , pmid = 15217949. https://dx.doi.org/10.1158/1078-0432.CCR-0578-03.

Chen, S. T. Smiley and M Reers and C Mottola-Hartshorn and M Lin and A Chen and T W Smith and G D Steele and L B. 1991. "Intracellular Heterogeneity in Mitochondrial Membrane Potentials Revealed by a J-Aggregate-Forming Lipophilic Cation Jc-1." *Proceedings of the National Academy of Sciences of the United States of America* 88 (5): 3671-5 , pmid = 2023917 , publisher = National Academy of Sciences. https://dx.doi.org/10.1073/PNAS.88.9.3671.

Christine, L. Chaffer and Erik W. Thompson and Elizabeth D. Williams. 2007. "Mesenchymal to Epithelial Transition in Development and Disease." *Cells Tissues Organs* 185: 7-19 , pmid = 17587803. https://dx.doi.org/10.1159/000101298.

Christophe Heinrich and Robert Blum and Sergio Gascón and Giacomo Masserdotti and Pratibha Tripathi and Rodrigo Sánchez and Steffen Tiedt and Timm Schroeder and Magdalena Götz and Benedikt, Berninger. 2010. "Directing Astroglia from the Cerebral Cortex into Subtype Specific Functional Neurons." *PLoS Biology* 8 (5): e1000373 , publisher = Public Library of Science. https://dx.doi.org/10.1371/journal.pbio.1000373.

Chuan-hai Zhang and Feng-Lin Guo and Ge-Liang Xu and Wei-Dong Jia and Yong-Sheng, Ge. 2014. "Stat3 Activation Mediates Epithelial-to-Mesenchymal Transition in Human Hepatocellular Carcinoma Cells." *Hepato-gastroenterology* 61 (6): 1082-9 , pmid = 26158169.

Derek, K. Smith and Jianjing Yang and Meng-Lu Liu and Chun-Li Zhang. 2016. "Small Molecules Modulate Chromatin Accessibility to Promote Neurog2-Mediated Fibroblast-to-Neuron Reprogramming." *Stem cell reports* 7 (11): 955-969 , pmid = 28157484 , publisher = Elsevier. https://dx.doi.org/10.1016/j.stemcr.2016.09.013.

DiCicco-Bloom, G. Mairet-Coello and A. Tury and E. 2009. "Insulin-Like Growth Factor-1 Promotes G1/S Cell Cycle Progression through Bidirectional Regulation of Cyclins and Cyclin-Dependent Kinase Inhibitors Via the Phosphatidylinositol 3-Kinase/Akt Pathway in Developing Rat Cerebral Cortex." *Journal of Neuroscience* 29 (1): 775-788 , pmid = 19158303. https://dx.doi.org/10.1523/JNEUROSCI.1700-08.2009.

Elena Scarpa and Andrá, S. Szabó and Anne Bibonne and Eric Theveneau and Maddy Parsons and Roberto Mayor Correspondence. 2015. "Cadherin Switch During Emt in Neural Crest Cells Leads to Contact Inhibition of Locomotion Via Repolarization of Forces." *Developmental Cell* 34: 421-434. https://dx.doi.org/10.1016/j.devcel.2015.06.012.

Esther , Y. Son and Justin K Ichida and Brian J Wainger and Jeremy S Toma and Victor F Rafuse and Clifford J Woolf and Kevin Eggan. 2011. "Conversion of Mouse and Human Fibroblasts into Functional Spinal Motor Neurons." *Cell Stem Cell* 9 (9): 205-218 , publisher = Cell Press. https://dx.doi.org/10.1016/J.STEM.2011.07.014.

Feng and Fuhui Wang and Xiao Zhang and Yiping Guo and Duanqing Pei and Hui, Zheng, Songwei He and Jinlong Chen and Yixin Zhang and Mengdan Zhang and Xiao Yang and Yuan Li and Hao Sun and Lilong Lin and Ke Fan and Lining Liang and Chengqian. 2017. "Sequential Emt-Met Induces Neuronal Conversion through Sox2." *Cell discovery* 3: 17017 , pmid = 28580167 , publisher = Nature Publishing Group. https://dx.doi.org/10.1038/celldisc.2017.17.

Fran Supek and Matko Bošnjak and Nives Škunca and Tomislav, Šmuc. 2011. "Revigo Summarizes and Visualizes Long Lists of Gene Ontology Terms." *PLoS ONE* 6 (7): e21800 , publisher = Public Library of Science. https://dx.doi.org/10.1371/journal.pone.0021800.

Giacomo Masserdotti and Sébastien Gillotin and Bernd Sutor and Daniela Drechsel and Martin Irmler and Helle, F. Jørgensen and Steffen Sass and Fabian J. Theis and Johannes Beckers and Benedikt Berninger and François Guillemot and Magdalena Götz. 2015. "Transcriptional Mechanisms of Proneural Factors and Rest in Regulating Neuronal Reprogramming of Astrocytes." *Cell stem cell* 17 (7): 74-88 , pmid = 26119235 , publisher = Elsevier. https://dx.doi.org/10.1016/j.stem.2015.05.014.

Houbo Jiang and Zhimin Xu and Ping Zhong and Yong Ren and Gaoyang Liang and Haley, A. Schilling and Zihua Hu and Yi Zhang and Xiaomin Wang and Shengdi Chen and Zhen Yan and Jian Feng. 2015. "Cell Cycle and P53 Gate the Direct Conversion of Human Fibroblasts to Dopaminergic Neurons." *Nature Communications* 6 (12): 10100 , publisher = Nature Publishing Group. https://dx.doi.org/10.1038/ncomms10100.

Huh, C. J., B. Zhang, M. B. Victor, S. Dahiya, L. F. Batista, S. Horvath, and A. S. Yoo. 2016. "Maintenance of Age in Human Neurons Generated by Microrna-Based Neuronal Conversion of Fibroblasts." *Elife* 5 (09 20). https://dx.doi.org/10.7554/eLife.18648.

Jerome Mertens and Apuã, C. M. Paquola and Manching Ku and Emily Hatch and Lena Böhnke and Shauheen Ladjevardi and Sean McGrath and Benjamin Campbell and Hyungjun Lee and Joseph R. Herdy and J. Tiago Gonçalves and Tomohisa Toda and Yongsung Kim and Jürgen Winkler and Jun Yao and Martin W. Hetzer and Fred H. Gage. 2015. "Directly Reprogrammed Human Neurons Retain Aging-Associated Transcriptomic Signatures and Reveal Age-Related Nucleocytoplasmic Defects." *Cell stem cell* 17 (10): 705-718 , pmid = 26456686 , publisher = Elsevier. https://dx.doi.org/10.1016/j.stem.2015.09.001.

Jiang and Zhiqiang Cai and Hui Sun and Kang Zhang and Yi Zhang and Ju Chen and Xiang-Dong, Fu, Yuanchao Xue and Kunfu Ouyang and Jie Huang and Yu Zhou and Hong Ouyang and Hairi Li and Gang Wang and Qijia Wu and Chaoliang Wei and Yanzhen Bi and Li. 2013. "Direct Conversion of Fibroblasts to Neurons by Reprogramming Ptb-Regulated Microrna Circuits." *Cell* 152 (1): 82-96 , pmid = 23313552. https://dx.doi.org/10.1016/j.cell.2012.11.045.

Jun Guo and Yuexiu Wang and Frederick Sachs and Fanjie, Meng. 2014. "Actin Stress in Cell Reprogramming." *Proceedings of the National Academy of Sciences of the United States of America* 111 (12): E5252-61 , pmid = 25422450 , publisher = National Academy of Sciences. https://dx.doi.org/10.1073/pnas.1411683111.

Karin Ehrenreiter and Daniela Piazzolla and Vanishree Velamoor and Izabela Sobczak and, J. Victor Small and Junji Takeda and Thomas Leung and Manuela Baccarini. 2005. "Raf-1 Regulates Rho Signaling and Cell Migration." *The Journal of Cell Biology* 168.

Kitamura, T. Nosaka and T Kawashima and K Misawa and K Ikuta and A L Mui and T. 1999. "Stat5 as a Molecular Regulator of Proliferation, Differentiation and Apoptosis in Hematopoietic Cells." *The EMBO journal* 18 (9): 4754-65 , pmid = 10469654 , publisher = European Molecular Biology Organization. https://dx.doi.org/10.1093/emboj/18.17.4754.

Kumi Sakurai and Indrani Talukdar and Veena, S. Patil and Jason Dang and Zhonghan Li and Kung-Yen Chang and Chih-Chung Lu and Violaine Delorme-Walker and Celine Dermardirossian and Karen Anderson and Dorit Hanein and Chao-Shun Yang and Dongmei Wu and Yang Liu and Tariq M. Rana. 2014. "Kinome-Wide Functional Analysis Highlights the Role of Cytoskeletal Remodeling in Somatic Cell Reprogramming." *Cell stem cell* 14 (4): 523-34 , pmid = 24702998 , publisher = NIH Public Access. https://dx.doi.org/10.1016/j.stem.2014.03.001.

Laloraya, A. P. Renjini and Shiny Titus and Prashanth Narayan and Megha Murali and Rajesh Kumar Jha and Malini. 2014. "Stat3 and Mcl-1 Associate to Cause a Mesenchymal Epithelial Transition." *Journal of cell science* 127 (4): 1738-50 , pmid = 24481815 , publisher = The Company of Biologists Ltd. https://dx.doi.org/10.1242/jcs.138214.

Louise, C. Parr-Brownlie and ClÃ©mentine Bosch-Bouju and Lucia Schoderboeck and Rachel J. Sizemore and Wickliffe C. Abraham and Stephanie M. Hughes. 2015. "Lentiviral Vectors as Tools to Understand Central Nervous System Biology in Mammalian Model Organisms." *Frontiers in Molecular Neuroscience* 8 (5): 14 , publisher = Frontiers. https://dx.doi.org/10.3389/fnmol.2015.00014.

Mak, M. Agostini and F Romeo and S Inoue and M V Niklison-Chirou and A J Elia and D Dinsdale and N Morone and R A Knight and T W. 2016. "Metabolic Reprogramming During Neuronal Differentiation." *Cell Death & Differentiation* 23 (9): 1502-1514 , publisher = Nature Publishing Group. https://dx.doi.org/10.1038/cdd.2016.36.

Marisa Karow and Rodrigo Sánchez and Christian Schichor and Giacomo Masserdotti and Felipe Ortega and Christophe Heinrich and Sergio Gascón and Muhammad, A. Khan and D. Chichung Lie and Arianna Dellavalle and Giulio Cossu and Roland Goldbrunner and Magdalena Götz and Benedikt Berninger. 2012. "Reprogramming of Pericyte-Derived Cells of the Adult Human Brain into Induced Neuronal Cells." *Cell stem cell* 11 (10): 471-6 , pmid = 23040476 , publisher = Elsevier. https://dx.doi.org/10.1016/j.stem.2012.07.007.

Marisa Karow and Rodrigo Sánchez and Christian Schichor and Giacomo Masserdotti and Felipe Ortega and Christophe Heinrich and Sergio Gascón and Muhammad , A. Khan and D. Chichung Lie and Arianna Dellavalle and Giulio Cossu and Roland Goldbrunner and Magdalena Götz and Benedikt Berninger. 2012. "Reprogramming of Pericyte-

Derived Cells of the Adult Human Brain into Induced Neuronal Cells." *Cell Stem Cell* 11 (10): 471-476 , publisher = Cell Press. https://dx.doi.org/10.1016/J.STEM.2012.07.007.

Massimiliano Caiazzo and Maria Teresa Dell'Anno and Elena Dvoretskova and Dejan Lazarevic and Stefano Taverna and Damiana Leo and Tatyana, D. Sotnikova and Andrea Menegon and Paola Roncaglia and Giorgia Colciago and Giovanni Russo and Piero Carninci and Gianni Pezzoli and Raul R. Gainetdinov and Stefano Gustincich and Alexander Dityatev and Vania Broccoli. 2011. "Direct Generation of Functional Dopaminergic Neurons from Mouse and Human Fibroblasts." *Nature* 476 (7): 224-227 , publisher = Nature Research. https://dx.doi.org/10.1038/nature10284.

Matheus, B. Victor and Michelle Richner and Tracey O. Hermanstyne and Joseph L. Ransdell and Courtney Sobieski and Pan-Yue Deng and Vitaly A. Klyachko and Jeanne M. Nerbonne and Andrew S. Yoo. 2014. "Generation of Human Striatal Neurons by Microrna-Dependent Direct Conversion of Fibroblasts." *Neuron* 84 (10): 311-23 , pmid = 25374357 , publisher = Elsevier. https://dx.doi.org/10.1016/j.neuron.2014.10.016.

Meaghan, J. Jones and Sarah J. Goodman and Michael S. Kobor. 2015. "Dna Methylation and Healthy Human Aging." *Aging Cell* 14 (12): 924-932 , publisher = Wiley/Blackwell (10.1111). https://dx.doi.org/10.1111/acel.12349.

Meng-Lu Liu and Tong Zang and Chun-Li, Zhang. 2016. "Direct Lineage Reprogramming Reveals Disease-Specific Phenotypes of Motor Neurons from Human Als Patients." *Cell reports* 14 (1): 115-128 , pmid = 26725112 , publisher = Elsevier. https://dx.doi.org/10.1016/j.celrep.2015.12.018.

Meng-Lu Liu and Tong Zang and Yuhua Zou and Joshua, C. Chang and Jay R. Gibson and Kimberly M. Huber and Chun-Li Zhang. 2013. "Small Molecules Enable Neurogenin 2 to Efficiently Convert Human Fibroblasts into Cholinergic Neurons." *Nature Communications* 4 (7): ncomms3183 , publisher = Nature Publishing Group. https://dx.doi.org/10.1038/ncomms3183.

Mertens, J., A. C. M. Paquola, M. Ku, E. Hatch, L. Bohnke, S. Ladjevardi, S. McGrath, B. Campbell, H. Lee, J. R. Herdy, J. T. Goncalves, T. Toda, Y. Kim, J. Winkler, J. Yao, M. W. Hetzer, and F. H. Gage. 2015. "Directly Reprogrammed Human Neurons Retain Aging-Associated Transcriptomic Signatures and Reveal Age-Related Nucleocytoplasmic Defects." *Cell Stem Cell* 17, no. 6 (Dec 3): 705-718. https://dx.doi.org/10.1016/j.stem.2015.09.001.

Michael, K. Wendt and Nikolas Balanis and Cathleen R. Carlin and William P. Schiemann. 2014. "Stat3 and Epithelial-Mesenchymal Transitions in Carcinomas." *Jak-Stat* 3 (1): e28975 , pmid = 24843831 , publisher = Taylor & Francis. https://dx.doi.org/10.4161/jkst.28975.

Miquel Bosch and Jorge Castro and Takeo Saneyoshi and Hitomi Matsuno and Mriganka Sur and Yasunori, Hayashi. 2014. "Structural and Molecular Remodeling of Dendritic Spine Substructures During Long-Term Potentiation." *Neuron* 82 (4): 444-59 , pmid = 24742465 , publisher = NIH Public Access. https://dx.doi.org/10.1016/j.neuron.2014.03.021.

Mohammad Reza Omrani and Moein Yaqubi and Abdulshakour, Mohammadnia. 2018. "Transcription Factors in Regulatory and Protein Subnetworks During Generation of Neural Stem Cells and Neurons from Direct Reprogramming of Non-Fibroblastic Cell Sources." *Neuroscience* 380 (6): 63-77 , pmid = 29653196. https://dx.doi.org/10.1016/j.neuroscience.2018.03.033.

Orly , L. Wapinski and Thomas Vierbuchen and Kun Qu and Qian Yi Lee and Soham Chanda and Daniel R Fuentes and Paul G Giresi and Yi Han Ng and Samuele Marro and Norma F Neff and Daniela Drechsel and Ben Martynoga and Diogo S Castro and Ashley E Webb and Thomas C Südhof and Anne Brunet and Francois Guillemot and Howard Y Chang and Marius Wernig. 2013. "Hierarchical Mechanisms for Direct Reprogramming of Fibroblasts to Neurons." *Cell* 155 (10): 621-635 , pmid = 24243019. https://dx.doi.org/10.1016/j.cell.2013.09.028.

Philipp Koch and Oliver, Brüstle, Julia Ladewig and Jerome Mertens and Jaideep Kesavan and Jonas Doerr and Daniel Poppe and Finnja Glaue and Stefan Herms and Peter Wernet and Gesine Kögler and Franz-Josef Müller and. 2012. "Small Molecules Enable Highly Efficient Neuronal Conversion of Human Fibroblasts." *Nature Methods* 9 (6): 575-578 , publisher = Nature Publishing Group. https://dx.doi.org/10.1038/nmeth.1972.

Rachel Tsunemoto and Sohyon Lee and Attila Szűcs and Pavel Chubukov and Irina Sokolova and Joel, W. Blanchard and Kevin T. Eade and Jacob Bruggemann and Chunlei Wu and Ali Torkamani and Pietro Paolo Sanna and Kristin K. Baldwin. 2018. "Diverse Reprogramming Codes for Neuronal Identity." *Nature* 557 (5): 375-380 , publisher = Nature Publishing Group. https://dx.doi.org/10.1038/s41586-018-0103-5.

Samy Lamouille and Jian Xu and Rik, Derynck. 2014. "Molecular Mechanisms of Epithelial-Mesenchymal Transition." *Nature reviews. Molecular cell biology* 15 (3): 178-96 , pmid = 24556840 , publisher = NIH Public Access. https://dx.doi.org/10.1038/nrm3758.

Sean, M. Gross and Peter Rotwein. 2016. "Unraveling Growth Factor Signaling and Cell Cycle Progression in Individual Fibroblasts." *The Journal of biological chemistry* 291 (7): 14628-38 , pmid = 27226630 , publisher = American Society for Biochemistry and Molecular Biology. https://dx.doi.org/10.1074/jbc.M116.734194.

Seema, B. Plaisier and Richard Taschereau and Justin A. Wong and Thomas G. Graeber. 2010. "Rank–Rank Hypergeometric Overlap: Identification of Statistically Significant Overlap between Gene-Expression Signatures." *Nucleic Acids Research* 38 (9): e169-e169 , pmid = 20660011. https://dx.doi.org/10.1093/nar/gkq636.

Sergio Gascón and Elisa Murenu and Giacomo Masserdotti and Felipe Ortega and Gianluca , L. Russo and David Petrik and Aditi Deshpande and Christophe Heinrich and Marisa Karow and Stephen P Robertson and Timm Schroeder and Johannes Beckers and Martin Irmler and Carsten Berndt and José P Friedmann Angeli and Marcus Conrad and Benedikt Berninger and Magdalena Götz. 2016. "Identification and Successful Negotiation of a Metabolic Checkpoint in Direct Neuronal Reprogramming." *Cell Stem Cell* 18 (3): 396-409. https://dx.doi.org/10.1016/j.stem.2015.12.003.

Spitzer, S. S. Rosenberg and N. C. 2011. "Calcium Signaling in Neuronal Development." *Cold Spring Harbor Perspectives in Biology* 3 (10): a004259-a004259 , pmid = 21730044. https://dx.doi.org/10.1101/cshperspect.a004259.

Stuart, M. Chambers and Christopher A. Fasano and Eirini P. Papapetrou and Mark Tomishima and Michel Sadelain and Lorenz Studer. 2009. "Highly Efficient Neural Conversion of Human Es and Ips Cells by Dual Inhibition of Smad Signaling." *Nature biotechnology* 27 (3): 275-80 , pmid = 19252484 , publisher = NIH Public Access. https://dx.doi.org/10.1038/nbt.1529.

Stuart, M. Chambers and Lorenz Studer. 2011. "Cell Fate Plug and Play: Direct Reprogramming and Induced Pluripotency." *Cell* 145 (6): 827-30 , pmid = 21663788 , publisher = Elsevier. https://dx.doi.org/10.1016/j.cell.2011.05.036.

Thomas Vierbuchen and Austin Ostermeier and Zhiping, P. Pang and Yuko Kokubu and Thomas C. Südhof and Marius Wernig. 2010. "Direct Conversion of Fibroblasts to Functional Neurons by Defined Factors." *Nature* 463 (2): 1035-1041 , publisher = Nature Publishing Group. https://dx.doi.org/10.1038/nature08797.

Tiffany, J. Morris and Lee M. Butcher and Andrew Feber and Andrew E. Teschendorff and Ankur R. Chakravarthy and Tomasz K. Wojdacz and Stephan Beck. 2014. "Champ: 450k Chip Analysis Methylation Pipeline." *Bioinformatics* 30 (2): 428-430 , pmid = 24336642. https://dx.doi.org/10.1093/bioinformatics/btt684.

Vadodaria, K. C., J. Mertens, A. Paquola, C. Bardy, X. Li, R. Jappelli, L. Fung, M. C. Marchetto, M. Hamm, M. Gorris, P. Koch, and F. H. Gage. 2016. "Generation of Functional Human Serotonergic Neurons from Fibroblasts." *Mol Psychiatry* 21, no. 1 (Jan): 49-61. https://dx.doi.org/10.1038/mp.2015.161.

Valentina Lo Sardo and William Ferguson and Galina, A. Erikson and Eric J. Topol and Kristin K. Baldwin and Ali Torkamani. 2016. "Influence of Donor Age on Induced Pluripotent Stem Cells." *Nature Biotechnology* 35 (12): 69-74 , pmid = 27941802. https://dx.doi.org/10.1038/nbt.3749.

Victor, M. B., M. Richner, H. E. Olsen, S. W. Lee, A. M. Monteys, C. Ma, C. J. Huh, B. Zhang, B. L. Davidson, X. W. Yang, and A. S. Yoo. 2018. "Striatal Neurons Directly Converted from Huntington's Disease Patient Fibroblasts Recapitulate Age-Associated Disease Phenotypes." *Nat Neurosci* 21, no. 3 (03): 341-352. https://dx.doi.org/10.1038/s41593-018-0075-7.

Xiaoju Zhang and Guangzhi Liu and Yi Kang and Zhaogang Dong and Qiyu Qian and Xitao, Ma. 2013. "N-Cadherin Expression Is Associated with Acquisition of Emt Phenotype and with Enhanced Invasion in Erlotinib-Resistant Lung Cancer Cell Lines." *PLoS ONE* 8 (3): e57692 , publisher = Public Library of Science. https://dx.doi.org/10.1371/journal.pone.0057692.

Xinde Zheng and Leah Boyer and Mingji Jin and Jerome Mertens and Yongsung Kim and Li Ma and Li Ma and Michael Hamm and Fred, H. Gage and Tony Hunter. 2016. "Metabolic Reprogramming During Neuronal Differentiation from Aerobic Glycolysis to Neuronal Oxidative Phosphorylation." *eLife* 5 (6): e13374 , publisher = eLife Sciences Publications Limited. https://dx.doi.org/10.7554/eLife.13374.

Yi-Ping, Hsueh. 2012. "Neuron-Specific Regulation on F-Actin Cytoskeletons: The Role of Cttnbp2 in Dendritic Spinogenesis and Maintenance." *Communicative & integrative*

biology 5 (7): 334-6 , pmid = 23060955 , publisher = Taylor & Francis. https://dx.doi.org/10.4161/cib.20364.

Ying Zhang and Rik, Derynck. 1999. "Regulation of Smad Signalling by Protein Associations and Signalling Crosstalk." *Trends in Cell Biology* 9 (7): 274-279 , publisher = Elsevier Current Trends. https://dx.doi.org/10.1016/S0962-8924(99)01579-2.

Yu Tang and Meng-Lu Liu and Tong Zang and Chun-Li, Zhang. 2017. "Direct Reprogramming Rather Than Ipsc-Based Reprogramming Maintains Aging Hallmarks in Human Motor Neurons." *Frontiers in Molecular Neuroscience* 10 (11): 359 , publisher = Frontiers. https://dx.doi.org/10.3389/fnmol.2017.00359.

Yue Xu and Xiuwen Zhu and Heung Sik Hahm and Wanguo Wei and Ergeng Hao and Alberto Hayek and Sheng, Ding. 2010. "Revealing a Core Signaling Regulatory Mechanism for Pluripotent Stem Cell Survival and Self-Renewal by Small Molecules." *Proceedings of the National Academy of Sciences of the United States of America* 107 (5): 8129-34 , pmid = 20406903 , publisher = National Academy of Sciences. https://dx.doi.org/10.1073/pnas.1002024107.

Zhiping, P. Pang and Nan Yang and Thomas Vierbuchen and Austin Ostermeier and Daniel R. Fuentes and Troy Q. Yang and Ami Citri and Vittorio Sebastiano and Samuele Marro and Thomas C. Südhof and Marius Wernig. 2011a. "Induction of Human Neuronal Cells by Defined Transcription Factors." *Nature* 476 (8): 220-223 , pmid = 21617644. https://dx.doi.org/10.1038/nature10202.

---. 2011b. "Induction of Human Neuronal Cells by Defined Transcription Factors." *Nature* 476 (8): 220-223 , publisher = Nature Publishing Group. https://dx.doi.org/10.1038/nature10202.

CHAPTER 2: Increased Post-Mitotic Senescence in Aged Human Neurons is a Pathological Feature of Alzheimer's Disease.

Abstract

The concept of senescence as a phenomenon limited to proliferating cells has been challenged by growing evidence of senescence-like features in terminally differentiated cells, including neurons. The persistence of senescent cells late in life is associated with tissue dysfunction and increased risk of age-related disease. We found that Alzheimer's disease (AD) brains have significantly higher proportions of neurons that express senescence markers, and their distribution indicates bystander effects. AD patient-derived directly induced neurons (iNs) exhibit strong transcriptomic, epigenetic, and molecular biomarker signatures that illuminate a specific human neuronal senescence-like state. AD iN single-cell transcriptomics revealed that senescent-like neurons face oncogenic challenges, metabolic dysfunction, and display a proinflammatory signature. Integrative profiling of the inflammatory secretome of AD iNs and patient cerebral spinal fluid revealed a neuronal senescence-associated-secretory-phenotype, that could trigger astrogliosis in human astrocytes. Finally, we show that targeting senescence-like neurons with senotherapeutics could be a novel strategy for preventing or treating AD.

Introduction

The integration of mature, terminally differentiated neurons into elaborated networks is thought be one of the fundamental principles of neuronally encoded information in the brain. Across a human lifetime, neurons face immense evolutionary pressure to retain this post-mitotic, differentiated state indefinitely to preserve information. Life-long terminal differentiation is not without cost, however, and the inability to rejuvenate cellular components combined with the longevity of humans leads to the accumulation of numerous defects late in life, including DNA damage, mitochondrial dysfunction, epigenetic changes, and transcriptional drift (Mattson and Magnus 2006; Reid et al. 2021). When confronted with these late-life cellular stressors, cells may

undergo a process known as cellular senescence. Originally described as replicative arrest of fibroblasts *in vitro*, senescence has since become accepted as one of the pillars of organismal aging. Senescent cells increase in abundance during aging, where they contribute to tissue dysfunction and numerous age-related disorders (McHugh and Gil 2018). Recent studies have changed the perception of cellular senescence, expanding it from a response to serial passage to a central role in responding to stress, molecular damage, and oncogene activation. Importantly, post-mitotic neurons experience many of the same age-related stressors that trigger senescence in proliferating cells. Indeed, there are a growing number of recent reports of senescence-like signatures in non-dividing cells, including osteoclasts (Farr et al. 2016), mature adipocytes (Minamino et al. 2009), neurons (Paramos-de-Carvalho et al. 2021), and others (Sapieha and Mallette 2018). Like proliferating cells, senescence in neurons is linked to aging and cellular stress, yet there is an important gap in knowledge regarding the definition and understanding of the senescence-like state of aged human neurons.

Cellular reprogramming techniques have allowed for the *in vitro* generation of functional human neurons from accessible tissues such as blood or skin. Unfortunately, neurons generated from induced pluripotent stem cell (iPSC) reprogramming have limited applicability to the study of age-related phenotypes. Passing through the stem cell intermediate phase leads to a youthful rejuvenation of the epigenome, gene expression, long-lived proteins, mitochondria function, and telomere length in the resulting neurons (Mertens et al. 2018; Schafer et al. 2019; Huh et al. 2016; Handel et al. 2016).In contrast, induced neurons (iNs) can be generated by the direct transdifferentiation of human donor fibroblasts, without passing through a stem cell intermediate phase. Avoiding the stem cell intermediate phase also bypasses the dramatic epigenetic rejuvenation that occurs in iPSC reprogramming. As a result, iNs retain the age-related features of their donor and allow for modeling of human age and disease *in vitro* (Herdy et al. 2019; Mertens et al. 2015b; Huh, et al. 2016; Victor et al. 2018). Importantly, age-equivalent iNs retain

transcriptional, epigenetic, and metabolic profiles of aging (Kim et al. 2018; Mertens, et al. 2015b). Therefore, the iN system allows us to study endogenous age-related processes in neurons instead of resorting to using exogenous stressors to accelerate aging.

Despite decades of research, Alzheimer's Disease (AD) remains a debilitating, progressive, and ultimately fatal dementia with no disease-modifying treatment options. The vast majority of cases (>95%) are sporadic, with no known cause aside from advanced age (Van Cauwenberghe, Van Broeckhoven, and Sleegers 2016). As the population over age 65 grows, the burden of AD is destined to grow in lockstep. As early as the 1990s several observations were made that suggested neuronal senescence might be a feature of AD, but the prevailing view that senescence was restricted to proliferating cells limited the impact of this work (Arendt et al. 1996; McShea et al. 1997). However, the growing reports of a senescence-like phenotype in neurons in a variety of aging or injury contexts led to the hypothesis that aged human neurons can enter a senescence-like state and contribute to AD pathology. Here, we show that AD patient-derived iNs enter a functionally impaired senescent-like state more frequently than age-matched healthy control donor-derived iNs. Deep multi-omic profiling revealed that many molecular features are shared with proliferative senescence and further extends our understanding of the senescence-like neuronal state as epigenomic and transcriptomic biomarkers of AD iNs, which are consistent with senescence induction. Strikingly, the culture supernatants of AD iNs mirror the pro-inflammatory signature of AD patient cerebral spinal fluid (CSF), and this neuronal senescence-associated-secretory-phenotype (SASP) secretome triggers reactive astrogliosis. Finally, we show that senescent-like AD iNs can be cleared by the senolytic drug cocktail of Dasatinib and Quercetin (DQ). Our data support the hypothesis that neurons can enter a senescent-like state and that these cells have the potential to initiate and contribute to AD-related neuroinflammation.

Further, our results suggest that targeting senescent cells in the brain could be a novel therapy for treating AD-related neurodegeneration.

Materials and Methods

Subjects

Subjects were participants at the Shiley-Marcos Alzheimer's Disease Research Center (ADRC) at UCSD and provided written informed consent; all procedures were approved by local human subjects committees. Both AD and control subjects underwent rigorous clinical assessment as part of the ADRC study, including detailed neuropsychological testing and brain imaging (MRI), and the subjects selected for biopsies were stratified to show either a clear non-demented clinical picture or clear phenotype of AD (classified as probable AD until pathological confirmation). They were followed for at least 2 years after biopsy with no evidence of cognitive decline (controls) and with evidence of progressive impairment (AD). Punch skin biopsies were obtained at the Altman Clinical & Translational Research Institute (ACTRI) at UCSD, and fibroblast derivation was performed by standard procedures in serum-containing media. Additional familial AD fibroblast lines were described previously(Israel et al. 2012), and 4 old control and 3 young control fibroblast lines were obtained from Coriell (Baltimore longitudinal study of aging) and also described previously(Kim, et al. 2018; Mertens et al. 2015a). Table 2.1 contains post mortem PFC slice information.

Astrocytes

Human cortical, cerebellar, and hippocampal astrocytes were acquired from a commercial vendor and cultured in astrocyte medium according to the manufacturer's specifications (ScienCell 1800, 1801). For CM experiments, 48-hour iN conditioned supernatant was pooled from six AD and six CTL iN lines and spiked in at a 1:3 ratio with untreated astrocyte medium for 48 hours. Protein input between pooled samples was normalized to total protein as measured by qubit (ThermoFisher). Cells were then fixed for ICC or harvested with Trizol for RNA extraction.

Fibroblasts and iNs

Primary human dermal fibroblasts from donors between 0 and 88 years of age were obtained from the Coriell Institute Cell Repository, the University Hospital in Erlangen and Shiley-Marcos Alzhiemer's Disease Research Center. Protocols were previously approved by the Salk Institute Institutional Review Board and informed consent was obtained from all subjects. Fibroblasts were cultured in DMEM containing 15% tetracycline-free fetal bovine serum and 0.1% NEAA (Thermo Fisher Scientific) transduced with lentiviral particles for EtO and XTP-Ngn2:2A:Ascl1 (E+N2A) or the combined tetOn system cassette consisting of the rtTAAdv [Clonech] driven by the UbC promoter, Ngn2:2A:Ascl1 under control of the TREtight promoter [Clontech], and a puromycin-resistance gene driven by the PGK promoter (UNA, Sup Fig2A) and expanded in the presence of G418 (200 µg/ml; Thermo Fisher Scientific) and puromycin (1 µg/ml; Sigma Aldrich), or puromycin only, respectively, as 'iN-ready' fibroblast cell lines. Following at least 3 passages after viral transduction, 'iN-ready' fibroblasts were trypsinized and pooled into high densities (30,000 – 50,000 cells per cm^2 ; appx. a 2:1 – 3:1 split from a confluent culture) and, after 24h, the medium was changed to neuron conversion (NC) medium based on DMEM:F12/Neurobasal (1:1) for three weeks. NC contains the following supplements: N2 supplement, B27 supplement (both 1x; Thermo Fisher Scientific), doxycycline (2 µg/ml, Sigma Aldrich), Laminin (1 µg/ml, Thermo Fisher Scientific Scientific), dibutyryl cyclic-AMP (100 µg/ml, Sigma Aldrich), human recombinant Noggin (150 ng/ml; Preprotech), LDN-193189 (500 nM; Fisher Scientific Co) and A83-1 (500 nM; Santa Cruz Biotechnology Inc.), CHIR99021 (3 µM, LC Laboratories), Forskolin (5 µM, LC Laboratories) SB-431542 (10 µM; Cayman Chemicals), pyrintegrin (1 µM; Tocris), ZM336372 (.175 µM; Cayman), AZ960 (0.1 µM; Cayman), and KC7F2 (7.5 µM; Fischer Scientific). Medium was changed every third day. For further maturation up to six weeks, iNs were switched to BrainPhys (STEMCELL Technologies)-based neural maturation media (NM) containing N2, B27, GDNF, BDNF (both 20 ng/ml, R&D), dibutyryl cyclicAMP (100 µg/ml, Sigma Aldrich), doxycycline (2 µg/ml, Sigma-Aldrich) and laminin (1 µg/ml, Thermo Fisher

Scientific). For maturation on astrocytes for morphological analysis and calcium imaging, iNs were carefully trypsinized during week 4 and replated on a feeder layer of mouse astrocytes and cultured in NM media containing 2% KOSR (Thermo Fisher Scientific).

iPSCs and iPSC-iNs

Human iPSCs were reprogrammed using the four Yamanaka factors transferred using the Cyto-Tune Sendai reprogramming kit (Invitrogen) or standard retroviral vectors as previously described(Mertens et al. 2021), and cultured as colonies on Geltrex (Thermo Fisher)-coated plates in iPS-Brew (Miltenyi Biotec). For iPSC-iN transgene delivery, iPSCs were transferred to a monolayer PluriPro (Cell Guidance Systems) condition, transduced with lentiviral particles for pLVX-UbC-rtTA-Ngn2:2A:EGFP (UNG), and expanded in the presence of puromycin (0.5 mg/ml; Sigma Aldrich) as 'iPSC-iN-ready' iPSC-UNG lines as previously described(Schafer, et al. 2019). To initiate conversion, confluent iPSC-UNG monolayer cultures were transferred into NC media to achieve neuronal conversion of the cultures within 3 weeks before fixing and staining, or isolation by flow cytometry for RNA purification.

Flow Cytometry

For isolation of iNs and iPSC-iNs from three-week cultures, cells were detached with TrypLE (Thermo Fisher) and stained for PSA-NCAM directly conjugated to APC (Miltenyl Biotec, 1x) for 1 hour at 4 C in sorting buffer (250 mM myo-inositol and 5 mg/ml polyvinyl alcohol in PBS) containing 1% KOSR (Thermo Fisher). Cells were washed and resuspended in sorting buffer containing EDTA and DNAse and filtered using a 40-um cell strainer. For C_{12}FDG analysis, cells were first treated with 100 nM bafilomycin A1 for 1 hour in fresh culture medium at 37 C, 5% CO_2. Next, a 2 mM C_{12}FDG solution was added to the cell culture medium for a final concentration of 33 uM and incubated for an additional hour. Cells were then washed twice with PBS and detached with TrypLE and prepared for FACS as described above.

Immunofluorescence

Formalin-fixed, paraffin-embedded slices of human pre-frontal cortex tissue were obtained from the Shiley-Marcos Alzheimer's Disease Research Center. Slides were deparaffinized and heat antigen retrieval was performed in 10 mM Sodium Citrate buffer (pH 6.0). Slides were permeabilized by two 10-minute washes in PBS with 0.4% Triton X-100 (PBS-T) and 1% serum, followed by a 1-hour block in PBS-T and 5% serum. Primary antibodies (Mouse NeuN MAB377 1:1000, Rabbit p16INK4a EPR1473 1:1000) were diluted with 1% serum in PBS and incubated at room temperature for 1 hour, followed by an overnight incubation at 4C in a humidified chamber. Sections were then washed twice in PBS-T for 10 minutes followed by secondary antibody (Donkey Anti-Mouse IgG Alexa Fluor 488 and Donkey Anti-Rabbit IgG Alexa Fluor 555, both 1:250) incubation for 2 hours at room temperature. Sections were then stained for nuclei with DAPI (1:10,000 Sigma-Aldrich) and washed twice for 10 minutes with PBS-T. After washing, slides were mounted and coverslips sealed with nail polish.

Cells were cultured on tissue culture-treated ibidi µ-slides for imaging. Cells were fixed with 4% PFA for 20 minutes at room temperature and washed 3 × 15 minutes with TBS, followed by a 1-hr block with TBS containing 10% serum and 0.1% Triton X-100. Primary antibodies (H2AFJ provided by Carl Mann 1:200, p16INK4a Abcam 1:250, TuJ Covance 1:3000, NeuN EMD Millipore 1:250, GFAP EMD Millipore 1:1000) were applied overnight at 4C. Following two 10-minute washes with TBS, nuclei were stained with DAPI (1:10,000 Sigma-Aldrich) and secondary antibodies (Donkey Anti-Mouse IgG Alexa Fluor 488/555 and Donkey Anti-Rabbit IgG Alexa Fluor 488/555, and Donkey Anti-Chicken IgG Alexa Fluor 488/555, all 1:250) were incubated for 2 hours at room temperature. After washing, slides were mounted in PVA-DAPCO (Sigma Aldrich). TUNEL staining was performed with the Click-iT™ Plus TUNEL Assay 594. SA-B-Gal staining was performed with the Biopioneer cellular senescence detection kit (CS-001). Confocal images were taken on standard fluorescence microscopes or Zeiss LSM780 confocal microscopes.

ImageJ software analyze particles was used for regions of interest (ROI) selection and quantification of immunofluorescent signals within ROIs. Proximity analysis was performed with

MorphoLibJ. All data for one experiment were acquired from cells cultured or tissue processed in parallel on the same microscope with the exact same setting used.

Whole Genome mRNA-seq and Analysis

Total bulk RNA was extracted from fibroblasts and iPSCs and from flow cytometry-isolated iNs and iPSC-iNs following three weeks of conversion using Trizol LS reagent (Thermo Fischer), followed by TURBO DNase digestion (Agilent). RNA integrity was assessed before library preparation using the TruSeq Stranded mRNA Sample Prep Kit according to the manufacturer's instructions (Illumina). Libraries were sequenced paired-end 125 bp using the Illumina HiSeq 2500 platform. Read trimming was performed using TrimGalore, read mapping was performed using STAR, raw counts were generated using HOMER, and variance stabilizing transformation normalization (vst) and differential expression analyses were performed in DESeq2. Statistical values were corrected for false discovery rates (FDR) using the Benjamini-Hochberg method implemented in R. Transcripts per million for all samples were generated by RSEM using standard paired-end or single-end settings as appropriate. CDKN2A, NeuN, and GFAP expression in post-mortem human brain samples from the Allen Brainspan Atlas (https://www.brainspan.org/static/download.html) and Aging, Dementia, and TBI study (https://aging.brain-map.org/rnaseq/search) was based on FPKM and differential expression analysis of NeuN, GFAP and CDKN2A was performed using DESeq2 with the default test (Wald test). Analysis of CDKN2A expression across aging was performed with a simple regression analysis t-test in R. Donor metadata for the Aging, Dementia and TBI study can be found here: https://aging.brain-map.org/download/index, and metadata for the Allen Brainspan Atlas at http://help.brain-map.org/display/devhumanbrain/Documentation. Rank Rank Hypergeometric Overlap (RRHO) was performed using the UCLA online tool.

For single cell RNAseq, following three weeks of conversion bulk cultures were harvested with TrypLE without sorting and 10,000 cells per patient were loaded in parallel and processed using the 10x Single Cell 3' v3 protocol (Illumina). Libraries were prepared following the manufacturer's

protocol. Briefly, cells were partitioned into Gel Beads in Emulsion in the GemCode/Chromium instrument followed by cell lysis and barcoded reverse transcription of mRNA, followed by amplification, shearing, and 5' adapter and index attachment. cDNA was amplified for 11 cycles, and the resulting whole transcriptome was measured and quality assessed by Bioanalyzer. Twenty-five percent of the whole-transcriptome material was processed through v3 library construction according to the manufacturer's protocol. The resulting libraries were quality assessed and quantified again by BioAnalyzer. Libraries were then pooled and sequenced on one lane of a NovaSeq 6000 (S1 100).

Single-Cell Data Analysis

Sequenced samples were initially processed using CellRanger software version 3.0.2 (10x Genomics) and were aligned to the GRCh38 (hg38) human reference genome. CellRanger digital expression matrices (DGE) were generated containing the raw unique molecular identified (UMI) counts for each sample. Count tables were then loaded into R and analyzed using the Seurat package. All cells with fewer than 300 genes or more than 10,000 genes or mitochondrial reads > 30% were excluded using Seurat's subset function. Using these parameters, we were able to keep 29,515 cells for downstream analysis. For each cell, UMI counts were log normalized and scaled. Cells were then clustered based on the top 3,000 variable genes identified using the FindVariableFeatures function. Variable genes were then used to perform principal components (PC) analysis, and the first 15 PCs were used for both AD and CTL cells. We then identified clusters using the FindClusters tool and visualized clusters using the uniform manifold approximation and projection (UMAP) dimensionality reduction. Marker genes for each cluster were identified using the FindMarkers function using default parameters.

For monocle analysis, cellranger processed UMIs were imported using the load_cellranger_data function, combined, preprocessed using the preprocess_cds function (num dim = 100), and dimensionality reduced using UMAP with the reduce_dimensions fuction. Cells were then clustered using cluster_cells (resolution = 1e-5). To assess differentiation of fibroblasts to iNs,

trajectory analysis was performed using the learn_graph tool. Differential expression analysis between clusters, disease status, or other metadata was performed using graph_test (knn neighbor graph) followed by fit_models with the relevant formula (eg ~Disease + Patient, etc). Residues from the differential expression were then obtained with the coefficient_table function. Genes with a min expression > 0.1 in the iN cluster were used to order cells in pseudotime, and the root node was selected programmatically by first grouping the cells according to which trajectory graph node they were nearest to, calculating the fraction of cells at each node from the earliest time point, and then picking the node that was most heavily occupied by early cells and returning that node as a root. The function plot_genes_in_pseudotime was then used to interrogate how specific genes behaved along pseudotime.

Senescence scoring was done using the AddModuleScore in Seurat, taking the average expression of senescence genes in R-HSA-2559583 subtracted by the aggregate expression of a randomly selected set of control feature sets (n=100). All analyzed features were binned based on averaged expression, and the control features were randomly selected from each bin.

Telomere Length Estimation

DNA for telomere estimation was extracted from bulk fibroblast using the DNEasy Blood and Tissue kit (Qiagen). Concentrations were measured via qubit and all samples were diluted to 5ng/uL. Telomere length was assessed via a qPCR strategy as described previously (O'Callaghan 2011). All oligomers used were HPLC purified, and a standard curve was obtained using an 84mer oligonucleotide containing only the TTAGGG repeat. The gene 36B4 was selected as a single copy gene standard to control for genome abundance between samples. All qPCR was performed with SYBR green (Life Technologies) on a BioRad CFX384 thermocycler.

Genome-Wide DNA Methylation Analysis

Genomic DNA was extracted from flow cytometry-isolated iNs or bulk fibroblast cultures using the DNEasy Blood and Tissue Kit (Qiagen). DNA methylation assays were performed on the Illumina MethylEPIC BeadChip as per the standard manufacturers protocol. Raw IDAT files

were processed and analyzed in R using the ChAMP and RnBeads packages and were normalized using the BMIQ procedure. Beta values were used as methylation residues for downstream analysis and correlation with RNAseq datasets.

Whole Genome Assay for Transposase-Accessible Chromatin Using Sequencing (ATACseq) and Analysis

ATAC-Seq was performed as described earlier (Buenrosto 2013). Briefly, 50,000 iNs were lysed in 50 ul lysis buffer (10 mM Tris-HCl ph 7.5, 10 mM NaCl, 3 mM MgCl2, 0.1% IGEPAL, CA-630, in water), pelleted and resuspended in 50 µL transposase reaction mix (1x Tagment DNA buffer, 2.5 µL Tagment DNA enzyme I in water (Illumina)), and incubated at 37°C for 30 min. DNA was purified with Zymo ChIP DNA concentrator columns (Zymo Research). DNA was then amplified with PCR mix (1.25 µM Nextera primer 1, 1.25 µM Nextera primer 2-bar code, 0.6x SYBR Green I (Life Technologies, S7563), 1x NEBNext High-Fidelity 2x PCR MasterMix, (NEBM0541) for 7-10 cycles, run on an agarose gel for size selection of fragments (160-500 bp), and extracted from the gel and paired-end 75 bp sequencing using the Illumina NextSeq 500 platform. Reads were trimmed using TrimGalore and mapped to the UCSC genome build hg38 using STAR. Peaks were then calculated and annotated using the HOMER software package. For agnostic genome-wide characterization of the peaks, sequence depth-normalized bigWig files were used for generating chromatin accessibility profiles using deepTools software. Next, differential accessibility analysis of all identified ATAC-Seq peaks was performed using differential peaks function in HOMER, and fold changes and significance of the resulting differential peaks were plotted as volcano plot using R ggplot2. Genome-wide integration of the ATAC-Seq data with the RNA-Seq data on a gene-by-gene level was performed based on comparing the fold changes of differentially accessible peaks (HOMER differential ATAC peaks) with the fold changes of differentially expressed genes (RNA-Seq expression), using R, and visualization was performed using R ggplot2 and GraphPad Prism software. GSEA of annotated Promoter-TSS peaks was performed using STRING, and overlapping with the Riessland et al dataset was

performed using shared GO terms and enrichment scores present in both datasets. Motif enrichment analysis was performed in HOMER. Statistical enrichment of motifs was performed by using all control iNs as background for AD iN peak and subsequent motif calling. The resulting q-values generated through this method are marked in the figures. Comparisons of peak height between AD and CTL iNs was performed in deeptools using the plotHeatmap function.

ProteinSimple Analysis

ProteinSimple Jess (biotechne) was used for low-input digital capillary Western blot-like protein analysis. FACS-purified iNs were plated on Geltrex-coated wells and harvested with PBS. Pellets were then resuspended in RIPA Lysis and Extraction Buffer (Thermo Fisher) containing the cOmplete EDTA-free Protease Inhibitor Cocktail and PhosSTOP phosphatase inhibitors (Sigma Aldrich). Samples were pooled from 9 CTL and AD lines and analyzed using the 12-230 kDa Jess Separation Module. Concentrations of primary antibodies (CDKN2A 1:100) were adjusted to the technology. All assays were run using the standard default settings provided by ProteinSimple Inc., with the exception of an increased 60-min incubation time for the primary antibodies. Data analysis was performed using Compass software (biotechne).

Statistical Analysis

Statistical tests for NGS datasets were performed using built in normalization and significance correction tools in R, GSEA, STRING, HOMER, DESeq2, and deepTools, Seurat, Monocle, and RnBeads. Adjusted p values (padj) indicate that values were corrected for multiple testing using false discovery rates (FDR). Non-omics quantitative data statistics were calculated using GraphPad Prism software with the method indicated for each figure or methods section; for control versus AD comparisons, unpaired t tests and ANOVAs were used. Significance evaluations are marked as $*p < 0.05$; $**p < 0.01$; $***p < 0.001$; and **** $p < .0001$ in the figures.

Results

The human pre-frontal cortex of AD patients harbors an increased proportion of senescent neurons.

The CDKN2A gene, which encodes the senescence-activating proteins p16INK4a and p14ARF, is consistently upregulated in senescent cells and is considered to be one of the most specific genetic markers of senescence(Rayess, Wang, and Srivatsan 2012). Therefore, we examined CDKN2A expression in postmortem brains from 30 AD patients and 99 sex- and age-matched cognitively normal (NC) controls from the Allen Aging, Dementia, and Traumatic Brain Injury (TBI) study. We found that CDKN2A mRNA abundance was significantly increased in the neuron-rich pre-frontal cortex (PCx) of AD patients (Fig2.1A) (Miller et al. 2017); by contrast, no CDKN2A expression changes were detected in the frontal white matter (FWM), which contains mostly axons and glia (Fig2.1A, SupFig2.1A). CDKN2A expression also trended higher in other neuron-rich areas of AD patients, and CDKN2A increased in expression during aging in the human brain (SupFig2.1B-C). Given the field's evolving understanding of cellular senescence as a phenomenon whose features can materialize in non-dividing cells late in life (Sapieha and Mallette 2018), and the reports of neuronal senescence in rodents and humans (Moreno-Blas et al. 2019; Arendt, et al. 1996), we asked if neurons contribute to increased CDKN2A expression in the PCx. We obtained PCx brain tissue from a clinically characterized cohort of mid-stage AD patients (Braak III-IV, n=10) and age/sex-matched cognitively normal controls (n=10) and performed fluorescence immunohistochemistry for p16INK4a (p16) and the mature neuron marker NeuN (Fig2.1B, Table2.1). Remarkably, we observed a distinct subpopulation of NeuN/p16 double-positive neurons in all aged brains, and these cells were significantly (about 3-fold) more abundant in AD brains (Fig2.1B-C). NeuN/p16 double-positive cells represented a minority of NeuN-positive cells, and the majority of p16-positive cells in the brain were NeuN-negative (Fig2.1C). The sparse number of p16-positive cells is consistent with the general view that senescent cells represent a minority within their resident tissue and supports the notion that senescent neurons are less abundant than senescent glia(Jurk et al. 2012). Further, these rates are consistent with a recent eigengene approach to estimate the abundance of senescent neurons in the cortex of AD patients(Dehkordi et al. 2021). Due to bystander effects, senescent

cells tend to cluster in their resident niche (da Silva et al. 2019), so we examined p16 clustering by calculating adjacency scores of p16 in reference to NeuN or DAPI loci(Andrey et al. 2010). As expected, p16 localization showed a clear clustering pattern, with p16 foci significantly closer to their nearest neighbor than a randomized subsampling of tissue loci (Fig2.1D-E). Notably, p16-positive cells were significantly more likely to cluster around NeuN-positive cells, indicating that senescent-like neurons represent a potential source for secreted bystander factors and might act as a starting point for senescent cell clusters in the aged human brain. This effect appeared to be neuron-specific, as we detected significantly weaker clustering of p16 near DAPI foci than NeuN loci (Fig2.1D). Further, clustering tended to be elevated in AD (SupFig2.1D). These data suggest that neurons expressing p16INK4a are more common in the brains of AD patients and that senescent-like cells, including neurons, tend to cluster together in a pattern consistent with bystander senescence initiation.

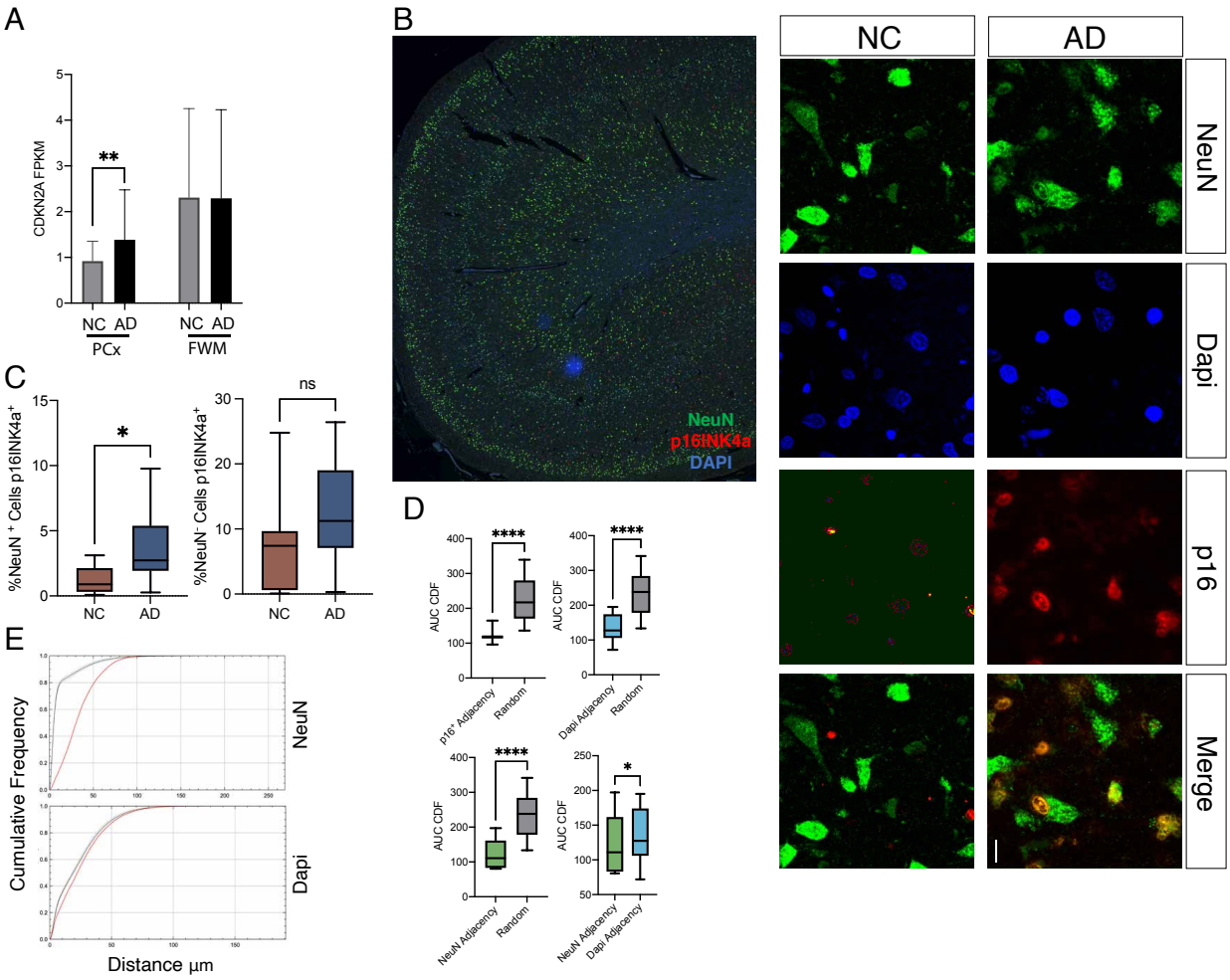

Figure 2.1: The human AD brain harbors an increased proportion of senescent neurons (A) Expression of CDKN2A in the brains of Alzheimer's disease (AD) patients and cognitively normal (NC) controls in the prefrontal cortex (PCx) and frontal white matter (FWM) (Wald test DESeq2, n=30 AD; 99 NC). (B) Fluorescence microscopy analysis of p16 expression in postmortem PCx tissue from AD and NC patients, left 20X, right 63X, scale bar=16 µm. (C) Quantification of p16 expression in NeuN+ cells (left) and DAPI+ nuclei (right) (n=10 AD; 10 NC, unpaired t-test). (D) Clustering analysis of p16 signal adjacent to other p16+ loci (top left), DAPI+ loci (top right), NeuN+ loci (bottom left), and NeuN adjacency compared to DAPI adjacency (bottom right) (n=10 AD; 10 NC, paired t-test). (E) Example cumulative distribution function for p16 signal near NeuN+ and DAPI+ loci used to calculate the adjacency AUC in D. * $p < .05$, ** $p < .01$, **** $p < .0001$.

Senescent transcriptomic and epigenomic patterns in age-equivalent AD iNs

Given the increased abundance of p16-expressing neurons in AD patient brains, we next sought to examine the extent to which aged iNs from AD patients display senescence-related features. To functionally assess the molecular features of senescence in human neurons in AD, we generated iNs from a cohort of AD patients and non-demented controls. Briefly, we obtained punch biopsies from 16 AD (13 sporadic, 3 familial) patients and 19 non-demented controls (CTL) for iNs. It has been shown that donor-specific iNs capture age- and disease-specific molecular pathologies, including transcriptomic, mitochondrial, and epigenetic aging signatures in aging iNs, (Mertens, et al. 2015b; Kim, et al. 2018; Herdy, et al. 2019) cell fate instability in AD iNs, (Mertens, et al. 2021) and other phenotypes (Huh, et al. 2016; Victor, et al. 2018; Tang et al. 2018). Our cohort includes patients aged 57-88 (Fig2.2A), and control donors were further matched according to age, sex, and ApoE genotypes to mitigate genetic bias. Following direct Ngn2/Ascl1-mediated iN conversion for 21 days and PSA-NCAM FACS-based purification, we obtained mature cortical iNs as previously reported (Ladewig et al. 2012; Mertens, et al. 2015b; Mertens, et al. 2021; Kim, et al. 2018; Vadodaria et al. 2016) (SupFig2.2A), with equivalent efficiency in AD and CTL lines (SupFig2.2B-C). To explore AD-associated changes in senescence gene expression in AD iNs, we collected whole transcriptome RNA-Seq data from the iNs (n=35). To identify changes specific to aged neurons, we also prepared RNA-Seq from three control groups: i) isogenic iPSC-derived neurons (iPSC-iNs) that appear transcriptionally fetal relative to a human brain development atlas (n=20), ii) the corresponding unconverted fibroblasts (n=35), and iii) unconverted iPSC lines from the same cohort (n=20) (Fig2.2A). Differential expression analyses of AD vs CTL for all four cell types (iNs, iPSC-iNs, fibroblasts, and iPSCs) were ranked separately according to significance then log2FC for Gene Set Enrichment Analysis (GSEA) of a list of canonical senescence genes (Reactome R-HSA-2559583). Interestingly, we observed a strong and significant enrichment of senescence genes exclusively in AD iNs but no significant enrichment in rejuvenated AD iPSC-derived neurons, fibroblasts, or iPSCs (Fig2.2B-C).

Importantly, senescence genes are predominantly upregulated in AD iNs and include 33 significantly upregulated genes such as the classic senescence and inflammation markers CDKN2A, MMP3, CXCL8, CXCL5, CDKN1C, and IL6. Only three were significantly downregulated (Coppé et al. 2010). Notably, two of these three downregulated senescence genes also have neuron-specific functions (NMDA receptor-associated RAB5B gene, and the neuronal morphogenesis IGSF3 gene), which might explain why they are not upregulated (Fig2.2C) (Mertens, et al. 2021; Chen et al. 2015; Usardi et al. 2017). Senescence genes were also significantly upregulated in iNs relative to iPSC-iNs for all patients, highlighting the adult-specific and age-dependent nature of this activation (SupFig2.2D). To validate and better characterize the relative contribution of senescence genes in human neurons, we integrated our iN transcriptome data with RNA-Seq data of human embryonic stem cell-derived neurons where senescence was induced by knockout of SATB1 (Riessland et al. 2019). In addition to a significant loss of SATB1 expression in AD iNs, rank rank hypergeometric order (RRHO) analysis confirmed the hypothesis that AD iNs are transcriptionally closer to senescent SATB1-knockout neurons than to wild type (WT) neurons (SupFig2.2E). Next, we examined the overlap in genes that were significantly differentially expressed between both AD and CTL iNs and SATB1 KO and WT neurons, which revealed 59 co-upregulated and 44 co-downregulated genes (padj < .05). GO analysis of upregulated genes identified a significant enrichment of genes related to extracellular matrix (ECM) reorganization, including metallopeptidases (ADAMTS5), collagenases (COL11A1), and glypicans (GPC4). Thus, endogenous transcriptional activation of a neuronal senescence gene expression profile is specific to aged human neurons and enriched in neurons from AD patients. The neuronal senescence profile is characterized by functional genetic markers of senescence, including increased CDKN family expression, ECM modification, and inflammatory gene expression.

In response to aging-related stress, state transition towards senescence is known to be deeply anchored in epigenomic landscape changes that establish senescence-associated gene

expression. To assess if the increased expression of senescence genes in AD neurons is founded in their epigenomes, we examined chromatin accessibility using assay for transposase-accessible chromatin sequencing (ATAC-Seq) of PSA-NCAM purified iNs (n=10 AD; 11 CTL) and CpG DNA methylation (DNAm) status using the Illumina MethylEPIC chip (n=8 AD; 8 CTL). Consistent with their higher gene expression, ATAC-Seq revealed that senescence genes were markedly more accessible in AD iNs, with an average of 31% more peaks per gene (Fig2.2D). Similarly, average promoter DNAm in CTL iNs inversely correlated with expression on a gene-by-gene basis and showed the expected overall negative relationship between promoter methylation and expression of senescence genes (Fig2.2E). Interestingly, increased methylation of senescence gene promoters in AD iNs appeared to be insufficient to dampen their expression, and AD samples counterintuitively displayed an overall positive correlation of promoter methylation to gene expression (Fig2.2E). At the same time, overall senescence gene promoter methylation was largely similar in both groups (SupFig2.2F). Thus, as high promoter methylation is typically associated with decreased expression (Moore, Le, and Fan 2013), these findings indicate a disruption of gene regulation by promoter methylation in senescence genes of AD iNs. Next, to specifically assess neuron-specific functions that are rooted in epigenetic and transcriptomic changes, we filtered for all the genes that showed increased promoter ATAC-Seq accessibility, lower promoter methylation, and increased RNA-Seq expression exclusively in the AD iNs but not in fibroblasts from the same patients (n=1225 genes). We then performed GSEA, which revealed that five of the top 20 enriched pathways were senescence-related terms, including Oxidative Stress Induced Senescence, DNA Damage Induced Senescence, and the Senescence Associated Secretory Phenotype (Fig2.2F). Consistently, many gene sets were shared with ATAC-Seq data from SATB1-knockout neurons, further indicating a compromised neuronal chromatin landscape (SupFig2.2G) (Riessland, et al. 2019). This notion is supported by analysis of the replication-independent histone variant H2AFJ, which is preferentially upregulated in senescent cells (Contrepois et al. 2017). H2AFJ transcripts as well as its associated gene targets

were significantly upregulated in AD iNs (SupFig2.2H), and immunocytochemistry of H2AFJ revealed significantly brighter H2AFJ staining in AD iNs (Fig2.2G). We next probed for potential key upstream effectors in our ATAC-Seq data that had the potential to override DNAm marks and drive senescent gene expression in AD iNs. We found that regions containing the binding motif for the transcription factor ETS1 were significantly more open in AD iNs (Fig2.2H), and ETS1 is known to drive expression of p16INK4a and bind both hypo- and hyper-methylated promoters in replicative senescence (Ohtani et al. 2001; Hänzelmann et al. 2015). Thus, ETS1 is a tangible example of a factor that can drive senescence gene expression despite increased promoter methylation in human neurons (Fig2.2H).

Although we did not observe substantial senescence gene activation in fibroblasts and used passage-equivalent lines in our experiments, telomere attrition during fibroblast passaging might contribute to a compromised neuronal chromatin landscape. Therefore, we sought to determine if iN senescence was independent of telomere attrition by measuring telomere content by qPCR in PSA-NCAM purified AD and CTL iNs (n=9 AD; 9 CTL) across 22 population doublings (passages 10-32). No significant difference in the rate of telomere attrition between AD and CTL was detected in the fibroblasts (Fig2.2I). Likewise, the average absolute telomere content per genome was unchanged (234 Kb in AD and 228 Kb in control iNs)(Cawthon 2002; O'Callaghan et al. 2008). Another independent estimation of population doublings by CpG methylation indicated no significant difference in doublings of iN or parent fibroblast lines (SupFig2.2I) (Koch and Wagner 2013). Telomere shortening may occur in replication-independent scenarios upon downregulation of the telomere factor *POT1* and shelterin subunit *TERF2;* however, we observed no difference in the expression of these two genes in AD and CTL iNs (SupFig2.2J) (Denchi and de Lange 2007).

Taken together these data indicate that a compromised epigenetic landscape in AD iNs, including relaxation of chromatin at senescence genes, upregulation of a senescence-related histone, dysregulation of methylation at senescence promoters, and ETS1 transcription factor

binding, all contribute to the increased expression of senescence genes in AD neurons, and this expression is independent of telomere attrition and not a ‘carryover’ of proliferative senescence in parent fibroblasts.

Figure 2.2: Senescence changes in the transcriptome and epigenome of aged AD neurons. (A) Experimental schema. (B) GSEA of differential expression of AD and CTL in four cell types - iNs (aged induced neurons n=35), iPSC-iNs (rejuvenated young neurons, n=20), iPSCs (n=20), and fibroblasts (n=35) - indicates a significant enrichment exclusively (q-value = .012) in AD iNs. (C) Volcano plot of genes used for GSEA in B in iNs. Genes above the significance threshold (padj < .05, Log2FC >1) are colored red. (D) Histogram of peaks averaged from 10 AD and 10 CTL iN samples across senescence genes, including the transcription start site (TSS) and transcription end site (TES) and 2kb window (left). Peak counts in senescence genes are significantly higher in AD iNs than in CTLs (right); each point represents the number of peaks in a single gene in our senescence gene list (MannWhitney test). (E) Increased promoter methylation is negatively associated with senescence gene expression in CTL iNs and positively associated with expression in AD iNs (n=8 AD; 8 CTL). (F) GO analysis of genes with low promoter methylation and high expression in AD iNs. (G) H2AFJ is expressed significantly higher in AD iNs (right) and shows significantly brighter staining by ICC (left); scale bar = 16 μm. (H) The binding motif for the transcription factor ETS1 is significantly enriched in open chromatin in AD (Target) relative to CTL (Background) iNs. (I) There are no significant differences between telomere erosion in AD and CTL parent fibroblast lines or in total telomere content, as measured by qPCR. * p < .05, ** p < .01.

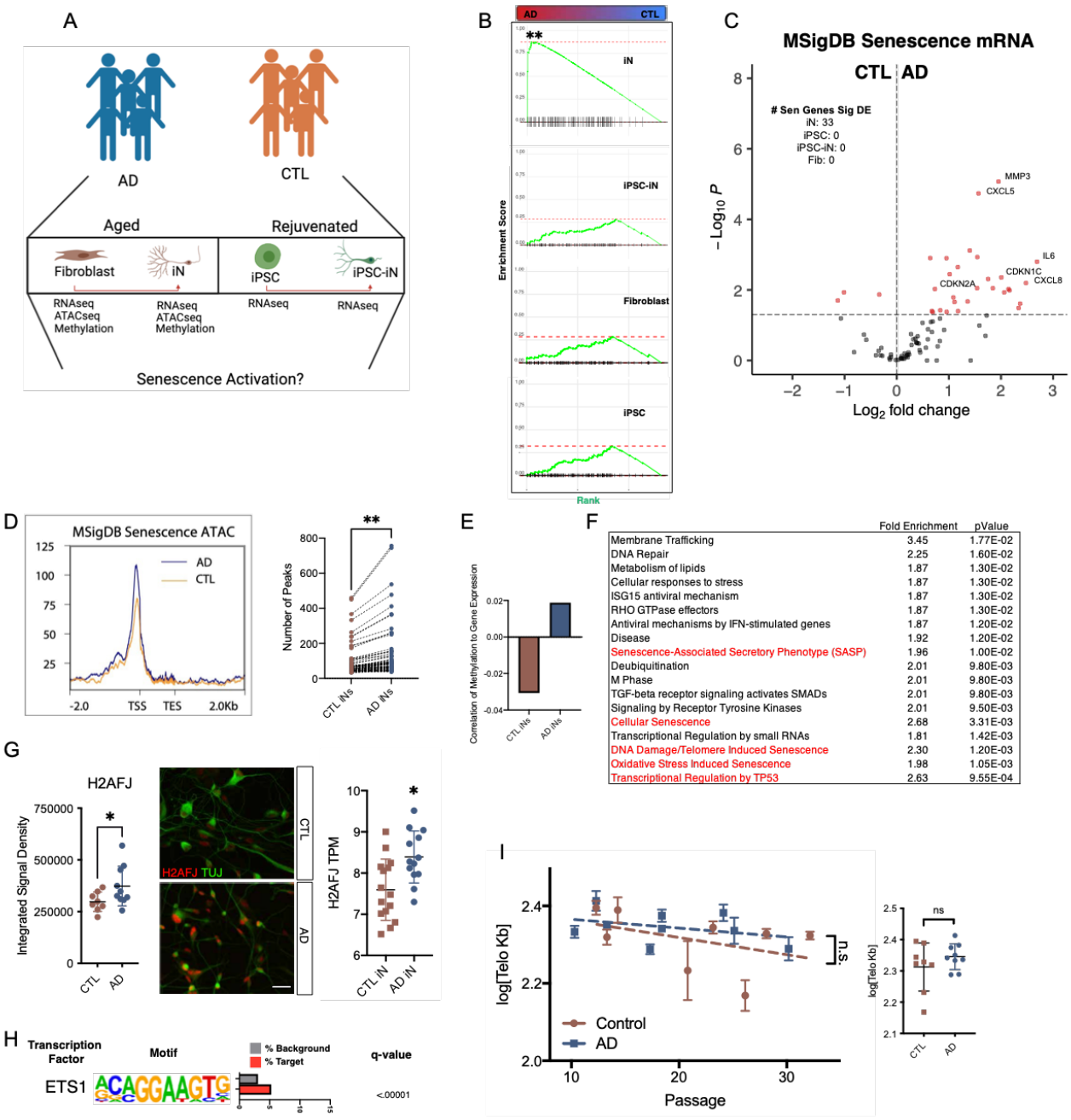
A
AD
CTL
Aged
Rejuvenated
Fibroblast
iN
iPSC
iPSC-iN
RNAseq
ATACseq
Methylation
RNAseq
ATACseq
Methylation
RNAseq
RNAseq
Senescence Activation?
B
AD
CTL
**
iN
iPSC-iN
Fibroblast
iPSC
Enrichment Score
Rank
C
MSigDB Senescence mRNA
CTL
AD
Sen Genes Sig DE
iN: 33
iPSC: 0
iPSC-iN: 0
Fib: 0
MMP3
CXCL5
IL6
CDKN1C
CXCL8
CDKN2A
−Log10 P
Log2 fold change
D
MSigDB Senescence ATAC
AD
CTL
-2.0
TSS
TES
2.0Kb
**
Number of Peaks
CTL iNs
AD iNs
E
Correlation of Methylation to Gene Expression
CTL iNs
AD iNs
F
Fold Enrichment
pValue
Membrane Trafficking 3.45 1.77E-02
DNA Repair 2.25 1.60E-02
Metabolism of lipids 1.87 1.30E-02
Cellular responses to stress 1.87 1.30E-02
ISG15 antiviral mechanism 1.87 1.30E-02
RHO GTPase effectors 1.87 1.30E-02
Antiviral mechanisms by IFN-stimulated genes 1.87 1.20E-02
Disease 1.92 1.20E-02
Senescence-Associated Secretory Phenotype (SASP) 1.96 1.00E-02
Deubiquitination 2.01 9.80E-03
M Phase 2.01 9.80E-03
TGF-beta receptor signaling activates SMADs 2.01 9.80E-03
Signaling by Receptor Tyrosine Kinases 2.01 9.50E-03
Cellular Senescence 2.68 3.31E-03
Transcriptional Regulation by small RNAs 1.81 1.42E-03
DNA Damage/Telomere Induced Senescence 2.30 1.20E-03
Oxidative Stress Induced Senescence 1.98 1.05E-03
Transcriptional Regulation by TP53 2.63 9.55E-04
G
H2AFJ
Integrated Signal Density
CTL
AD
H2AFJ TUJ
CTL
AD
H2AFJ TPM
CTL iN
AD iN
H
Transcription Factor
Motif
% Background
% Target
q-value
ETS1
<.00001
I
log[Telo Kb]
Control
AD
Passage
n.s.
ns
CTL
AD

AD iNs mirror postmortem neuronal senescence of patient brains and present bona fide in vitro markers of cellular senescence.

Because an increased fraction of NeuN-positive cells in the AD patient brains expressed p16, and because the CDKN2A locus was more accessible and CDKN2A mRNAs for the p16 isoform were more abundant in AD iNs, we next sought to examine the p16 protein in our iN model (SupFig2.3A). Consistently, a capillary Western blot analysis of protein extracted from PSA-NCAM purified iNs confirmed increased p16 protein levels in AD iNs (Fig2.3A). Immunocytochemical analysis showed that AD iNs had significantly more p16-positive cells and a higher fluorescence intensity of p16 staining within the positive fraction (Fig2.3B). Notably, the three-fold increase in the number of p16-postitive neurons in AD iNs over controls was remarkably similar to what we observed in postmortem tissue, though the overall abundance of senescent neurons was larger *in vitro* than *in vivo* by four-fold. These results suggest that iNs faithfully recapitulate the senescence activation observed in NeuN-expressing cells in the AD brain and that iNs can be used to model spontaneous neuronal senescence *in vitro*.

We next explored if AD iNs present classic biomarkers of senescence. First, we tested for the common senescence marker senescence-associated beta galactosidase (BGal)(Moreno-Blas, et al. 2019; Chow et al. 2019). Consistently, AD iNs were significantly more likely to be BGal-positive than control iNs (Fig2.3C), and no increased BGal abundance was observed in parallel fibroblast cultures (SupFig2.3B). Importantly, neuronal senescence appeared to be largely independent of the number of BGal-positive cells in the fibroblast culture or the donor ages at biopsy, as neither rate correlated with the fraction of BGal-positive iN cultures (SupFig2.3C). We also observed no significant differences in senescence marker abundance when comparing sex as a biological variable in our cohort (SupFig2.3D-E). As a secondary measure of BGal activity, we used a C_{12}FDG strategy that offers a fluorogenic readout of BGal activity that can be measured via FACS. We observed clear population separation between C_{12}^{+} and C_{12}^{-} in PSA-NCAM^{+} cells, and AD iNs had a significantly larger C_{12} population than CTL lines measured in a subset of our

cohort (n=8) (Fig2.3D). Because other characteristic features of senescent cells are increased cytoplasmic and nuclear volumes (McHugh and Gil 2018), we extracted cellular volumes from forward scatter area (FSC-A) data and measured the nuclear area of purified iNs by DAPI staining. Indeed, FSC-A values were substantially higher (SupFig2.3F), and ROI-based nuclear areas were significantly larger in AD iNs compared to controls (Fig2.3E), and AD nuclei tended to be larger in post-mortem tissue, though not significantly (SupFig2.1E). Two common changes accompanied by alterations in nuclear size in senescent cells are the loss of Lamin B1 in the nuclear envelope and formation of senescence associated heterochromatin foci (SAHF). We examined AD and CTL iN lines for these two markers but did not detect any differences in Lamin B1 (SupFig2.3G) or the formation of SAHF (Data not shown); these markers may be more common features of senescence in replicative cells.

We next sought to test if senescence markers were specific to aged neurons or if they also appeared in young neurons from the same patients. Matched PSA-NCAM purified iPSC-iNs from three AD patients from our cohort lacked BGal signal and p16 immunoreactivity (Fig2.3F-G). Consistently, p16 mRNA was not detected in iPSC-iNs by RNA-Seq (Fig2.3H). These data, together with the low level of senescent gene expression observed in iPSC-iNs (SupFig2.2D), suggest that senescence activation is more likely to occur in aged neurons and that rejuvenated fetal-like iPSC-iNs have lower rates of spontaneous senescence under baseline culture conditions (Fig2.3I).

Figure 2.3: iNs present *bona fide* markers of cellular senescence. (A) AD iNs have increased p16 protein measured by chemiluminescence in a capillary Western blot analysis (n=9 AD; 9 CTL, unpaired t-test). (B) Example confocal images of p16 co-stained with Tuj in PSA-NCAM-sorted iNs; scale bar = 16 μm (left). AD iNs have a significantly increased population and intensity of $p16^+$ cells (right). (n=9 AD; 8 CTL, unpaired t-test). (C) Example picture of PSANCAM-sorted iNs stained for SA-B-Gal and co-stained for mature neuron marker NeuN (left); scale bar = 8 μm. Quantification of $BGal^+$ rates in AD and CTL iN cultures (right). (n=17 AD, 16 CTL, unpaired t-test). (D) Example FACS gating to separate $C12^+$ from $C12^-$ cells (left). AD iNs have a significantly larger $C12^+$ population as indicated by a higher geometric mean of C12 signal (right). (n=4 AD; 4 CTL, unpaired t-test). (E) Example images of CTL and AD nuclei stained with DAPI (left). AD iNs have increased nuclear area measured by integrated DAPI signal (right). (n= 10 AD and 10 CTL patients, unpaired t-test). (F) Example images of p16 and UNG:GFP in iPSC-derived AD iNs; scale bar = 16 μm (left). Quantification of p16 signal intensity in iPSC-derived AD iNs (right). (n=3 iPSC-iN; 3 iN, unpaired t-test). (G) Example BGal staining in iPSC-iN cultures; scale bar = 8 μm (left). Quantification of $BGal^+$ rates in AD iPSC-iNs or fibroblast iNs (right). (n=3 iPSC-iN; 3 iN, unpaired t-test). (H) p16ink4a is not expressed in iPSC-iNs. (I) Senescent-like phenotypes manifest only in aged human neurons, but young rejuvenated iPSC-iNs do not present senescence markers under baseline conditions. * $p < .05$, ** $p < .01$, *** $p < .001$, **** $p < .0001$.

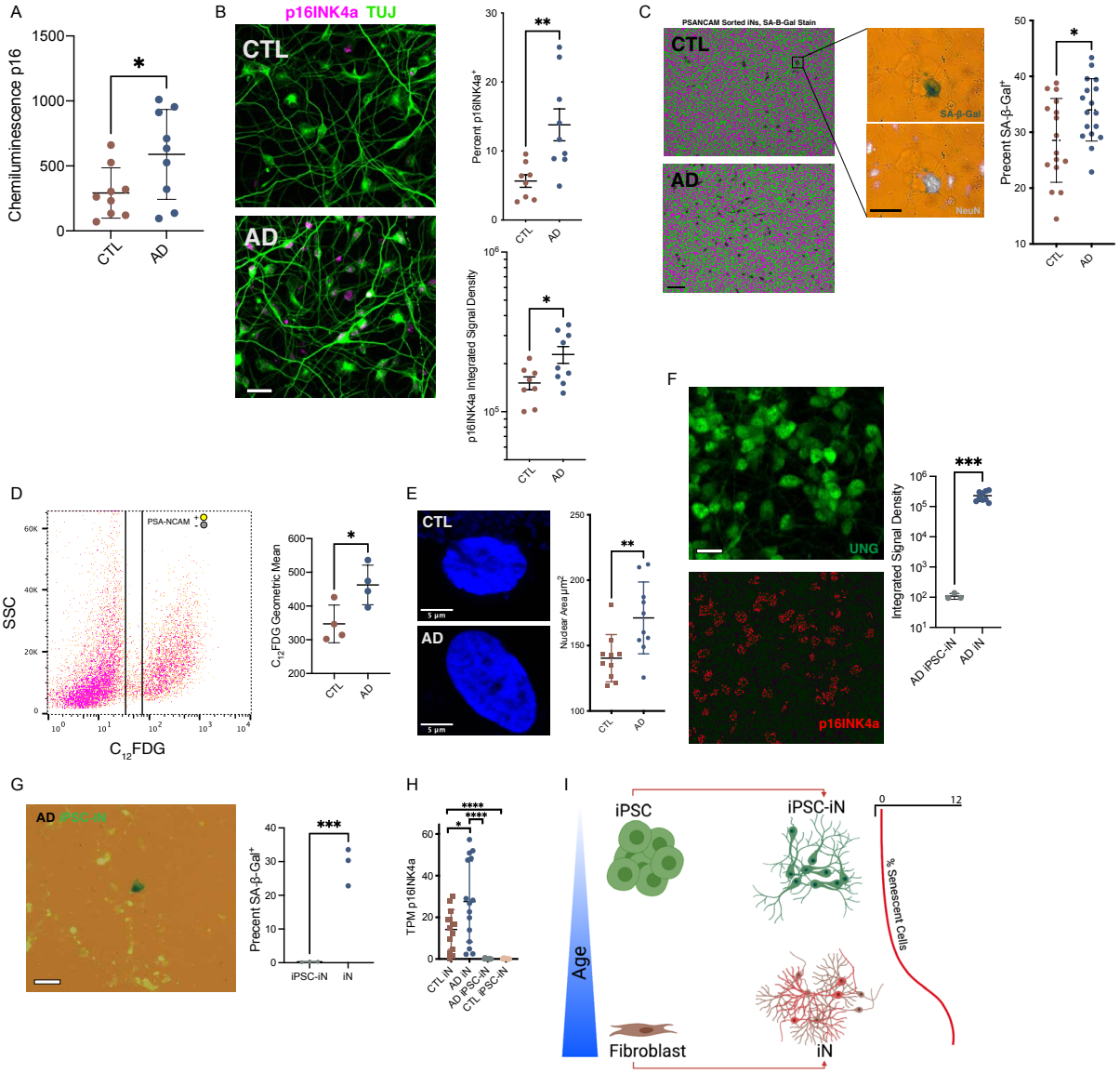
A
Chemiluminescence p16
CTL
AD
B
p16INK4a TUJ
CTL
AD
Percent p16INK4a+
p16INK4a Integrated Signal Density
C
PSANCAM Sorted iNs, SA-B-Gal Stain
CTL
AD
SA-β-Gal
NeuN
Precent SA-β-Gal+
D
PSA-NCAM
SSC
C12FDG
C12FDG Geometric Mean
E
CTL
AD
Nuclear Area µm2
F
UNG
p16INK4a
Integrated Signal Density
AD iPSC-iN
AD iN
G
AD iPSC-iN
Precent SA-β-Gal+
iPSC-iN
iN
H
TPM p16INK4a
CTL iN
AD iN
AD iPSC-iN
CTL iPSC-iN
I
iPSC
iPSC-iN
Age
Fibroblast
iN
% Senescent Cells

Single-cell transcriptomics reveal a neuronal senescence trajectory that culminates in oncogenic challenges and metabolic dysfunction in senescent-like neurons.

Similar to the aged brain, iN cultures from AD and CTL donors show a high degree of heterogeneity with regards to various senescence markers. Thus, some genetic features specific to the minority of senescent neurons might be masked in our initial bulk transcriptome data from 16 AD patients and 19 CTLs. To capture mosaic transcriptional features that describe the path from normal to a senescent-like neuron, and to extract the key features of fully senescent neurons, we performed single-cell transcriptome analysis of non-FACS purified AD and CTL iN cultures (Fig2.4A). In this one case we opted to perform scRNAseq on unsorted cultures that contain a mixture of iNs and unconverted fibroblasts, in contrast to all other previous experiments on PSA-NCAM-purified neurons, to minimize the viability loss caused by flow sorting. We retrieved reliable libraries from 29,515 cells (n= 4 AD, 3 CTL, Table2.2), and we employed a partition-based graph abstraction strategy to resolve transcriptional topology using Monocle3(Cao et al. 2019). UMAP dimensionality reduction identified five transcriptionally distinct clusters in our dataset after filtering for low quality cells (Fig2.4B, SupFig2.4A). As anticipated, we observed undifferentiated and only partially converted fibroblasts that separated from successfully converted iNs based on UMAP clustering. These were characterized by low expression of neuronal fate genes and high expression of fibroblast fate genes (SupFig2.4B). Further, RNA trajectory analysis indicated a clear differentiation continuum from fibroblast to neuron identity (SupFig2.4C), with one cluster capturing fully converted iNs. Pseudo-bulk differential expression analysis between the fibroblast cluster and iN cluster significantly correlated with the transcriptome profiles of bulk fibroblasts versus iNs (SupFig2.4E), and the fraction of cells allocated to the iN cluster was also consistent with the percentage of stringent PSA-NCAM-positive neurons typically observed during FACS purification (SupFig2.4D). AD and CTL iNs differentiated at equal efficiencies, and there was no significant difference in the correlation of AD or CTL iNs to fibroblast gene expression. Finally, we assessed the transcriptional neuronal subtype identity within the iN cluster and, consistent with

bulk data, we found that most iNs expressed glutamatergic or GABAergic markers but virtually no dopaminergic, cholinergic, or serotonergic cells (SubFig2.4F).

Next, we sought to isolate senescent from non-senescent cells within the iN cluster by assigning cells a senescent module score. On the pseudo-bulk level, AD iNs had a higher overall senescence module score than CTLs, but no significant difference was detected in fibroblasts (Fig2.4C, SupFig2.5A). We separated the top and bottom 15% of module-scored iNs to obtain sen-high and sen-low bins and performed differential expression analysis (Fig2.4D). Sen-low and sen-high iNs significantly differed in their expression of CDKN2A, indicating that our scoring approach was successful (SupFig2.5B). Unbiased differential expression analysis of the sen-low and sen-high populations revealed 865 genes that were significantly differentially expressed (qvalue < .05); 644 upregulated and 221 downregulated in sen-high iNs (Fig2.4D, SupFig2.5C). GSEA of these genes revealed that senescence in neurons is accompanied by decreased expression of synaptic and neuronal functionality genes, indicating that in human neurons the senescent state underlies compromised cellular functionality (Fig2.4E). Further, we detected changes in gene sets for major metabolism pathways in senescent iNs, with a significant loss of oxidative phosphorylation and TCA electron transport (Fig2.4E). Notably, senescent-like iNs showed a significant gain in the expression of several functional gene sets, including genes related to extracellular matrix organization, DNA damage repair pathways, and pro-inflammatory SASP. Although these are all classic features of cellular senescence in other cell types, the marked increase in SASP-related mRNA abundance in iNs was surprising. Importantly, this SASP signature was absent from fibroblasts and occurred specifically in iNs from AD patients (SupFig2.5F). We hypothesize that neurons themselves might secrete SASP factors, which could explain the bystander effects observed in post-mortem AD brain tissues, and that senescent neurons might trigger pro-inflammatory cascades in AD.

To evaluate molecular features specific to senescence in AD neurons, we contrasted AD from control iNs that binned into sen-low and sen-high groups (SupFig2.5D). Interestingly,

differential expression analysis detected more transcriptional differences between AD and control iNs in the sen-high group (n=227 genes) than in the sen-low group (n=62 genes), and 36 genes were shared between the groups (SupFig2.5D). Next, we examined putative functional protein-protein interaction networks of genes upregulated in AD iN in sen-high and sen-low groups separately. Two distinct networks were upregulated in sen-low: i) neuron development (including terms related to morphogenesis, nephron development, and nervous system development), and ii) metabolic changes (including nucleoside metabolism, ATP synthesis, and electron transport chain). In contrast, sen-high AD iNs gained a pro-inflammatory transcriptional network, with a trio of cytokine- and interleukin-related terms, as well as a significantly expanded network of metabolic changes (Fig2.4F). This finding indicates that, in non-senescent neurons, AD iNs experience initial metabolic changes and neuron development challenges that proceed to an expanded metabolic reprogramming and inflammatory activation after senescence induction. To further examine the senescence trajectory in aged human neurons, we employed reverse graph embedding to order single cells along a pseudotime corresponding to increased CDKN2A expression, allowing us to examine genes that changed across this trajectory and the relative abundance of patient populations (Fig2.4G). Consistent with their increased senescence score, AD iNs were overrepresented at late, high CDKN2A pseudotimes (Fig2.4H). In addition to CDKN2A, CDKN1D and CDKN1C followed this trajectory of increased expression across pseudotime. Notably CDKN1A was the exception, as its expression fell at late pseudotimes. Interestingly, CDKN1A is known to be active early in senescence and to decrease during late senescence when other genes such as CDKN2A become active, suggesting that this pattern is maintained in senescence in neurons (Stein et al. 1999). Other genes that increased across senescence pseudotime include potent inflammatory genes, including CXCL5/8, CST5, and IL7 (Fig2.4H, SupFig2.5E).

Finally, we sought to validate these results in an independently generated post-mortem AD scRNAseq dataset (SupFig2.5G) (Morabito et al. 2021). We extracted 6,369 excitatory

neurons from this dataset (4,725 AD, n= 11 and 1,644 healthy, n=7), as excitatory neurons are reported to be the most prone to senescence-related changes in AD. Cells were then arranged in pseudotime corresponding to increased CDKN2A expression, where we again observed an overrepresentation of AD neurons at late, high-senescence pseudotimes. Likewise, inflammatory gene expression, matrix-modifying genes, and co-expression of CDKN family members followed a similar trajectory in post-mortem neurons as iNs. Differential expression analysis across senescence pseudotime captured gene networks related to neurodegeneration and loss of functional synaptic genes, as well as metabolic dysfunction with the loss of CAMP signaling (SupFig2.5H). The prominent loss of synapse-related genes further suggests that senescent neurons have impaired function both *in vitro* and *in vivo.* Thus, both a scoring and reverse graph embedding approach identified increased senescence gene expression in AD iNs, suggesting that early versus late senescence in neurons can be distinguished by initial metabolic and oncogenic challenges that culminate in a pro-inflammatory response and metabolic reprogramming in deep senescence.

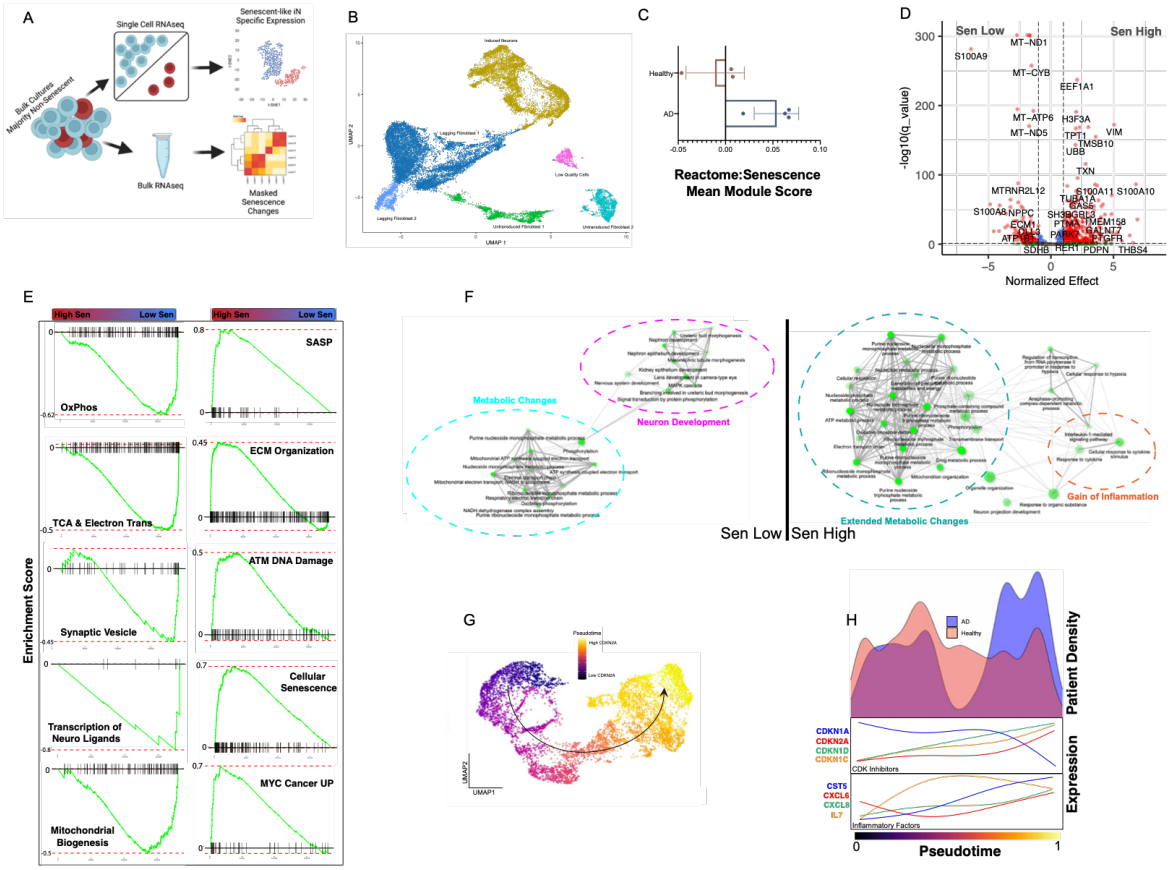

Figure 2.4: scRNAseq indicates oncogenic challenges and metabolic dysfunction in senescent neurons. (A) scRNAseq allows us to discriminate senescent gene expression from the majority of non-senescent cells that mask expression in bulk RNAseq. (B) UMAP clustering of all unsorted fibroblast to iN cultures after 3 weeks of conversion from 4 AD and 3 CTL patients. (C) Mean module score for each patient in iNs. (D) Volcano plot of genes differentially expressed between sen-low and sen-high iNs. (E) GSEA of gene sets enriched (right) or depleted (left) in sen-high cells. (F) Gene network analysis of genes enriched in AD iNs in sen-low (left) or sen-high (right) populations. (G) UMAP projection of iNs colored by their rank in pseudotime analysis tracking the expression of CDKN2A. (H) Density plot of patient proportions across CDKN2A pseudotime and gene expression changes across pseudotime.

AD iN SASP-conditioned media triggers astrogliosis.

A minority of senescent cells can have an outsized impact on tissue homeostasis through paracrine pro-inflammatory SASP molecules (Coppé, et al. 2010), and reactive astrogliosis is now widely considered to be one of the defining pathological features of AD(Rodríguez et al. 2009). Our single-cell RNA-Seq data indicate that deep neuronal senescence is characterized by a pro-inflammatory SASP-related gene expression signature specifically in AD iNs, and we wondered if AD iNs were capable of releasing SASP factors into the media, which could trigger astrogliosis. We obtained CSF from a cohort of 184 patients (n= 102 AD, 82 NC) and separately prepared conditioned media (CM) from six AD and six CTL PSA-NCAM-purified iN cultures. We measured inflammation traces using a proximity extension assay based on oligonucleotide-linked antibodies (Fig2.5A). Remarkably, 21 of the 40 overlapping probes showed the same direction of change between AD and CTL patient samples from both CSF and iN CM samples, indicating that these signaling factors were indeed released by neurons in an AD-specific manner (Fig2.5B, Table2.3). Notably, AD patients' CSF had increased levels of known SASP proteins, including CXCL5/6/9, CCL23/11, IL7, and MMP10 (Basisty et al. 2020). CST5, an inflammatory factor recently described to be active at the earliest stages following traumatic brain injury, was also upregulated in both CSF and iN samples (Hill et al. 2018). Furthermore, three of the identified upregulated proteins in AD CSF and AD iNs (MMP10, STAMBP, and EIF4EBP1) were previously discovered as AD biomarkers(Whelan et al. 2019). To directly assess if AD iN-derived SASP factors were a sufficient source to trigger astrocyte reactivity, we exposed healthy ApoE3 homozygous primary human cortical astrocytes, which expressed the appropriate receptors for our identified inflammatory targets, to CM from AD and control iN cultures (Fig2.5A, SupFig2.6A-B,E-F). Interestingly, both AD and control iN CM triggered an increase in $GFAP^+$ area, indicating that the secretome of aged human iNs was sufficient to activate human astrocytes. Importantly, we observed that the AD iN's, but not fibroblast or iPSC-iN's, CM initiated a hyperreactive state in the astrocytes, which was evident from higher $GFAP^+$ area and significantly brighter GFAP signals

(SupFig2.6B-D). Although higher GFAP is associated with astrocyte reactivity, it is also expressed in non-reactive astrocytes. To validate and further assess astrocyte reactivity in response to AD iN-derived SASP factors, we assessed the transcriptomes of human astrocyte cultures by RNA-Seq exposed to either control or AD iN CM. Differential expression analysis identified 1,071 genes upregulated and 981 genes downregulated in astrocytes in response to AD iN CM (padj <.05, abs[log2FC] > 1)(Fig2.5C). Genes known to characterize reactive astrogliosis were widely upregulated following exposure to AD CM, including genes related to the cytoskeleton (nestin, vimentin), metabolism (ALDOC, FABP7), chaperones (CRYAB), secreted proteins (C3, Serpina3n, IL6), signaling receptors (NTRK2, IL17R), and downregulation of glutamate transporters (EAAT1/2) (Fig2.5D) (Escartin et al. 2021). Interestingly, the most significantly downregulated gene was TIMP3, a matrix metalloprotease inhibitor whose targets include MMP10, one of the factors we identified as significantly increased in AD CSF and secreted by AD iNs (Visse and Nagase 2003). Next, we mapped our data to single-cell RNA-Seq data from post-mortem tissue astrocytes extracted from patients with or without AD pathology (Mathys et al. 2019). We found that 177 of the 537 genes that were differentially expressed (padj <.05, log2FC > 1) in AD astrocytes *in vivo* were also significantly differentially expressed after exposure to AD CM, including loss of glutamate transporters and synapse-related genes (SupFig2.6G). Consistently, RRHO of the log2FC-ranked differentially expressed genes between AD and CTL iN CM-treated astrocytes compared to postmortem astrocytes with or without AD pathology found a 1.662-fold increase in control and a 1.625-fold increase in AD gene enrichment in response to AD CM (Fig2.5F).

Because SASP factors can not only trigger inflammatory cascades but also elicit bystander senescence in neighboring cells, we were curious if AD iN CM-treated astrocytes would themselves enter a senescent state. To test this, we compared astrocyte transcriptome profiles to non-senescent vs irradiation-induced senescent astrocytes (Limbad et al. 2020). Interestingly, we found that 83% of the genes whose expression significantly changed after exposure to AD

CM were also significantly differentially expressed in senescent astrocytes. Likewise, RRHO indicated that AD CM-treated astrocytes appeared transcriptionally closer to senescent astrocytes than non-senescent controls (1.21- and 1.2-fold enrichment, respectively) (SupFig2.6H). Together, these results suggest that senescent human neurons can trigger neighboring neurons as well as astrocytes to enter senescence in response to pro-inflammatory SASP factors that are specifically secreted by AD iNs. Further, neuronal paracrine effects trigger a disease-related reactive pro-inflammatory transcriptomic response and senescent astrocytic state that closely mirror those of reactive astrocytes in the diseased human brain, including cytokine release, loss of synaptic maintenance, changes in metabolism, and morphological changes (Fig2.5E).

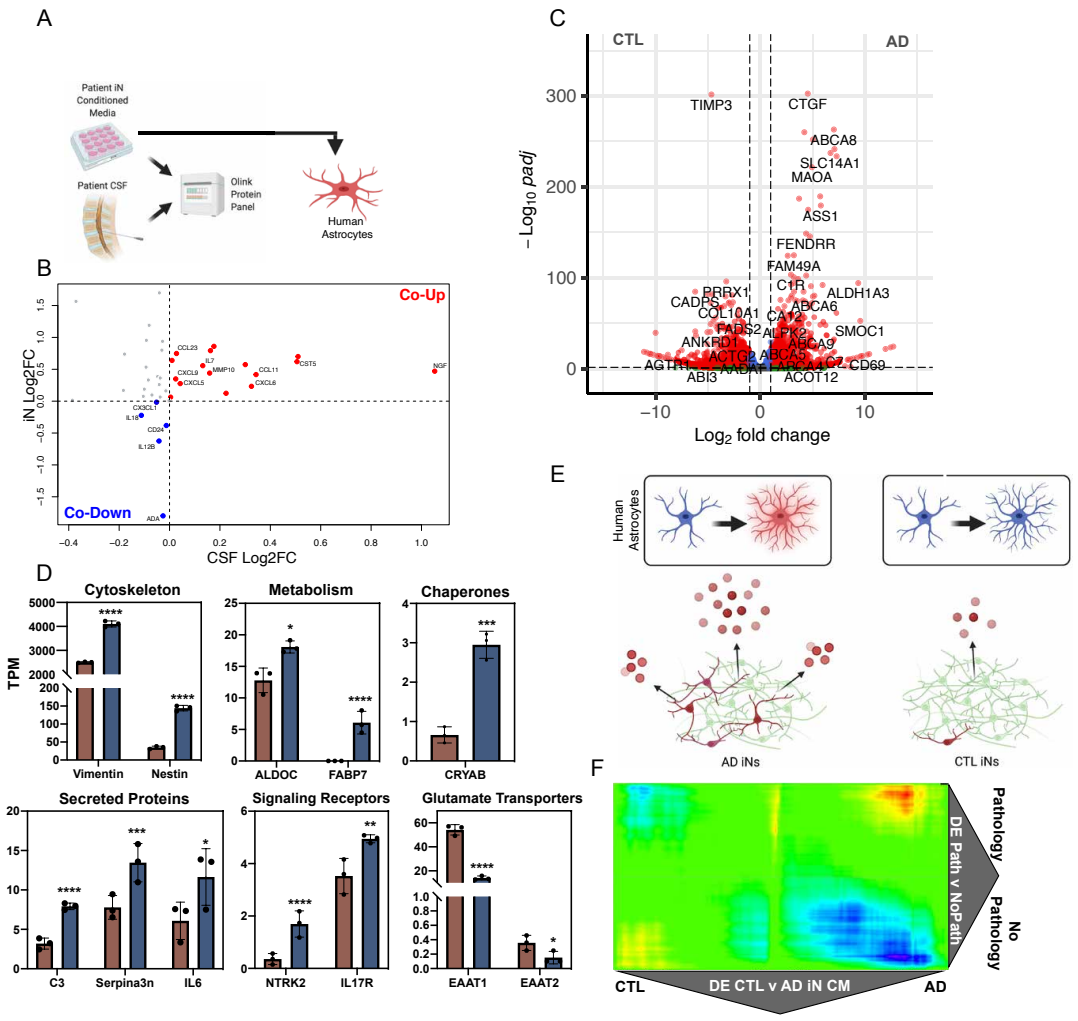

Figure 2.5: AD conditioned media triggers reactive astrogliosis. (A) Experimental paradigm. Cerebral spinal fluid (CSF) and patient iN conditioned media (CM) were submitted for a multiplex inflammation panel, and CM was applied to human astrocytes to evaluate reactivity. (B) Overlap of log2FC of inflammatory probes (AD/CTL) from CSF and iN CM. Co-upregulated in AD in red and co-downregulated in blue. (C) Differential expression analysis between AD and CTL CM-treated astrocytes reveals 981 genes significantly differentially expressed (n=3 astrocyte cell lines). (D) Expression of reactive astrocyte markers in AD or CTL treated astrocytes (n=3, Wald test DESeq2). (E) A larger population of senescent-like neurons triggered a hyperreactive state in human astrocytes. (F) RRHO mapping of the transcriptional overlap between astrocytes from post-mortem patients with or without AD pathology and between astrocytes treated with AD or CTL CM *in vitro*. * $p < .05$, ** $p < .01$, *** $p < .001$, **** $p < .0001$.

Senescence in neurons can be triggered by oncogenes and eliminated with senotherapeutics.

A wide variety of cellular stressors can trigger senescence, but whether these are sufficient to induce senescence in neurons is largely unexplored. Our previous study found that AD iNs experience an oncogenic challenge and de-differentiation stress, and oncogenic stress is one of the most robust methods for senescence induction(Mertens, et al. 2021; Yaswen and Campisi 2007). Therefore, we tested if overexpression of an oncogene could trigger oncogene-induced senescence (OIS) in iNs. Following differentiation, iNs were transduced with a lentivirus for the overexpression of KRasG12V:GFP, an oncogenic form of Ras used widely to trigger senescence, or a GFP control virus (Fig2.6A) (Collado and Serrano 2010). After a week of transgene overexpression, cells were fixed and stained for p16 and NeuN to assess activation of senescence in neurons. Similar to reports in proliferating cells, Ras-induced iNs had significantly higher amounts of p16-positive cells compared to GFP controls (Fig2.6B). Importantly, this senescence activation was not accompanied by a loss of neuronal fate, and proportions of NeuN-positive cells did not differ between Ras- or GFP-treated groups (SupFig2.7A). Further, we did not observe the formation of SAHF in Ras-induced cells that are characteristic of OIS in proliferating cells, indicating that a full DNA damage response (DDR) and consequent establishment of heterochromatin lie downstream of p16 activation as has been reported(Bartkova et al. 2006). However, it remains possible that longer Ras treatments could culminate in DDR and SAHF formation in neurons. These results confirm that oncogenic Ras is sufficient to produce a senescence response in neurons, and that OIS is a robust activator of senescence in both proliferating and non-proliferating cells.

Clearance of senescent cells in the brain has beneficial effects in mouse models of AD (Bussian et al. 2018; Musi et al. 2018; Zhang et al. 2019), and genetic elimination of senescent cells alleviates age-related brain inflammation and cognitive impairment in mice (Ogrodnik et al. 2021). Pharmacological elimination using the senescent targeting drug combination Dasatinib and Quercetin (D+Q) has provided similar results (Zhang, et al. 2019). Therefore, we tested

whether PSA-NCAM-sorted AD iNs cultures were more sensitive to D+Q treatment than healthy iN cultures. Indeed, iN cultures treated with the D+Q cocktail (0.5 – 1.5 μM) for 48 hours showed significantly higher levels of TUNEL-positive neurons than CTL iNs exposed to the same treatment (Fig2.6C-D). Although TUNEL-positive cells increased slightly in CTL cultures after D+Q, the change was much less pronounced than in AD patient lines, and doses of D+Q above 1 μM could produce significant differences in apoptosis between AD and CTL lines. We observed that an average of 6.2% of cells were removed at the highest tested concentration of D+Q, lower than the average $p16^{+}$ cells in AD cultures, suggesting that full removal was incomplete and higher doses of D+Q could be necessary to completely eliminate senescent iNs. However, 1.5 μM of D+Q was able to lower p16 abundance in AD cultures to levels comparable to CTL cultures (Fig2.6E). Taken together, these results suggest that senolytic drugs can specifically remove senescent neurons and restore senescent neuron abundance in AD neurons to that of healthy controls (Fig2.6F).

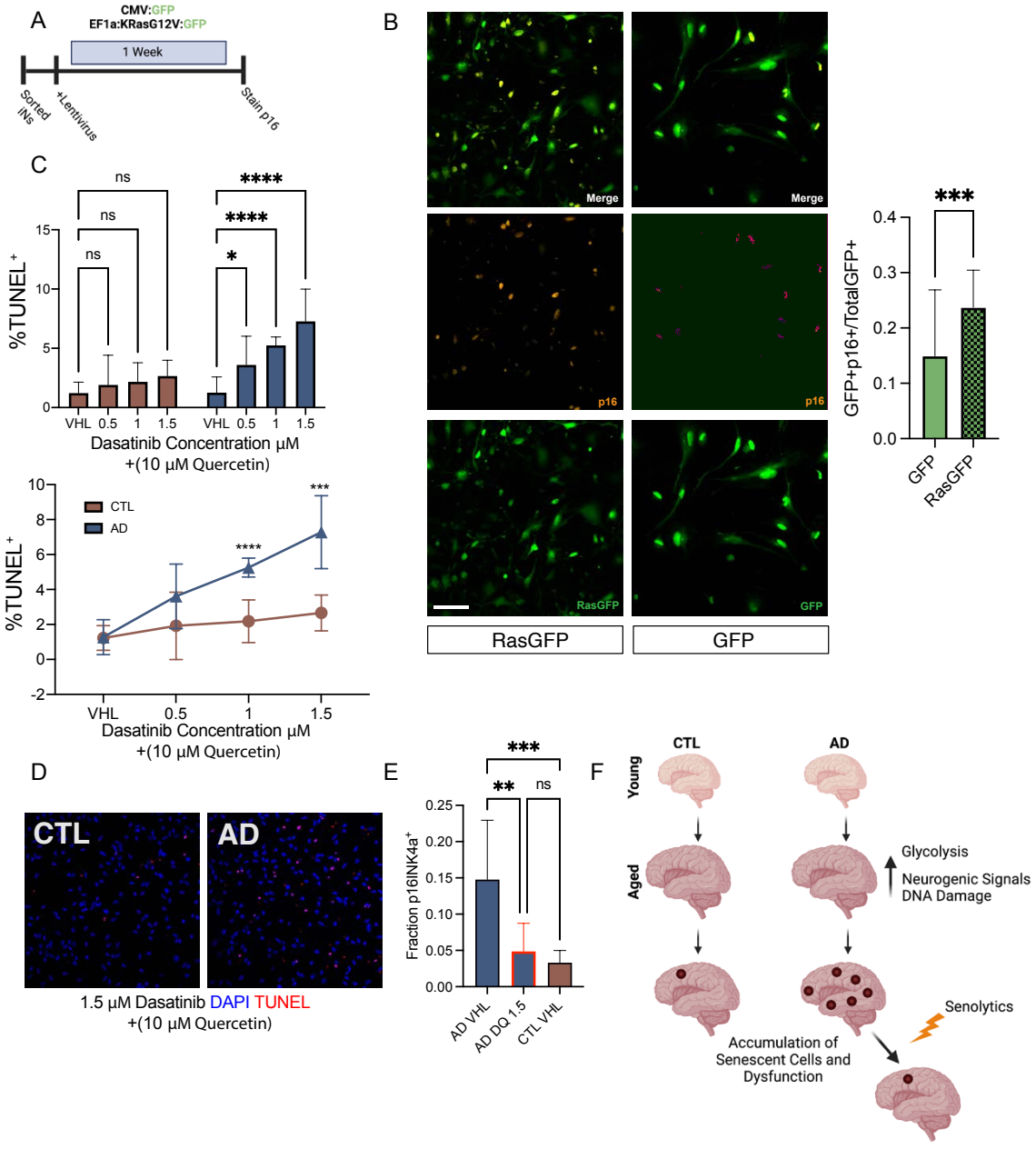

Figure 2.6: Senescence in neurons can be triggered by oncogenes and eliminated with senotherapeutics. (A) Ras overexpression experimental scheme. (B) Representative image of Ras- or GFP-treated iNs and p16 staining (left). Ras-treated iNs are significantly more likely to be p16^{+} than GFP controls (right). (n=8 biological replicates per condition, paired t-test). (C) AD iN cultures experience a dose-dependent increase in number of TUNEL^{+} cells after exposure to senolytic cocktail dasatinib + 10 µM quercetin. (n=3 AD; 3 CTL, Two-way ANOVA). (D) Representative field of iN cultures from AD or CTL patients treated with 1.5 µM dasatinib + 10 µM quercetin. (E) AD cultures have significantly reduced p16^{+} cells after D+Q treatments that are comparable to CTL p16 levels (n=3 AD; 3 CTL, One-way ANOVA). (F) Theory cartoon. * p < .05, ** p < .01, *** p < .001, **** p < .0001.

Neuronal senescence manifests in impaired electrical activity.

Electrical activity and the transmission of information are the principal functions of neurons. Entry into senescence typically results in impaired or altered cellular functionality, and our scRNAseq dataset indicated that senescent neurons lost expression of functional neuron genes. Therefore, we sought to test if senescent iN cultures had impaired electrical activity by examining spontaneous neuronal spiking by multi electrode array (MEA). Senescence was induced in aged iN cultures by p16INK4a overexpression, a strategy used to induce senescence both *in vitro* and *in vivo*, and we confirmed senescence activation in iNs by measuring BGal rates in p16 overexpressing cells relative to a GFP control (SupFig2.8A)(McConnell et al. 1998; Azazmeh et al. 2020). PSA-NCAM-sorted iN cultures from an aged healthy individual were treated with p16 or GFP control virus and synapsin:dsred to monitor cultures, and then cells were replated onto polyornithine laminin-coated MEA plates with a feeder layer of support astrocytes (Fig2.7A). Field potentials from iNs were recorded in media optimized to replicate physiological conditions in the human brain (SupFig2.8B). Following a recovery period of two weeks while iNs re-elaborated their dendritic network, GFP:iNs showed a robust increase in spontaneous activity as assessed by mean firing rate, which could be specifically ablated by treatment with tetrodotoxin (TTX) (Fig2.7B,D). However, p16:iNs did not recover electrical activity and had significantly lower levels of spontaneous firing than controls by four weeks of recording (Fig2.7B,C). Notably, there were no significant differences between spiking of GFP:iNs and p16:iNs when triggered to fire by electrical stimulation (Fig2.7E), suggesting that the capacity to fire is preserved in senescent neurons, but their spontaneous activity is decreased relative to controls under baseline, unstimulated conditions. Taken together, these results confirm that a consequence of senescence in neurons is impaired spontaneous firing, which could manifest as disruption in information processing in the brain.

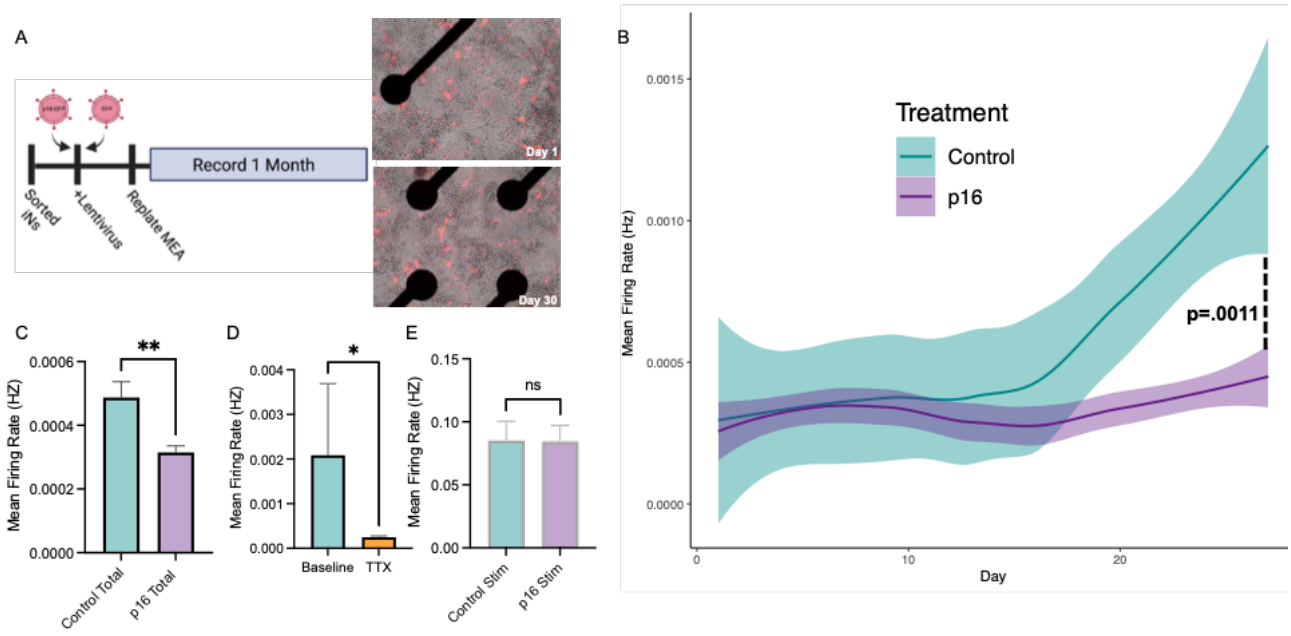

Figure 2.7: Neuronal senescence manifests in impaired electrical activity. (A) Experimental schema. Sorted iNs were treated with p16 or control lentivirus and cultured on multi electrode array (MEA) plates for one month of recording (left). Example images of synpasin:dsred labeled iNs on an MEA plate at 24 hours and one month after replating (right). (B) Ribbon plot of mean firing rate of p16 or GFP iNs. The slope of activity change over time was significantly higher in GFP than in p16-expressing iNs (n=18 recording wells for each condition. Two-tailed t-test). (C) The cumulative mean firing rate across all 30 days of recording in GFP iNs was significantly higher than p16 iNs. Measurements across all wells were averaged into a single point for a given day. (n=30, paired t-test). (D) Activity of iNs could be ablated with treatment of 1 uM tetrodotoxin. (n=18 recording wells, paired t-test). (E) There were no significant differences in the mean firing rate of GFP and p16 iNs following electrical stimulation (Stim) (n=18 recording wells for each condition, paired t-test).

Discussion

The concept of cellular senescence has evolved substantially since its original formulation as a proliferative arrest of human skin cells *in vitro*. The evidence of senescent cells across tissues of aged animals highlights senescence as a conventional strategy for responding to age-related stress in many cell types. Conversely, senescent cells have been observed early in development, before extensive age-related changes have occurred, and recent studies have uncovered functional roles of senescent cells in regeneration and in response to wound healing (Storer et al. 2013; Demaria et al. 2014). These observations suggest a coordinated and programmed cellular state induced by senescence that is dynamic but tightly regulated. Indeed, current knowledge favors a model where transient and controlled induction of senescent cells is adaptive but accumulation or chronic persistence of these cells results in dysfunction. The explicit cause for the increased prevalence of senescent cells late in life is still a subject of investigation, but it is likely due to a variety of other molecular changes associated with aging, including epigenetic changes, oxidative stress, DNA damage, and proteotoxic stress, all molecular hallmarks that are also shared with neurodegenerative diseases like AD. Here, we report that there in an increased burden of senescent neurons in the brains of AD patients, that we can model these cells *in vitro* using an aged human neuron culture system, and that senescent neurons constitute a neurogenic source of late-life brain inflammation in AD. The consequences of the presence of even a small population of senescent neurons in advanced ages could be quite profound for brain function. A single neuron can make many thousands of connections to its neighbors through extensive synaptic networks, providing ample opportunity for SASP-mediated dysfunction to spread (Mederos, González-Arias, and Perea 2018).

Our observations of senescent neurons in the AD brain led us to examine senescent features in aged AD neurons *in vitro* using iNs. Our characterization is consistent with a multi-marker strategy recommended to identify senescent cells with more accuracy (González-Gualda

et al. 2021). As in other cell types, senescence in neurons results in cellular dysfunction, including reduced spontaneous activity. Reports of senescence in non-dividing cells have occasionally come into conflict with the original conception of senescence as a state limited to proliferating cells, yet cells exhibiting features of senescence have been reported in many non-dividing cell types. Post-mitotic neurons are perhaps the most extensively reported non-dividing cell type to exhibit senescence phenotypes, and they are largely associated with aging or disease-related stress (Musi, et al. 2018; Jurk, et al. 2012; Riessland, et al. 2019; Chow, et al. 2019; Welch et al. 2022). We have shown that aged AD neuron cultures gain an inflammatory SASP that is capable of triggering reactive astrogliosis and that the transcriptional changes observed in these astrocytes resemble previously reported changes in post-mortem AD astrocytes. Much of the literature surrounding senescence in the brain has identified astrocytes as the cell type that most frequently presents features of senescence(Han et al. 2020). The SASP is known to induce senescence in a paracrine manner in neighboring cells, and it is tempting to speculate that the increased prevalence of senescent astrocytes in AD is due at least in part to a senescence-triggering SASP released by nearby senescent neurons. Indeed, our AD CM-treated astrocytes exhibit many of the transcriptional changes seen in irradiation-induced senescence in human astrocytes from a previous study (Limbad, et al. 2020). Thus, a neurogenic, irreconcilable inflammatory response driven by a minority of SASP-releasing neurons could be a potent source of AD-related neuroinflammation seen even at the earliest stages of AD progression.

Ultimately, we show that p16-expressing iNs can be eliminated with a senolytic cocktail of Dasatinib + Quercetin, reducing the number of p16-expressing cells in AD cultures to a level comparable with CTL cultures. The removal of chronic or overabundant senescent cells from the tissues of aged animals is generally associated with improvements in function and tissue homeostasis, and genetic elimination of senescent cells improved cognitive function of mice late in life, suggesting that targeting senescent cells in the AD brain for elimination could be a novel

approach for slowing neuroinflammation and subsequent neurodegeneration in AD. However, given the reports of senescent cells involved in wound healing and regeneration, we stress that more experiments will be necessary to understand the contributions that senescent neurons make to AD pathogenesis, or what the ultimate consequences of removing these neurons would have on overall brain function.

There are many known triggers for senescence induction. Previously we reported that induced neurons from our AD cohort had a loss of neuronal identity and appeared hypomature, expressed many genes associated with cancer, and had metabolic changes resembling a neoplastic Warburg shift (Traxler et al. 2022; Mertens, et al. 2021). These changes are especially pronounced in the cells undergoing senescence in our system. Among other potential causes for a senescence response preferentially in AD neurons, our data support the notion that de-differentiation stress is sufficient to trigger enough of a cell cycle response in a subset of neurons that they commit to the senescent phenotype, and cell cycle re-entry has been proposed as a molecular feature of AD (Herrup 2010). Indeed, challenging healthy neurons with oncogenic Ras produced a senescence response, implicating a common strategy of senescence activation in both proliferating and non-proliferating cells to cancerous transformation. Early in life, during wound healing and regeneration, transient senescence is beneficial, and recent studies suggest that senescence activation late in life could be an attempt to re-activate the wound-healing process (Wilkinson and Hardman 2020). For reasons that are not fully understood, during aging this process goes awry and senescent cells persist and ultimately contribute to tissue dysfunction. Therefore, there is also a possibility that neurons attempting to repair AD-related damage senesce but, in the context of the aged brain, they are incapable of repairing the damage and eventually contribute to an inflammatory feedback loop. Given the complexity of both the activation of senescence and the senescent phenotype itself, more studies will be necessary to fully evaluate senescence in neurons and AD.

Encouragingly, cellular models like the iN system have given us access to otherwise unreachable aged human neurons to directly evaluate the molecular basis for senescence in these cells. There have been many proposed sources for the persistent neuroinflammation observed in AD but, so far, the ultimate trigger has remained elusive. Here, we propose that a higher propensity of AD patient cells to senesce and release paracrine triggers to neighboring cells provides a plausible mechanism for AD neuroinflammation and pathogenic spread through the cortex. Further, this model is consistent with epidemiological studies that have suggested that AD patients have a lower incidence of cancer (Gillispie et al. 2021; Lanni et al. 2021; Li et al. 2014), where their senescing response could protect them earlier in life but be detrimentally activated in neurons late in life. Our data indicate that senescing human neurons can be specifically eliminated using senolytic drugs, suggesting that pharmacological removal of pathogenic inflammatory neurons could be possible in the AD brain, and we suggest that ongoing studies of senolytics that can cross the blood brain barrier should be evaluated for any effect on cognitive impairment late in life. However, with the growing number of reports of a senescence-like response in neurons, especially in the context of aging and disease, we think that it is prudent for future studies to consider these cells as a novel therapeutic target for modulating neurodegeneration.

Limitations of this Study

Fibroblasts to induced neuron conversions are heterogeneous and produce mixed populations of successfully converted neurons and a subset of undifferentiated cells. Here we used a FACS strategy to isolate neurons from unconverted fibroblasts, and we stress that pure populations be used for evaluation of senescence in these cells as fibroblasts, which readily senescence, have the potential to mask signal originating from neurons. Further, our p16 overexpression strategy produced a large proportion of senescent neurons which is likely larger than proportions present physiologically in the brain. Finally, despite the relatively large size of

our clinically characterized cohort there is the potential that our sample size might not fully represent the entirety of AD patient diversity.

Table T2.1: Clinically characterized cohort of AD and age-matched cognitively normal controls (NC) to investigate senescence markers in prefrontal cortex.

PATHID	BRAAK	Group	PATHDX1	AGE	SEX
5628	1	NC	Normal	80	F
5567	1	NC	Alzheimer's changes	86	M
5803	2	NC	Alzheimer neurofibrillary	103	F
5699	2	NC	Alzheimer's changes	92	F
5662	2	NC	Alzheimer's changes	93	F
5589	2	NC	Alzheimer's changes	94	F
5864	2	NC	Primary Age-Related Tau changes	96	M
5709	2	NC	Normal	94	M
5601	2	NC	Alzheimer's changes	89	M
5434	2	NC	Alzheimer's changes	86	M
5835	3	Early/Mid AD	Alzheimer's disease	85	F
5816	3	Early/Mid AD	Alzheimer's changes	83	F
5784	3	Early/Mid AD	Alzheimer's changes	89	F
5808	3	Early/Mid AD	Alzheimer's changes	98	M
5836	4	Early/Mid AD	Alzheimer's disease	93	F
5785	4	Early/Mid AD	Alzheimer's disease	87	F
5837	4	Early/Mid AD	Alzheimer's disease	90	M
5648	4	Early/Mid AD	Alzheimer's disease	70	M
5620	4	Early/Mid AD	Alzheimer's disease	86	M
5533	4	Early/Mid AD	Alzheimer's disease	88	M

Table T2.2: scRNAseq QC parameters

# Input Cells per patient	10,000
% cDNA sequenced	25
Chemistry	Single cell 3' v3
Culture Conditions	Bulk iN cultures, 2x 6cm culture plates per patient, 3 weeks NK, TrypLE to remove from plate
# samples multiplexed	7
Total Genes Dtected in at least 1 cell	28553

Patient	# cells retained	# reads Per Cell	# reads total for sample in library	median genes per cell	Sequencing Saturation (%)	cDNA conc (ng/uL)
14096	4,597	19,886	91,321,949	672	6	64
8020	1863	15472	28,823,884	1436	5.7	14.1
3158	6065	14183	86021552	771	6.6	36.9
2608	3706	26063	96588981	1332	8.8	38.1
3093	2635	15974	42090751	1002	7.3	14.1
8149	5126	16655	85374880	1630	7.2	42.9
8150	5523	14955	74606223	1691	6.3	27.3
Average	4,216	17,598	72,118,317	1,219	7	34

Table T2.3: Olink probes detected in iN supernatant samples.

$p < .05$ AD v CTL	Present in Aged iN Supernatant	Absent from Aged iN Supernatant
CCL2	IL8	IL2
CCL8	IL7	IL4
CCL20	IL17A	IL5
CXCL6	CCL3	IL10
CSF1	CCL7	IL13
IL6	CCL11	IL20
IL18R1	CCL13	IL18
EIF4EBP1	CCL19	IL24
CASP8	CXCL1	IL33
STAMBP	CXCL5	IL1A
KITLG	CXCL10	IL17C
NT3	MMP1	CCL4
	MMP10	CCL23
	TGFA	CCL25
	TGFB1	CCL2I
	VEGFA	CXCL9
	OPG	CXCL11
		CX3CL1
		TNF
		IFNG
		OSM

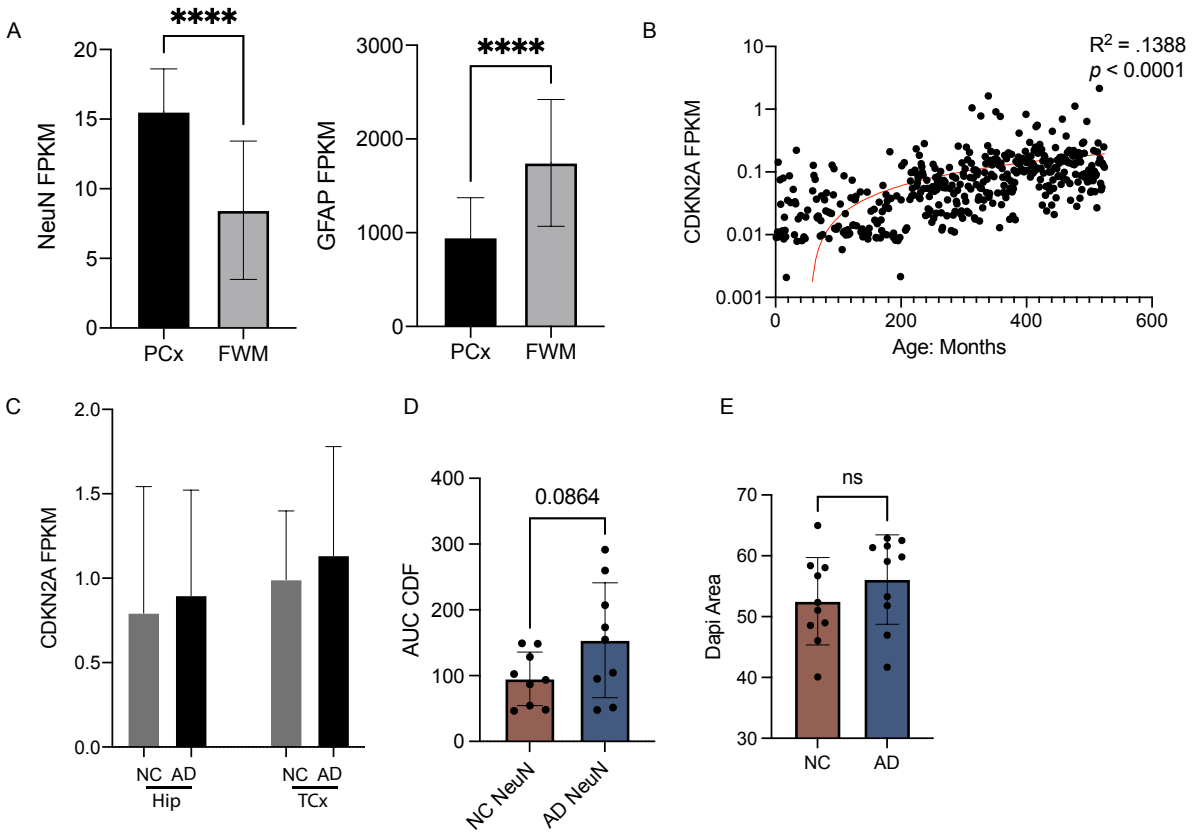

Supplemental Figure S2.1: (A) Prefrontal cortex (PCx) tissue contains more neuronal cell bodies, as indicated by higher NeuN expression, and frontal white matter (FWM) contains more glia, as indicated by higher GFAP expression (Wald test DESeq2, n=30 AD; 99 NC). (B) CDKN2A expression increases during aging in the human PCx (red line = simple linear regression, t-test, n=524). (C) Two neuron-rich brain regions, the hippocampus (Hip) and the temporal cortex (TCx), trend higher in CDKN2A expression. (n=30 AD; 99 NC). (D) p16 clustering tends to be higher adjacent to $NeuN^+$ nuclei (n=10 AD; 10 NC, unpaired t-test). (E) There was no significant difference in nuclear area for all cells between AD and NC nuclei. **** p < .0001.

Supplemental Figure S2.2: (A) Tet inducible system for the overexpression of NGN2 and ASCL1 for iN conversion (UNA). (B) Representative images of fibroblast cultures prior to conversion and iN cultures following 21 days of conversion from an AD and a CTL donor; scale bar = 16 μm (C) Example scatter plot and gating for FAC purification of iNs by PSA-NCAM (left). Percent yields of PSA-NCAM$^+$ iNs did not differ between AD and CTL donors (right). (n=16 AD; 19 CTL, unpaired t-test). (D) GSEA of senescence genes shows a significant enrichment in aged fibroblast iNs over rejuvenated iPSC-iNs. (E) SATB1 expression is significantly decreased in AD iNs (left). RRHO indicates that AD iNs are transcriptionally closer to SATB1 KO neurons than wild type (WT) cells (right). (F) Absolute levels of promoter methylation of senescence genes is consistent between AD and CTL iNs. (G) Density plot of enrichment FDR scores from GO analysis of ATAC peaks shared between Riessland et al (Riessland, et al. 2019) and iN datasets. (H) H2AFJ and downstream target genes are upregulated transcriptionally in AD iNs. (Wald test DESeq2) (I) Estimation of population doublings by DNA methylation shows no differences between AD and CTL donors for iNs or fibroblasts. (J) Expression of replication-independent telomere enzymes is equivalent between AD and CTL iNs. * $p < .05$, ** $p < .01$, *** $p < .001$.

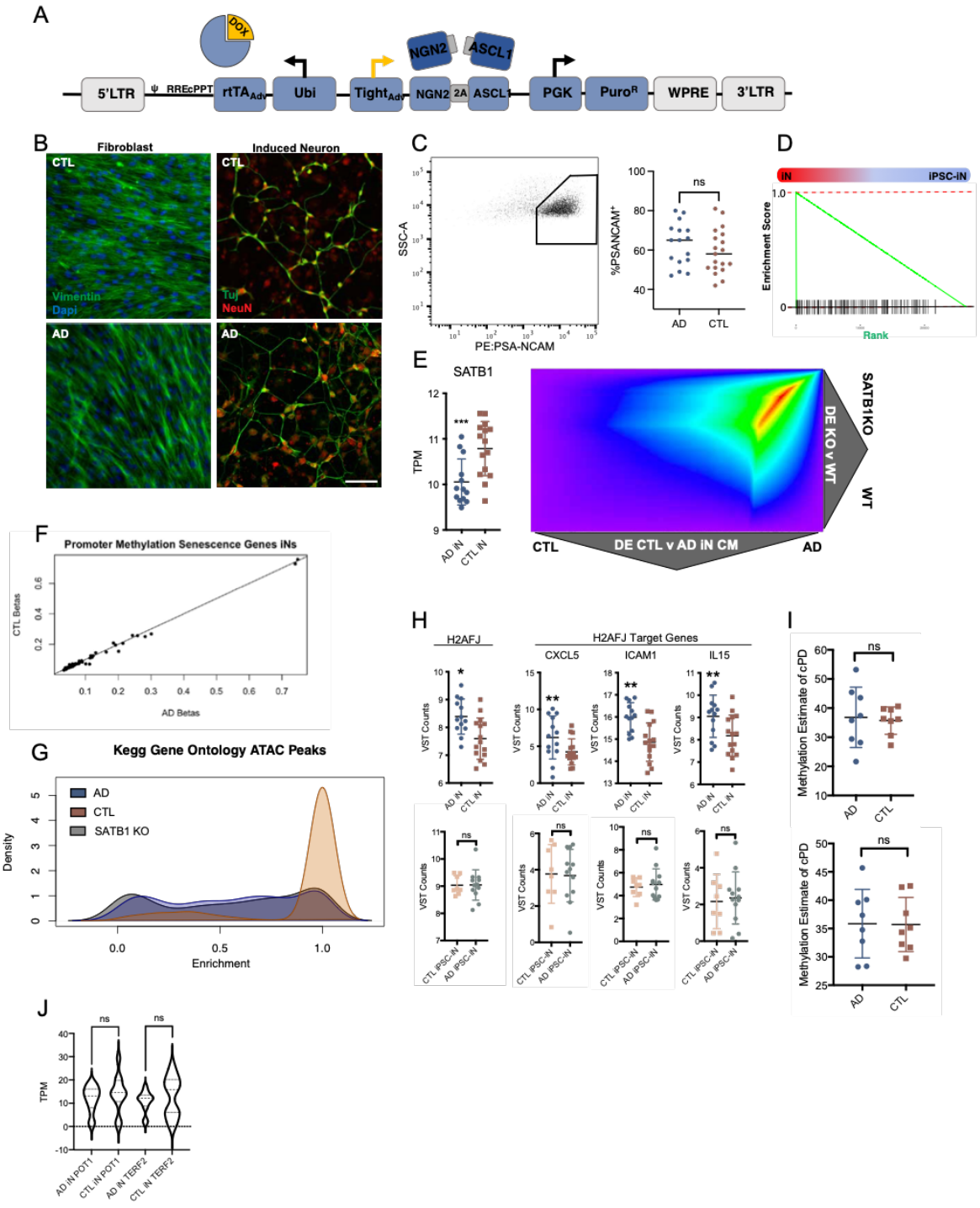
A
DOX
NGN2
ASCL1
5'LTR
ψ RREcPPT
rtTA Adv
Ubi
Tight Adv
NGN2 2A ASCL1
PGK
Puro R
WPRE
3'LTR
B
Fibroblast
Induced Neuron
CTL
CTL
Vimentin
Dapi
Tuj
NeuN
AD
AD
C
SSC-A
PE:PSA-NCAM
%PSANCAM+
ns
AD
CTL
D
iN
iPSC-iN
Enrichment Score
Rank
E
SATB1
TPM
***
AD iN
CTL iN
SATB1KO
DE KO v WT
WT
CTL
DE CTL v AD iN CM
AD
F
Promoter Methylation Senescence Genes iNs
CTL Betas
AD Betas
G
Kegg Gene Ontology ATAC Peaks
AD
CTL
SATB1 KO
Density
Enrichment
H
H2AFJ
H2AFJ Target Genes
CXCL5
ICAM1
IL15
VST Counts
CTL iPSC-iN
AD iPSC-iN
I
Methylation Estimate of cPD
ns
AD
CTL
J
TPM
AD iN POT1
CTL iN POT1
AD iN TERF2
CTL iN TERF2

Supplemental Figure S2.3: (A) Expression of full length CDKN2A, p14ARF, and p16INK4a mRNAs in AD and CTL iNs. (B) Example image of SA-B-Gal stain in AD and CTL fibroblast cultures (left); scale bar = 8 μm. Quantification of B-Gal rates (right). (n=8 AD; 8 CTL, unpaired t-test). (C) ANOVA analysis finds no significant relationship in BGal-positive rates in iNs based on the age of the donor or the rates of BGal-positive cells in parent fibroblast cultures. (D) Senescence marker rates and (E) gene expression show no sex-specific differences from patients in our cohort. (F) Density plot of forward scatter area (FSC) in PSA-NCAM-positive cells indicates a larger average FSC area in AD iNs. (G) AD and CTL iN cultures have equivalent levels of LaminB1 (n= 4 AD; 4 CTL, unpaired t-test, scale bar = 16 μm). * $p < .05$, ** $p < .01$.

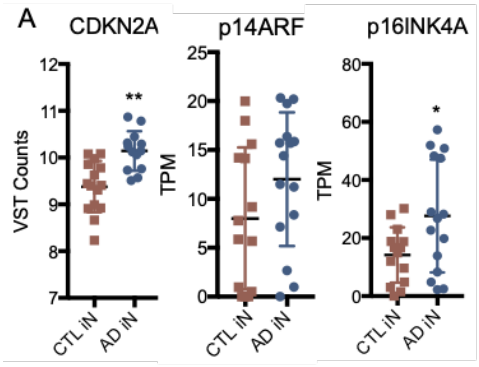

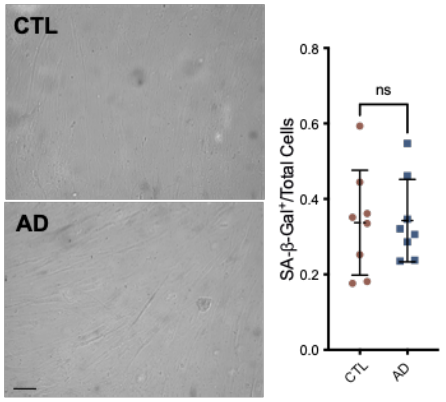

C

ANOVA Age iN

	df	SS	MS	F	Significance F
Regression	1	2.58187	2.58187	0.06487	0.800171548
Residual	43	1711.418	39.80042		
Total	44	1714			

ANOVA Age Fibroblast

	df	SS	MS	F	Significance F
Regression	1	1.825918	1.825918	0.045857	0.831448944
Residual	43	1712.174	39.818		
Total	44	1714			

ANOVA iN v Fibroblast

	df	SS	MS	F	Significance F
Regression	1	0.01927334	0.019273	1.147613	0.2900254
Residual	43	0.72215387	0.016794		
Total	44	0.74142721			

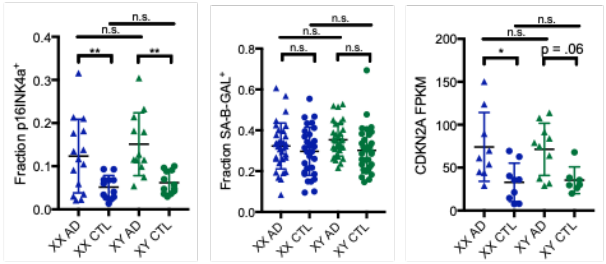

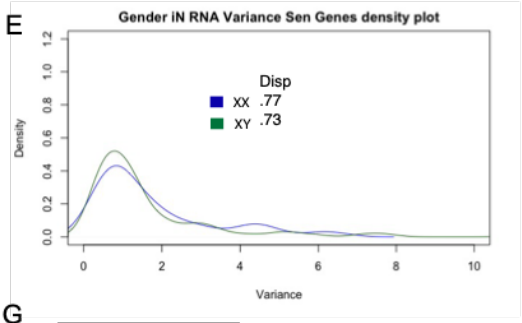

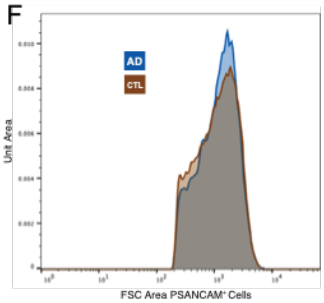

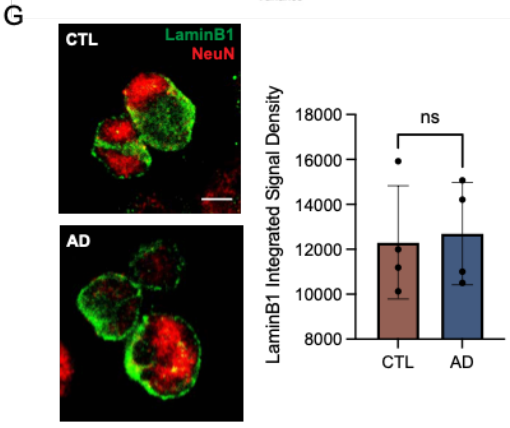

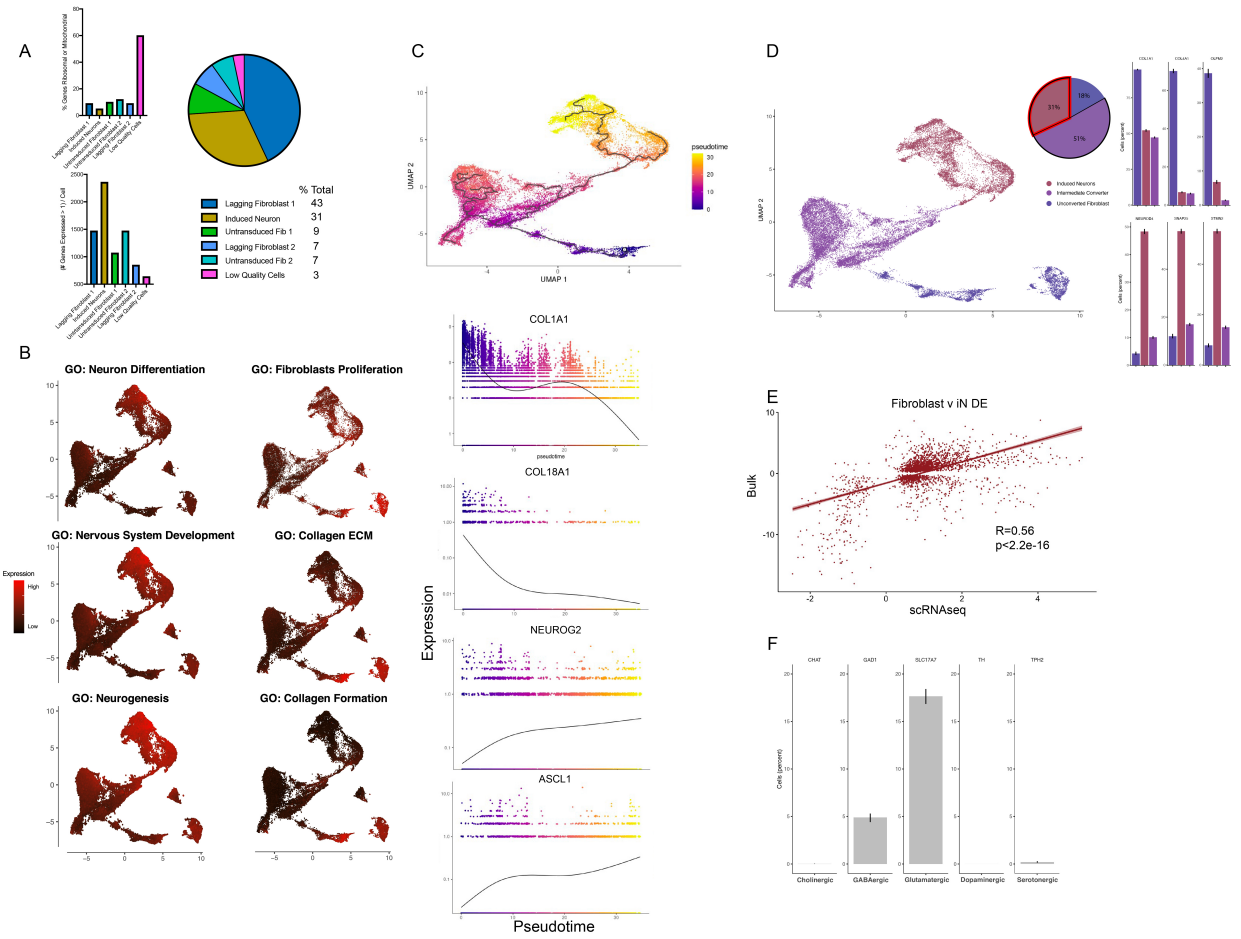

Supplemental Figure S2.4: (A) Genes expressed across UMAP clusters and proportions of cells within each cluster. (B) Expression pattern of neuron-related gene sets and fibroblast-related gene sets indicates cluster 2 as *bona fide* iNs. (C) Pseudotime ordering of cells indicates a clear differentiation trajectory from fibroblast to iN with the gain of NGN2 and ASCL1 and loss of fibroblast genes such as collagenases. (D) UMAP with annotation labels for fibroblasts, intermediate cells, and fully differentiated iNs (left). Marker gene expression in the 3 annotated classes (right). (E) Correlation analysis of differential expression (DE) between fibroblasts and iNs from bulk and single cell sequencing shows a significant overlap in gene expression changes. (F) Estimation of neuron subtype by marker gene expression indicates a majority of glutamatergic iNs with a small subset of GABAergic cells and rare instances of serotonergic, cholinergic, and dopaminergic neurons.

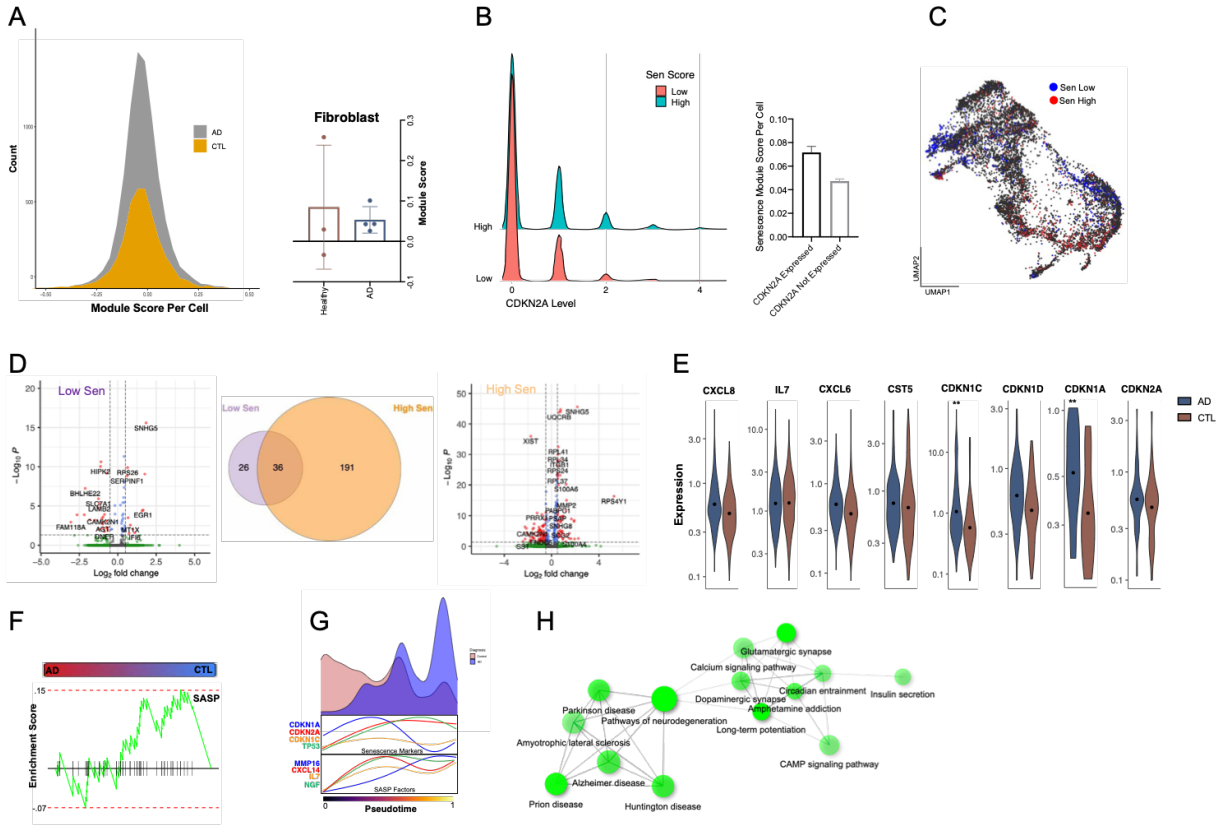

Supplemental Figure S2.5: (A) Density plot of mean module score per cell in AD or CTL iNs (left). Senescence module score in AD or CTL fibroblasts (right). (B) Density plot of sen-high and sen-low groups across CDKN2A expression (left). CDKN2A is expressed higher in populations with a high senescent score than in cells with a low senescence score (right). (C) Distribution of sen-high and sen-low cells across iNs in UMAP space. (D) Differential expression analysis between AD and CTL iNs in either sen-low or sen-high groups indicates a larger transcriptional difference between high-sen cells. (E) Expression of CDKN family members and inflammatory markers that increase across pseudotime are also upregulated at the pseudobulk levels in AD iNs relative to control. (F) GSEA of SASP genes showed no enrichment in AD fibroblasts. (G) Density plot of patient proportions across CDKN2A pseudotime in human post-mortem excitatory neurons and gene expression changes across pseudotime. (H) Gene network analysis of differentially expressed genes across CDKN2A pseudotime in human post-mortem excitatory neurons. ** p < .01

Supplemental Figure S2.6: (A) Representative image of primary human cortical astrocytes staining positive for astrocyte markers GFAP and S100B; scale bar = 16 μm. (B) Example images (right) and quantification (left) of human astrocytes treated with CM from AD or CTL iN cultures for 24 hours reveals increased reactivity as assessed by GFAP area and intensity (n=12 iNs; 3 astrocyte cell lines, unpaired t-test). (C) Human astrocytes treated with CM from AD or CTL fibroblast cultures for 24 hours (n=12 fibroblasts, 3 astrocyte cell lines, unpaired t-test). (D) Human astrocytes treated with CM from AD iN or AD iPSC-iN cultures for 24 hours (n=3 AD iN or iPSC-iNs, 3 astrocyte cell lines, unpaired t-test). (E) Expression of relevant receptors to identified iN cytokines in untreated astrocytes. (F) Pearson correlation of gene expression in untreated astrocytes to a human brain cell atlas showed highest correlation to cells annotated as astrocytes. (G) GO enrichment analysis of gene overlap from iN AD CM-treated and *in vivo* AD human astrocytes. (H) RRHO of irradiation in induced senescent (IR) or non-senescent (NS) astrocytes compared to AD or CTL-CM treated astrocytes. * $p < .05$, ** $p < .01$, *** $p < .001$.

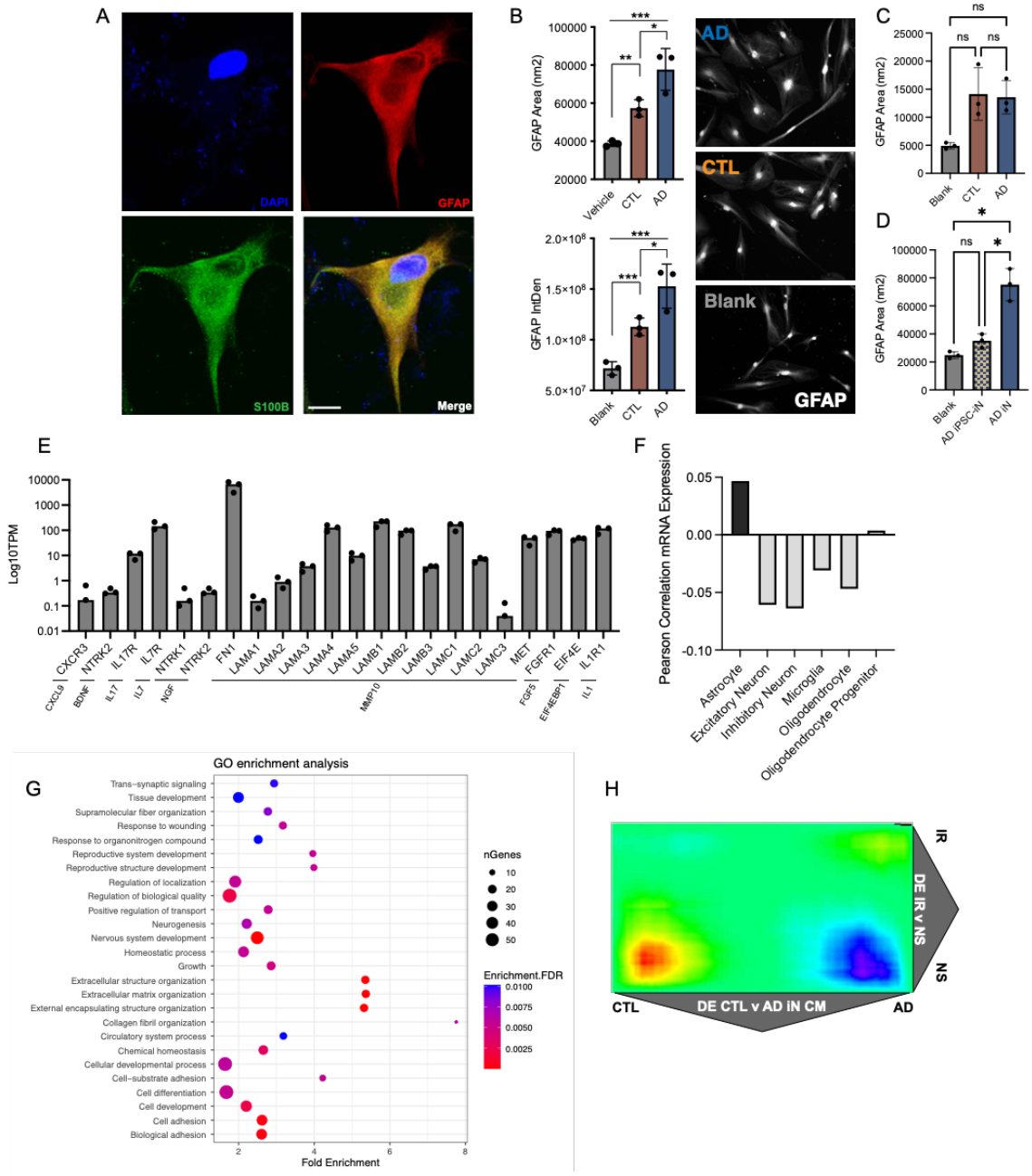
A
DAPI
GFAP
S100B
Merge
B
GFAP Area (nm2)
Vehicle
CTL
AD
GFAP IntDen
AD
CTL
Blank
GFAP
C
GFAP Area (nm2)
Blank
CTL
AD
D
GFAP Area (nm2)
Blank
AD iPSC-iN
AD iN
E
Log10TPM
CXCR3
NTRK2
IL17R
IL7R
NTRK1
NTRK2
FN1
LAMA1
LAMA2
LAMA3
LAMA4
LAMA5
LAMB1
LAMB2
LAMB3
LAMC1
LAMC2
LAMC3
MET
FGFR1
EIF4E
IL1R1
CXCL9
BDNF
IL17
IL7
NGF
MMP10
FGFs
EIF4EBP1
IL1
F
Pearson Correlation mRNA Expression
Astrocyte
Excitatory Neuron
Inhibitory Neuron
Microglia
Oligodendrocyte
Oligodendrocyte Progenitor
G
GO enrichment analysis
Trans-synaptic signaling
Tissue development
Supramolecular fiber organization
Response to wounding
Response to organonitrogen compound
Reproductive system development
Reproductive structure development
Regulation of localization
Regulation of biological quality
Positive regulation of transport
Neurogenesis
Nervous system development
Homeostatic process
Growth
Extracellular structure organization
Extracellular matrix organization
External encapsulating structure organization
Collagen fibril organization
Circulatory system process
Chemical homeostasis
Cellular developmental process
Cell-substrate adhesion
Cell differentiation
Cell development
Cell adhesion
Biological adhesion
Fold Enrichment
nGenes
Enrichment.FDR
H
IR
DE IR v NS
NS
CTL
DE CTL v AD iN CM
AD

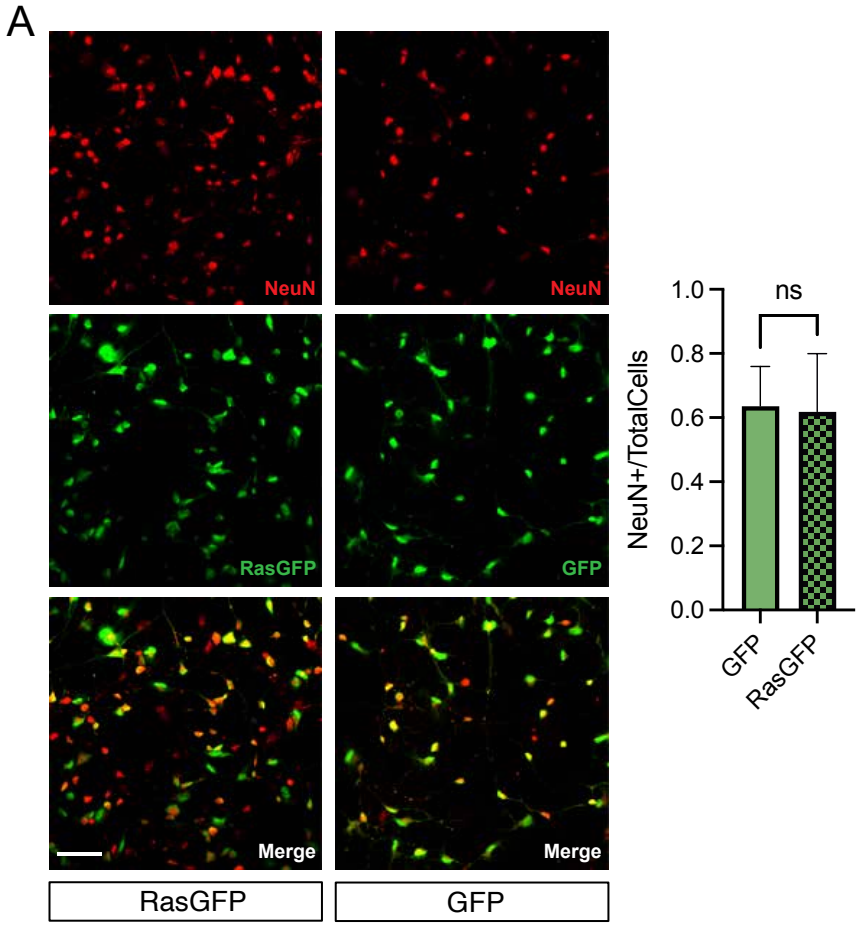

Supplemental Figure S2.7: (A) Representative images of Ras- or GFP-treated iNs and NeuN staining (left). Ras-treated iNs had equivalent levels of NeuN+ cells as GFP-treated controls (right); scale bar = 16 μm. (n=8 biological replicates per condition, paired t-test).

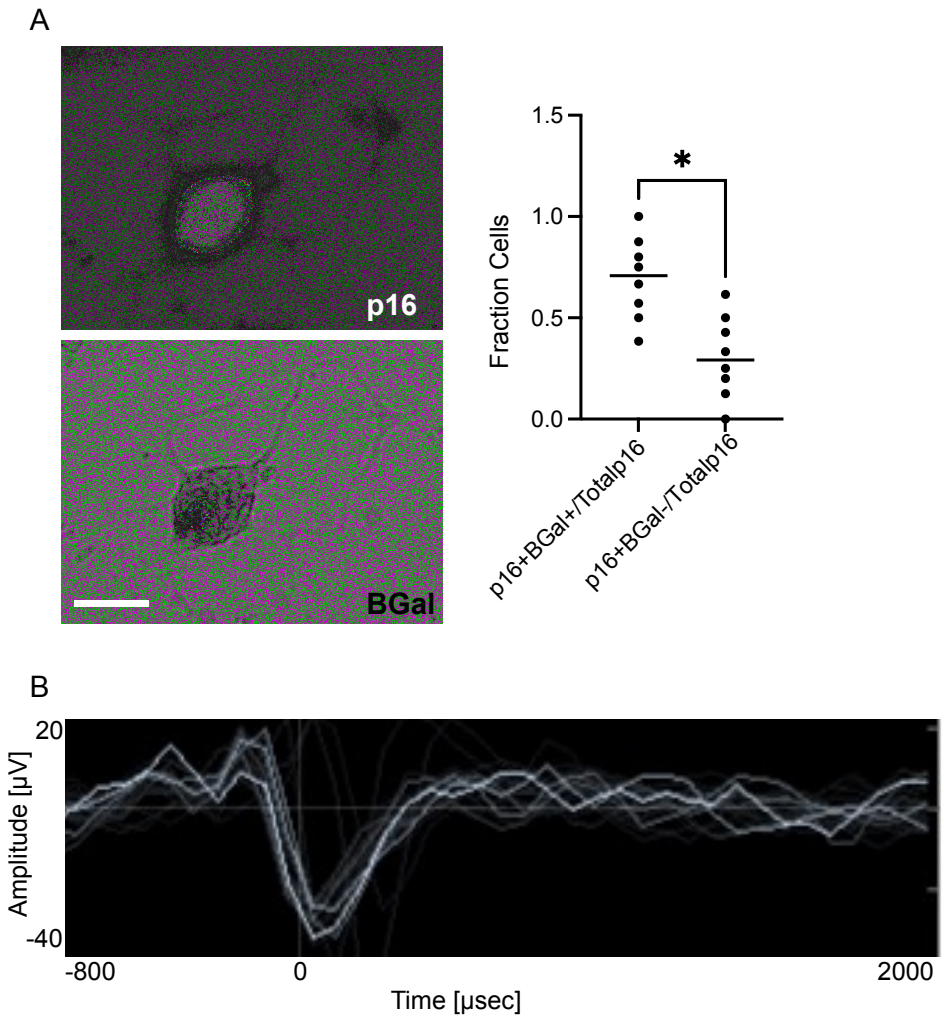

Supplemental Figure S2.8: (A) Example picture of p16- and BGal-co-positive iN (left). p16 overexpressing cells were significantly more likely to be $BGal^{+}$ than p16-negative cells (right); scale bar = 8 μm. (n=8 biological replicates, paired t-test). (B) Example MEA waveform from a GFP:iN control well. * $p < .05$.

Chapter 2, in full, is a reprint of the material as it appears in: Herdy, J. R., Traxler, L., Agarwal, R. K., Karbacher, L., Schlachetzki, J. C. M., Boehnke, L., Zangwill, D., Galasko, D., Glass, C. K., Mertens, J., & Gage, F. H. (2022). Increased post-mitotic senescence in aged human neurons is a pathological feature of Alzheimer's disease. Cell stem cell, 29(12), 1637–1652.e6. https://doi.org/10.1016/j.stem.2022.11.010. The dissertation author was the primary investigator and author of this paper.

References

Andrey, P., K. Kiêu, C. Kress, G. Lehmann, L. Tirichine, Z. Liu, E. Biot, P. G. Adenot, C. Hue-Beauvais, N. Houba-Hérin, V. Duranthon, E. Devinoy, N. Beaujean, V. Gaudin, Y. Maurin, and P. Debey. 2010. "Statistical Analysis of 3d Images Detects Regular Spatial Distributions of Centromeres and Chromocenters in Animal and Plant Nuclei." *PLoS Comput Biol* 6, no. 7 (Jul 08): e1000853. https://dx.doi.org/10.1371/journal.pcbi.1000853.

Arendt, T., L. Rödel, U. Gärtner, and M. Holzer. 1996. "Expression of the Cyclin-Dependent Kinase Inhibitor P16 in Alzheimer's Disease." *Neuroreport* 7, no. 18 (Nov 25): 3047-9. https://dx.doi.org/10.1097/00001756-199611250-00050.

Azazmeh, N., B. Assouline, E. Winter, S. Ruppo, Y. Nevo, A. Maly, K. Meir, A. K. Witkiewicz, J. Cohen, S. V. Rizou, E. Pikarsky, C. Luxenburg, V. G. Gorgoulis, and I. Ben-Porath. 2020. "Chronic Expression of P16." *Nat Commun* 11, no. 1 (06 01): 2711. https://dx.doi.org/10.1038/s41467-020-16475-3.

Bartkova, J., N. Rezaei, M. Liontos, P. Karakaidos, D. Kletsas, N. Issaeva, L. V. Vassiliou, E. Kolettas, K. Niforou, V. C. Zoumpourlis, M. Takaoka, H. Nakagawa, F. Tort, K. Fugger, F. Johansson, M. Sehested, C. L. Andersen, L. Dyrskjot, T. Ørntoft, J. Lukas, C. Kittas, T. Helleday, T. D. Halazonetis, J. Bartek, and V. G. Gorgoulis. 2006. "Oncogene-Induced Senescence Is Part of the Tumorigenesis Barrier Imposed by Dna Damage Checkpoints." *Nature* 444, no. 7119 (Nov 30): 633-7. https://dx.doi.org/10.1038/nature05268.

Basisty, N., A. Kale, O. H. Jeon, C. Kuehnemann, T. Payne, C. Rao, A. Holtz, S. Shah, V. Sharma, L. Ferrucci, J. Campisi, and B. Schilling. 2020. "A Proteomic Atlas of Senescence-Associated Secretomes for Aging Biomarker Development." *PLoS Biol* 18, no. 1 (01): e3000599. https://dx.doi.org/10.1371/journal.pbio.3000599.

Bussian, T. J., A. Aziz, C. F. Meyer, B. L. Swenson, J. M. van Deursen, and D. J. Baker. 2018. "Clearance of Senescent Glial Cells Prevents Tau-Dependent Pathology and Cognitive Decline." *Nature* 562, no. 7728 (10): 578-582. https://dx.doi.org/10.1038/s41586-018-0543-y.

Cao, J., M. Spielmann, X. Qiu, X. Huang, D. M. Ibrahim, A. J. Hill, F. Zhang, S. Mundlos, L. Christiansen, F. J. Steemers, C. Trapnell, and J. Shendure. 2019. "The Single-Cell Transcriptional Landscape of Mammalian Organogenesis." *Nature* 566, no. 7745 (02): 496-502. https://dx.doi.org/10.1038/s41586-019-0969-x.

Cawthon, R. M. 2002. "Telomere Measurement by Quantitative Pcr." *Nucleic Acids Res* 30, no. 10 (May 15): e47. https://dx.doi.org/10.1093/nar/30.10.e47.

Chen, J. L., D. J. Margolis, A. Stankov, L. T. Sumanovski, B. L. Schneider, and F. Helmchen. 2015. "Pathway-Specific Reorganization of Projection Neurons in Somatosensory Cortex During Learning." *Nat Neurosci* 18, no. 8 (Aug): 1101-8. https://dx.doi.org/10.1038/nn.4046.

Chow, H. M., M. Shi, A. Cheng, Y. Gao, G. Chen, X. Song, R. W. L. So, J. Zhang, and K. Herrup. 2019. "Age-Related Hyperinsulinemia Leads to Insulin Resistance in Neurons and Cell-Cycle-Induced Senescence." *Nat Neurosci* 22, no. 11 (11): 1806-1819. https://dx.doi.org/10.1038/s41593-019-0505-1.

Collado, M., and M. Serrano. 2010. "Senescence in Tumours: Evidence from Mice and Humans." *Nat Rev Cancer* 10, no. 1 (Jan): 51-7. https://dx.doi.org/10.1038/nrc2772.

Contrepois, K., C. Coudereau, B. A. Benayoun, N. Schuler, P. F. Roux, O. Bischof, R. Courbeyrette, C. Carvalho, J. Y. Thuret, Z. Ma, C. Derbois, M. C. Nevers, H. Volland, C. E. Redon, W. M. Bonner, J. F. Deleuze, C. Wiel, D. Bernard, M. P. Snyder, C. E. Rübe, R. Olaso, F. Fenaille, and C. Mann. 2017. "Histone Variant H2a.J Accumulates in Senescent Cells and Promotes Inflammatory Gene Expression." *Nat Commun* 8 (05 10): 14995. https://dx.doi.org/10.1038/ncomms14995.

Coppé, J. P., P. Y. Desprez, A. Krtolica, and J. Campisi. 2010. "The Senescence-Associated Secretory Phenotype: The Dark Side of Tumor Suppression." *Annu Rev Pathol* 5: 99-118. https://dx.doi.org/10.1146/annurev-pathol-121808-102144.

da Silva, P. F. L., M. Ogrodnik, O. Kucheryavenko, J. Glibert, S. Miwa, K. Cameron, A. Ishaq, G. Saretzki, S. Nagaraja-Grellscheid, G. Nelson, and T. von Zglinicki. 2019. "The Bystander Effect Contributes to the Accumulation of Senescent Cells in Vivo." *Aging Cell* 18, no. 1 (02): e12848. https://dx.doi.org/10.1111/acel.12848.

Dehkordi, Shiva Kazempour, Jamie Walker, Eric Sah, Emma Bennett, Farzaneh Atrian, Bess Frost, Benjamin Woost, Rachel E. Bennett, Timothy C. Orr, Yingyue Zhou, Prabhakar S. Andhey, Marco Colonna, Peter H. Sudmant, Peng Xu, Minghui Wang, Bin Zhang, Habil Zare, and Miranda E. Orr. 2021. "Profiling Senescent Cells in Human Brains Reveals Neurons with Cdkn2d/P19 and Tau Neuropathology." *Nature Aging* 1, no. 12 (2021/12/01): 1107-1116. https://dx.doi.org/10.1038/s43587-021-00142-3.

Demaria, M., N. Ohtani, S. A. Youssef, F. Rodier, W. Toussaint, J. R. Mitchell, R. M. Laberge, J. Vijg, H. Van Steeg, M. E. Dollé, J. H. Hoeijmakers, A. de Bruin, E. Hara, and J. Campisi. 2014. "An Essential Role for Senescent Cells in Optimal Wound Healing through Secretion of Pdgf-Aa." *Dev Cell* 31, no. 6 (Dec 22): 722-33. https://dx.doi.org/10.1016/j.devcel.2014.11.012.

Denchi, E. L., and T. de Lange. 2007. "Protection of Telomeres through Independent Control of Atm and Atr by Trf2 and Pot1." *Nature* 448, no. 7157 (Aug 30): 1068-71. https://dx.doi.org/10.1038/nature06065.

Escartin, C., E. Galea, A. Lakatos, J. P. O'Callaghan, G. C. Petzold, A. Serrano-Pozo, C. Steinhäuser, A. Volterra, G. Carmignoto, A. Agarwal, N. J. Allen, A. Araque, L. Barbeito, A. Barzilai, D. E. Bergles, G. Bonvento, A. M. Butt, W. T. Chen, M. Cohen-Salmon, C. Cunningham, B. Deneen, B. De Strooper, B. Díaz-Castro, C. Farina, M. Freeman, V. Gallo, J. E. Goldman, S. A. Goldman, M. Götz, A. Gutiérrez, P. G. Haydon, D. H. Heiland, E. M. Hol, M. G. Holt, M. Iino, K. V. Kastanenka, H. Kettenmann, B. S. Khakh, S. Koizumi, C. J. Lee, S. A. Liddelow, B. A. MacVicar, P. Magistretti, A. Messing, A. Mishra, A. V. Molofsky, K. K. Murai, C. M. Norris, S. Okada, S. H. R. Oliet, J. F. Oliveira, A. Panatier, V. Parpura, M. Pekna, M. Pekny, L. Pellerin, G. Perea, B. G. Pérez-Nievas, F. W. Pfrieger, K. E. Poskanzer, F. J. Quintana, R. M. Ransohoff, M. Riquelme-Perez, S. Robel, C. R. Rose, J. D. Rothstein, N. Rouach, D. H. Rowitch, A. Semyanov, S. Sirko, H. Sontheimer, R. A. Swanson, J. Vitorica, I. B. Wanner, L. B. Wood, J. Wu, B. Zheng, E. R. Zimmer, R. Zorec, M. V. Sofroniew, and A. Verkhratsky. 2021. "Reactive Astrocyte Nomenclature,

Definitions, and Future Directions." *Nat Neurosci* 24, no. 3 (03): 312-325. https://dx.doi.org/10.1038/s41593-020-00783-4.

Farr, J. N., D. G. Fraser, H. Wang, K. Jaehn, M. B. Ogrodnik, M. M. Weivoda, M. T. Drake, T. Tchkonia, N. K. LeBrasseur, J. L. Kirkland, L. F. Bonewald, R. J. Pignolo, D. G. Monroe, and S. Khosla. 2016. "Identification of Senescent Cells in the Bone Microenvironment." *J Bone Miner Res* 31, no. 11 (11): 1920-1929. https://dx.doi.org/10.1002/jbmr.2892.

Gillispie, G. J., E. Sah, S. Krishnamurthy, M. Y. Ahmidouch, B. Zhang, and M. E. Orr. 2021. "Evidence of the Cellular Senescence Stress Response in Mitotically Active Brain Cells-Implications for Cancer and Neurodegeneration." *Life (Basel)* 11, no. 2 (Feb 17). https://dx.doi.org/10.3390/life11020153.

González-Gualda, E., A. G. Baker, L. Fruk, and D. Muñoz-Espín. 2021. "A Guide to Assessing Cellular Senescence In vitro and In vivo." *FEBS J* 288, no. 1 (01): 56-80. https://dx.doi.org/10.1111/febs.15570.

Han, X., T. Zhang, H. Liu, Y. Mi, and X. Gou. 2020. "Astrocyte Senescence and Alzheimer's Disease: A Review." *Front Aging Neurosci* 12: 148. https://dx.doi.org/10.3389/fnagi.2020.00148.

Handel, A. E., S. Chintawar, T. Lalic, E. Whiteley, J. Vowles, A. Giustacchini, K. Argoud, P. Sopp, M. Nakanishi, R. Bowden, S. Cowley, S. Newey, C. Akerman, C. P. Ponting, and M. Z. Cader. 2016. "Assessing Similarity to Primary Tissue and Cortical Layer Identity in Induced Pluripotent Stem Cell-Derived Cortical Neurons through Single-Cell Transcriptomics." *Hum Mol Genet* 25, no. 5 (Mar 01): 989-1000. https://dx.doi.org/10.1093/hmg/ddv637.

Herdy, J., S. Schafer, Y. Kim, Z. Ansari, D. Zangwill, M. Ku, A. Paquola, H. Lee, J. Mertens, and F. H. Gage. 2019. "Chemical Modulation of Transcriptionally Enriched Signaling Pathways to Optimize the Conversion of Fibroblasts into Neurons." *Elife* 8 (05 17). https://dx.doi.org/10.7554/eLife.41356.

Herrup, K. 2010. "The Involvement of Cell Cycle Events in the Pathogenesis of Alzheimer's Disease." *Alzheimers Res Ther* 2, no. 3 (May 20): 13. https://dx.doi.org/10.1186/alzrt37.

Hill, L. J., V. Di Pietro, J. Hazeldine, D. Davies, E. Toman, A. Logan, and A. Belli. 2018. "Author Correction: Cystatin D (Cst5): An Ultra-Early Inflammatory Biomarker of Traumatic Brain Injury." *Sci Rep* 8, no. 1 (Mar 12): 4572. https://dx.doi.org/10.1038/s41598-018-22951-0.

Huh, C. J., B. Zhang, M. B. Victor, S. Dahiya, L. F. Batista, S. Horvath, and A. S. Yoo. 2016. "Maintenance of Age in Human Neurons Generated by Microrna-Based Neuronal Conversion of Fibroblasts." *Elife* 5 (09 20). https://dx.doi.org/10.7554/eLife.18648.

Hänzelmann, S., F. Beier, E. G. Gusmao, C. M. Koch, S. Hummel, I. Charapitsa, S. Joussen, V. Benes, T. H. Brümmendorf, G. Reid, I. G. Costa, and W. Wagner. 2015. "Replicative Senescence Is Associated with Nuclear Reorganization and with Dna Methylation at Specific Transcription Factor Binding Sites." *Clin Epigenetics* 7: 19. https://dx.doi.org/10.1186/s13148-015-0057-5.

Israel, M. A., S. H. Yuan, C. Bardy, S. M. Reyna, Y. Mu, C. Herrera, M. P. Hefferan, S. Van Gorp, K. L. Nazor, F. S. Boscolo, C. T. Carson, L. C. Laurent, M. Marsala, F. H. Gage, A. M. Remes, E. H. Koo, and L. S. Goldstein. 2012. "Probing Sporadic and Familial Alzheimer's Disease Using Induced Pluripotent Stem Cells." *Nature* 482, no. 7384 (Jan 25): 216-20. https://dx.doi.org/10.1038/nature10821.

Jurk, D., C. Wang, S. Miwa, M. Maddick, V. Korolchuk, A. Tsolou, E. S. Gonos, C. Thrasivoulou, M. J. Saffrey, K. Cameron, and T. von Zglinicki. 2012. "Postmitotic Neurons Develop a P21-Dependent Senescence-Like Phenotype Driven by a Dna Damage Response." *Aging Cell* 11, no. 6 (Dec): 996-1004. https://dx.doi.org/10.1111/j.1474-9726.2012.00870.x.

Kim, Y., X. Zheng, Z. Ansari, M. C. Bunnell, J. R. Herdy, L. Traxler, H. Lee, A. C. M. Paquola, C. Blithikioti, M. Ku, J. C. M. Schlachetzki, J. Winkler, F. Edenhofer, C. K. Glass, A. A. Paucar, B. N. Jaeger, S. Pham, L. Boyer, B. C. Campbell, T. Hunter, J. Mertens, and F. H. Gage. 2018. "Mitochondrial Aging Defects Emerge in Directly Reprogrammed Human Neurons Due to Their Metabolic Profile." *Cell Rep* 23, no. 9 (05 29): 2550-2558. https://dx.doi.org/10.1016/j.celrep.2018.04.105.

Koch, C. M., and W. Wagner. 2013. "Epigenetic Biomarker to Determine Replicative Senescence of Cultured Cells." *Methods Mol Biol* 1048: 309-21. https://dx.doi.org/10.1007/978-1-62703-556-9_20.

Ladewig, J., J. Mertens, J. Kesavan, J. Doerr, D. Poppe, F. Glaue, S. Herms, P. Wernet, G. Kögler, F. J. Müller, P. Koch, and O. Brüstle. 2012. "Small Molecules Enable Highly Efficient Neuronal Conversion of Human Fibroblasts." *Nat Methods* 9, no. 6 (Jun): 575-8. https://dx.doi.org/10.1038/nmeth.1972.

Lanni, C., M. Masi, M. Racchi, and S. Govoni. 2021. "Cancer and Alzheimer's Disease Inverse Relationship: An Age-Associated Diverging Derailment of Shared Pathways." *Mol Psychiatry* 26, no. 1 (01): 280-295. https://dx.doi.org/10.1038/s41380-020-0760-2.

Li, J. M., C. Liu, X. Hu, Y. Cai, C. Ma, X. G. Luo, and X. X. Yan. 2014. "Inverse Correlation between Alzheimer's Disease and Cancer: Implication for a Strong Impact of Regenerative Propensity on Neurodegeneration?" *BMC Neurol* 14 (Nov 14): 211. https://dx.doi.org/10.1186/s12883-014-0211-2.

Limbad, C., T. R. Oron, F. Alimirah, A. R. Davalos, T. E. Tracy, L. Gan, P. Y. Desprez, and J. Campisi. 2020. "Astrocyte Senescence Promotes Glutamate Toxicity in Cortical Neurons." *PLoS One* 15, no. 1: e0227887. https://dx.doi.org/10.1371/journal.pone.0227887.

Mathys, H., J. Davila-Velderrain, Z. Peng, F. Gao, S. Mohammadi, J. Z. Young, M. Menon, L. He, F. Abdurrob, X. Jiang, A. J. Martorell, R. M. Ransohoff, B. P. Hafler, D. A. Bennett, M. Kellis, and L. H. Tsai. 2019. "Single-Cell Transcriptomic Analysis of Alzheimer's Disease." *Nature* 570, no. 7761 (06): 332-337. https://dx.doi.org/10.1038/s41586-019-1195-2.

Mattson, M. P., and T. Magnus. 2006. "Ageing and Neuronal Vulnerability." *Nat Rev Neurosci* 7, no. 4 (Apr): 278-94. https://dx.doi.org/10.1038/nrn1886.

McConnell, B. B., M. Starborg, S. Brookes, and G. Peters. 1998. "Inhibitors of Cyclin-Dependent Kinases Induce Features of Replicative Senescence in Early Passage Human Diploid

Fibroblasts." *Curr Biol* 8, no. 6 (Mar 12): 351-4. https://dx.doi.org/10.1016/s0960-9822(98)70137-x.

McHugh, D., and J. Gil. 2018. "Senescence and Aging: Causes, Consequences, and Therapeutic Avenues." *J Cell Biol* 217, no. 1 (01 02): 65-77. https://dx.doi.org/10.1083/jcb.201708092.

McShea, A., P. L. Harris, K. R. Webster, A. F. Wahl, and M. A. Smith. 1997. "Abnormal Expression of the Cell Cycle Regulators P16 and Cdk4 in Alzheimer's Disease." *Am J Pathol* 150, no. 6 (Jun): 1933-9.

Mederos, S., C. González-Arias, and G. Perea. 2018. "Astrocyte-Neuron Networks: A Multilane Highway of Signaling for Homeostatic Brain Function." *Front Synaptic Neurosci* 10: 45. https://dx.doi.org/10.3389/fnsyn.2018.00045.

Mertens, J., J. R. Herdy, L. Traxler, S. T. Schafer, J. C. M. Schlachetzki, L. Böhnke, D. A. Reid, H. Lee, D. Zangwill, D. P. Fernandes, R. K. Agarwal, R. Lucciola, L. Zhou-Yang, L. Karbacher, F. Edenhofer, S. Stern, S. Horvath, A. C. M. Paquola, C. K. Glass, S. H. Yuan, M. Ku, A. Szücs, L. S. B. Goldstein, D. Galasko, and F. H. Gage. 2021. "Age-Dependent Instability of Mature Neuronal Fate in Induced Neurons from Alzheimer's Patients." *Cell Stem Cell* 28, no. 9 (09 02): 1533-1548.e6. https://dx.doi.org/10.1016/j.stem.2021.04.004.

Mertens, J., A. C. M. Paquola, M. Ku, E. Hatch, L. Bohnke, S. Ladjevardi, S. McGrath, B. Campbell, H. Lee, J. R. Herdy, J. T. Goncalves, T. Toda, Y. Kim, J. Winkler, J. Yao, M. W. Hetzer, and F. H. Gage. 2015a. "Directly Reprogrammed Human Neurons Retain Aging-Associated Transcriptomic Signatures and Reveal Age-Related Nucleocytoplasmic Defects." *Cell Stem Cell* 17, no. 6 (Dec 3): 705-718. https://dx.doi.org/10.1016/j.stem.2015.09.001.

Mertens, J., A. C. M. Paquola, M. Ku, E. Hatch, L. Böhnke, S. Ladjevardi, S. McGrath, B. Campbell, H. Lee, J. R. Herdy, J. T. Gonçalves, T. Toda, Y. Kim, J. Winkler, J. Yao, M. W. Hetzer, and F. H. Gage. 2015b. "Directly Reprogrammed Human Neurons Retain Aging-Associated Transcriptomic Signatures and Reveal Age-Related Nucleocytoplasmic Defects." *Cell Stem Cell* 17, no. 6 (Dec 03): 705-718. https://dx.doi.org/10.1016/j.stem.2015.09.001.

Mertens, J., D. Reid, S. Lau, Y. Kim, and F. H. Gage. 2018. "Aging in a Dish: Ipsc-Derived and Directly Induced Neurons for Studying Brain Aging and Age-Related Neurodegenerative Diseases." *Annu Rev Genet* 52 (11 23): 271-293. https://dx.doi.org/10.1146/annurev-genet-120417-031534.

Miller, J. A., A. Guillozet-Bongaarts, L. E. Gibbons, N. Postupna, A. Renz, A. E. Beller, S. M. Sunkin, L. Ng, S. E. Rose, K. A. Smith, A. Szafer, C. Barber, D. Bertagnolli, K. Bickley, K. Brouner, S. Caldejon, M. Chapin, M. L. Chua, N. M. Coleman, E. Cudaback, C. Cuhaciyan, R. A. Dalley, N. Dee, T. Desta, T. A. Dolbeare, N. I. Dotson, M. Fisher, N. Gaudreault, G. Gee, T. L. Gilbert, J. Goldy, F. Griffin, C. Habel, Z. Haradon, N. Hejazinia, L. L. Hellstern, S. Horvath, K. Howard, R. Howard, J. Johal, N. L. Jorstad, S. R. Josephsen, C. L. Kuan, F. Lai, E. Lee, F. Lee, T. Lemon, X. Li, D. A. Marshall, J. Melchor, S. Mukherjee, J. Nyhus, J. Pendergraft, L. Potekhina, E. Y. Rha, S. Rice, D. Rosen, A. Sapru, A. Schantz, E. Shen, E. Sherfield, S. Shi, A. J. Sodt, N. Thatra, M. Tieu, A. M. Wilson, T. J. Montine, E. B. Larson, A. Bernard, P. K. Crane, R. G. Ellenbogen, C. D. Keene, and E. Lein. 2017.

"Neuropathological and Transcriptomic Characteristics of the Aged Brain." *Elife* 6 (11 09). https://dx.doi.org/10.7554/eLife.31126.

Minamino, T., M. Orimo, I. Shimizu, T. Kunieda, M. Yokoyama, T. Ito, A. Nojima, A. Nabetani, Y. Oike, H. Matsubara, F. Ishikawa, and I. Komuro. 2009. "A Crucial Role for Adipose Tissue P53 in the Regulation of Insulin Resistance." *Nat Med* 15, no. 9 (Sep): 1082-7. https://dx.doi.org/10.1038/nm.2014.

Moore, L. D., T. Le, and G. Fan. 2013. "Dna Methylation and Its Basic Function." *Neuropsychopharmacology* 38, no. 1 (Jan): 23-38. https://dx.doi.org/10.1038/npp.2012.112.

Morabito, S., E. Miyoshi, N. Michael, S. Shahin, A. C. Martini, E. Head, J. Silva, K. Leavy, M. Perez-Rosendahl, and V. Swarup. 2021. "Single-Nucleus Chromatin Accessibility and Transcriptomic Characterization of Alzheimer's Disease." *Nat Genet* 53, no. 8 (08): 1143-1155. https://dx.doi.org/10.1038/s41588-021-00894-z.

Moreno-Blas, D., E. Gorostieta-Salas, A. Pommer-Alba, G. Muciño-Hernández, C. Gerónimo-Olvera, L. A. Maciel-Barón, M. Konigsberg, L. Massieu, and S. Castro-Obregón. 2019. "Cortical Neurons Develop a Senescence-Like Phenotype Promoted by Dysfunctional Autophagy." *Aging (Albany NY)* 11, no. 16 (08 30): 6175-6198. https://dx.doi.org/10.18632/aging.102181.

Musi, N., J. M. Valentine, K. R. Sickora, E. Baeuerle, C. S. Thompson, Q. Shen, and M. E. Orr. 2018. "Tau Protein Aggregation Is Associated with Cellular Senescence in the Brain." *Aging Cell* 17, no. 6 (12): e12840. https://dx.doi.org/10.1111/acel.12840.

O'Callaghan, N., V. Dhillon, P. Thomas, and M. Fenech. 2008. "A Quantitative Real-Time Pcr Method for Absolute Telomere Length." *Biotechniques* 44, no. 6 (May): 807-9. https://dx.doi.org/10.2144/000112761.

Ogrodnik, M., S. A. Evans, E. Fielder, S. Victorelli, P. Kruger, H. Salmonowicz, B. M. Weigand, A. D. Patel, T. Pirtskhalava, C. L. Inman, K. O. Johnson, S. L. Dickinson, A. Rocha, M. J. Schafer, Y. Zhu, D. B. Allison, T. von Zglinicki, N. K. LeBrasseur, T. Tchkonia, N. Neretti, J. F. Passos, J. L. Kirkland, and D. Jurk. 2021. "Whole-Body Senescent Cell Clearance Alleviates Age-Related Brain Inflammation and Cognitive Impairment in Mice." *Aging Cell* 20, no. 2 (02): e13296. https://dx.doi.org/10.1111/acel.13296.

Ohtani, N., Z. Zebedee, T. J. Huot, J. A. Stinson, M. Sugimoto, Y. Ohashi, A. D. Sharrocks, G. Peters, and E. Hara. 2001. "Opposing Effects of Ets and Id Proteins on P16ink4a Expression During Cellular Senescence." *Nature* 409, no. 6823 (Feb 22): 1067-70. https://dx.doi.org/10.1038/35059131.

Paramos-de-Carvalho, D., I. Martins, A. M. Cristóvão, A. F. Dias, D. Neves-Silva, T. Pereira, D. Chapela, A. Farinho, A. Jacinto, and L. Saúde. 2021. "Targeting Senescent Cells Improves Functional Recovery after Spinal Cord Injury." *Cell Rep* 36, no. 1 (Jul 06): 109334. https://dx.doi.org/10.1016/j.celrep.2021.109334.

Rayess, H., M. B. Wang, and E. S. Srivatsan. 2012. "Cellular Senescence and Tumor Suppressor Gene P16." *Int J Cancer* 130, no. 8 (Apr 15): 1715-25. https://dx.doi.org/10.1002/ijc.27316.

Reid, D. A., P. J. Reed, J. C. M. Schlachetzki, I. I. Nitulescu, G. Chou, E. C. Tsui, J. R. Jones, S. Chandran, A. T. Lu, C. A. McClain, J. H. Ooi, T. W. Wang, A. J. Lana, S. B. Linker, A. S. Ricciardulli, S. Lau, S. T. Schafer, S. Horvath, J. R. Dixon, N. Hah, C. K. Glass, and F. H. Gage. 2021. "Incorporation of a Nucleoside Analog Maps Genome Repair Sites in Postmitotic Human Neurons." *Science* 372, no. 6537 (04 02): 91-94. https://dx.doi.org/10.1126/science.abb9032.

Riessland, M., B. Kolisnyk, T. W. Kim, J. Cheng, J. Ni, J. A. Pearson, E. J. Park, K. Dam, D. Acehan, L. S. Ramos-Espiritu, W. Wang, J. Zhang, J. W. Shim, G. Ciceri, L. Brichta, L. Studer, and P. Greengard. 2019. "Loss of Satb1 Induces P21-Dependent Cellular Senescence in Post-Mitotic Dopaminergic Neurons." *Cell Stem Cell* 25, no. 4 (10 03): 514-530.e8. https://dx.doi.org/10.1016/j.stem.2019.08.013.

Rodríguez, J. J., M. Olabarria, A. Chvatal, and A. Verkhratsky. 2009. "Astroglia in Dementia and Alzheimer's Disease." *Cell Death Differ* 16, no. 3 (Mar): 378-85. https://dx.doi.org/10.1038/cdd.2008.172.

Sapieha, P., and F. A. Mallette. 2018. "Cellular Senescence in Postmitotic Cells: Beyond Growth Arrest." *Trends Cell Biol* 28, no. 8 (08): 595-607. https://dx.doi.org/10.1016/j.tcb.2018.03.003.

Schafer, S. T., A. C. M. Paquola, S. Stern, D. Gosselin, M. Ku, M. Pena, T. J. M. Kuret, M. Liyanage, A. A. Mansour, B. N. Jaeger, M. C. Marchetto, C. K. Glass, J. Mertens, and F. H. Gage. 2019. "Pathological Priming Causes Developmental Gene Network Heterochronicity in Autistic Subject-Derived Neurons." *Nat Neurosci* 22, no. 2 (02): 243-255. https://dx.doi.org/10.1038/s41593-018-0295-x.

Stein, G. H., L. F. Drullinger, A. Soulard, and V. Dulić. 1999. "Differential Roles for Cyclin-Dependent Kinase Inhibitors P21 and P16 in the Mechanisms of Senescence and Differentiation in Human Fibroblasts." *Mol Cell Biol* 19, no. 3 (Mar): 2109-17. https://dx.doi.org/10.1128/MCB.19.3.2109.

Storer, M., A. Mas, A. Robert-Moreno, M. Pecoraro, M. C. Ortells, V. Di Giacomo, R. Yosef, N. Pilpel, V. Krizhanovsky, J. Sharpe, and W. M. Keyes. 2013. "Senescence Is a Developmental Mechanism That Contributes to Embryonic Growth and Patterning." *Cell* 155, no. 5 (Nov 21): 1119-30. https://dx.doi.org/10.1016/j.cell.2013.10.041.

Tang, Y., S. Xiong, P. Yu, F. Liu, and L. Cheng. 2018. "Direct Conversion of Mouse Fibroblasts into Neural Stem Cells by Chemical Cocktail Requires Stepwise Activation of Growth Factors and Nup210." *Cell Rep* 24, no. 5 (07 31): 1355-1362.e3. https://dx.doi.org/10.1016/j.celrep.2018.06.116.

Traxler, L., J. R. Herdy, D. Stefanoni, S. Eichhorner, S. Pelucchi, A. Szücs, A. Santagostino, Y. Kim, R. K. Agarwal, J. C. M. Schlachetzki, C. K. Glass, J. Lagerwall, D. Galasko, F. H. Gage, A. D'Alessandro, and J. Mertens. 2022. "Warburg-Like Metabolic Transformation Underlies Neuronal Degeneration in Sporadic Alzheimer's Disease." *Cell Metab* 34, no. 9 (Sep 06): 1248-1263.e6. https://dx.doi.org/10.1016/j.cmet.2022.07.014.

Usardi, A., K. Iyer, S. M. Sigoillot, A. Dusonchet, and F. Selimi. 2017. "The Immunoglobulin-Like Superfamily Member Igsf3 Is a Developmentally Regulated Protein That Controls

Neuronal Morphogenesis." *Dev Neurobiol* 77, no. 1 (01): 75-92. https://dx.doi.org/10.1002/dneu.22412.

Vadodaria, K. C., J. Mertens, A. Paquola, C. Bardy, X. Li, R. Jappelli, L. Fung, M. C. Marchetto, M. Hamm, M. Gorris, P. Koch, and F. H. Gage. 2016. "Generation of Functional Human Serotonergic Neurons from Fibroblasts." *Mol Psychiatry* 21, no. 1 (Jan): 49-61. https://dx.doi.org/10.1038/mp.2015.161.

Van Cauwenberghe, C., C. Van Broeckhoven, and K. Sleegers. 2016. "The Genetic Landscape of Alzheimer Disease: Clinical Implications and Perspectives." *Genet Med* 18, no. 5 (05): 421-30. https://dx.doi.org/10.1038/gim.2015.117.

Victor, M. B., M. Richner, H. E. Olsen, S. W. Lee, A. M. Monteys, C. Ma, C. J. Huh, B. Zhang, B. L. Davidson, X. W. Yang, and A. S. Yoo. 2018. "Striatal Neurons Directly Converted from Huntington's Disease Patient Fibroblasts Recapitulate Age-Associated Disease Phenotypes." *Nat Neurosci* 21, no. 3 (03): 341-352. https://dx.doi.org/10.1038/s41593-018-0075-7.

Visse, R., and H. Nagase. 2003. "Matrix Metalloproteinases and Tissue Inhibitors of Metalloproteinases: Structure, Function, and Biochemistry." *Circ Res* 92, no. 8 (May 02): 827-39. https://dx.doi.org/10.1161/01.RES.0000070112.80711.3D.

Welch, G. M., C. A. Boix, E. Schmauch, J. Davila-Velderrain, M. B. Victor, V. Dileep, P. L. Bozzelli, Q. Su, J. D. Cheng, A. Lee, N. S. Leary, A. R. Pfenning, M. Kellis, and L. H. Tsai. 2022. "Neurons Burdened by Dna Double-Strand Breaks Incite Microglia Activation through Antiviral-Like Signaling in Neurodegeneration." *Sci Adv* 8, no. 39 (Sep 30): eabo4662. https://dx.doi.org/10.1126/sciadv.abo4662.

Whelan, C. D., N. Mattsson, M. W. Nagle, S. Vijayaraghavan, C. Hyde, S. Janelidze, E. Stomrud, J. Lee, L. Fitz, T. A. Samad, G. Ramaswamy, R. A. Margolin, A. Malarstig, and O. Hansson. 2019. "Multiplex Proteomics Identifies Novel Csf and Plasma Biomarkers of Early Alzheimer's Disease." *Acta Neuropathol Commun* 7, no. 1 (11 06): 169. https://dx.doi.org/10.1186/s40478-019-0795-2.

Wilkinson, H. N., and M. J. Hardman. 2020. "Senescence in Wound Repair: Emerging Strategies to Target Chronic Healing Wounds." *Front Cell Dev Biol* 8: 773. https://dx.doi.org/10.3389/fcell.2020.00773.

Yaswen, P., and J. Campisi. 2007. "Oncogene-Induced Senescence Pathways Weave an Intricate Tapestry." *Cell* 128, no. 2 (Jan 26): 233-4. https://dx.doi.org/10.1016/j.cell.2007.01.005.

Zhang, P., Y. Kishimoto, I. Grammatikakis, K. Gottimukkala, R. G. Cutler, S. Zhang, K. Abdelmohsen, V. A. Bohr, J. Misra Sen, M. Gorospe, and M. P. Mattson. 2019. "Senolytic Therapy Alleviates Aβ-Associated Oligodendrocyte Progenitor Cell Senescence and Cognitive Deficits in an Alzheimer's Disease Model." *Nat Neurosci* 22, no. 5 (05): 719-728. https://dx.doi.org/10.1038/s41593-019-0372-9.

CONCLUSION

To advance human health and understand human disease, we need access to models that allow us to study complex biological systems in a laboratory environment. Nowhere is this need greater than for studying the human brain, which is fundamentally difficult to access. The neuron is the individual coding unit in mammalian brains, which combined with billions of neighbors produces cognition, consciousness, and behavior. A more complete understanding of human neurons as the individual building blocks of the brain will then contribute to a greater understanding of the system as a whole.

Here, I have utilized the technology developed in the field of cellular reprogramming to generate human neurons derived from a skin biopsy using direct neuron transdifferentiation. In Chapter 1, I present a streamlined and state-of-the-art iN protocol, which uses a combined lentiviral vector and a pathway analysis derived small molecule cocktail to produce iNs from human skin with high efficiency. In Chapter 2, I apply this technology to a cohort of healthy and AD patient cells to produce age equivalent neurons to evaluate molecular markers of AD in aged human neurons. Therein, I discovered a population of senescent neurons that have neuroinflammatory and dysfunctional consequences for the aged human brain. My work shows that iNs are a relevant *in vitro* system for modeling neuronal senescence and lays the foundations for future work investigating how senescent neurons contribute to brain aging.

Senescence is a programmed cellular response that can be activated under conditions of stress and culminates in a change of cell fate. When faced with irreparable damage, especially during disease or chronic aging-related insults, cells can undergo apoptosis or shift to an apoptosis-resistant senescent state. Our understanding of the conditions under which cells can senesce has expanded dramatically since its initial discovery, changing our conception of senescence from a narrow response to proliferative stress to a diverse general strategy for mammalian cells to manage molecular damage and preserve tissue function and organismal health. Unfortunately, in aged individuals, senescent cells often persist within tissues and

ultimately contribute to tissue dysfunction. As evidence of the diversity of inputs that can trigger senescence grows, the reliability of any one given feature to distinguish senescent from non-senescent cells has become elusive. One challenging result has been the discovery of a senescence state shift in non-dividing cells, chiefly neurons, which by definition were thought to be incapable of experiencing the proliferative arrest hallmark of senescence. However, the results I have gathered suggests that neurons are also capable of a senescent state shift. This senescent state shift occurs more often in AD patients, placing senescent neurons at the threshold between healthy aging and disease in the geriatric human brain.

Moving forward, my work cautiously advocates for the use of senolytics for treating AD. Removal of neurons to treat neurodegeneration at first appears counterintuitive, but it is possible that the outsized impact senescent neurons have on their niche through inflammatory signaling and improper firing could mean their persistence is doing more harm than good, and removing them could slow the neuroinflammatory and neurodegenerative process. Indeed, patients are currently being recruited for clinical trials testing the D+Q cocktail in human patients to treat AD. I also advocate for the continued use of iNs to study neuronal senescence and develop new generations of neuron targeting senotherapeutics. As we advance our understanding of the pathways necessary for neurons to senesce, we can develop more targeted therapies to slow or reverse this process instead of resorting to the selective ablation of these cells entirely.

Currently, I anticipate the most important area of study for neuronal senescence is the SASP. Many of the genetic risk factors associated with AD involve immune related genes and glial reactivity, but how these changes manifest in neuronal degeneration or what are the initiating inflammatory events in AD pathogenesis remain unclear. The persistence of a neuronal SASP could link immune activation to a senescent neurogenic source, where an irreconcilable neuronal SASP perpetuates a pathogenic astrocyte and microglia state that slowly degrades tissue functionality until cells can no longer cope and begin to degenerate. The SASP is a highly heterogenous response, however, so identifying the critical factors will be no small undertaking.

Previous senescence literature has given us clues for likely candidates, and the consistencies of other molecular markers of senescence in neurons, e.g. p16 and H2AFJ, support the idea that a neuronal SASP might operate through a similar mechanism as proliferating cells. One rich area for investigation is the contribution of LINE1 transposable elements to a SASP. LINE1 transposons have been found to be necessary for maintaining a long term SASP response by providing a single stranded cDNA intermediate in the cytoplasm that maintains a cell autonomous immune response. Neurons have perhaps the highest rate of transposon activity of any somatic cell type. Therefore, it is possible that neurons rely on LINE1 for a chronic SASP response and that intervening in this signaling cascade could eliminate a neuronal SASP.

One limitation of this thesis is that it relies on neurons grown in a monoculture environment in the absence of other brain relevant cell types. Although we were able to model paracrine interactions through the application of neuronal conditioned media, it is likely that cellular crosstalk through physical cell-cell interactions is an important component of a neuronal senescence signaling cascade. Future work should use more physiologically relevant cellular models, like 3D cortical organoids, to examine the responses of other cell types to senescent neurons in a tissue relevant environment. Exciting results in the development of these models has made this work possible, and we are entering a new era of human *in vitro* culture systems that can take into account multiple cell types in a single experiment.

In conclusion, aging in a complex and stochastic process that can result in many different individual outcomes. As societies live to more advanced ages, learning to intervene in age-related disorders will vastly improve the human healthspan. The work I have presented here is an attempt to expand that knowledge, and I look forward to participating in continued investigation in this area to promote healthy brain again and reduce the devastating impacts of late-life neurodegeneration.